

# **Electrophysiological and Molecular Insights into Thalamocortical Rhythmicity and Hippocampal Theta Oscillations**

Inaugural – Dissertation

zur

Erlangung des Doktorgrades

der Mathematisch-Naturwissenschaftlichen Fakultät

der Universität zu Köln

vorgelegt von

**Magdalena Elisabeth Siwek**

aus Tschenstochau

Köln

Juni 2014



Referee/ Berichterstatter: **Prof. Dr. Ansgar Büschges**

**Prof. Dr. Wolfgang Walkowiak**

Tag der mündlichen Prüfung: 25.06.14



# Zusammenfassung

Neuronale Netzwerke sind mit verschiedenen spannungsgesteuerten Kalziumkanälen verknüpft, die eine Schlüsselrolle in der Entstehung von Oszillationen im Hippocampus, aber auch in der thalamokortikalen Rhythmizität einnehmen. Innerhalb einer Vielzahl von Oszillationen konnte gezeigt werden, dass der  $Ca_v2.3$  R-typ Kalziumkanal für die hippocampale Thetaaktivität maßgeblich verantwortlich ist. Thetaoszillationen im Frequenzbereich von 4-7 Hz repräsentieren ein spezifisches Aktivitätsmuster, das für kognitive Fertigkeiten, wie dem Abrufen von Gedächtnisinhalten, unerlässlich ist. Auf pharmakologischer Ebene werden zwei Subtypen von Thetaaktivität, der Atropin resistente Typ I und das Atropin sensitive Typ II Theta, differenziert. Typ II Theta wird dabei über eine durch den  $Ca_v2.3$  R-typ Kalziumkanal vermittelte, muskarinerge Signalkaskade in der hippocampalen CA1 Region generiert. Interessanterweise treten Theta Oszillationen auch während des paradoxen bzw. REM (rapid eye movement) Schlafs auf, was daraufhin deutet, dass Thetaaktivität vom zirkadianen Rhythmus abhängt. Da  $Ca_v2.3$  R-typ Kalziumkanäle ebenfalls im retikulär thalamischen Kern (RTN), der in die Schlafgenerierung eingebunden ist, exprimiert werden, kann vermutet werden, dass dem  $Ca_v2.3$  Kalziumkanal eine regulatorische Funktion beim Schlaf zukommt. Bislang konnte allerdings nicht geklärt werden, welche genaue Rolle  $Ca_v2.3$  R-typ Kalziumkanäle im thalamokortikalen Netzwerk übernehmen. Daher analysierten wir den  $Ca_v2.3$  R-typ Kalziumkanal in spontanen und pharmakologisch induzierten Schlaf von  $Ca_v2.3^{-/-}$  Mäusen und  $Ca_v2.3^{+/+}$  Kontrolltieren. Unsere Ergebnisse zeigen eine erhöhte Anzahl an Schlafübergängen sowie eine verminderte Gesamtwachdauer bei  $Ca_v2.3^{-/-}$  Mäusen und verdeutlichen folglich die tragende Rolle des  $Ca_v2.3$  R-typ Kalziumkanals in Bezug auf die Schlafmodulation.

Studien belegen, dass  $Ca_v2.3^{-/-}$  Mäuse auch Absence-Epilepsien ausbilden können, was die Rolle des  $Ca_v2.3$  R-typ Kalziumkanals in der Epileptogenese widerspiegelt. Pathologische Veränderungen in der zentralen Rhythmizität und eine damit einhergehende erhöhte Anfallswahrscheinlichkeit können unter anderem durch Akkumulation von A $\beta$  Plaques, wie sie bei der Alzheimererkrankung auftreten, gefördert werden. Dabei zeigte sich, dass in Mausmodellen der familiären Alzheimer-Demenz (FAD) erhöhte A $\beta$  Plaquebildung mit Veränderungen in der Proteinsynthese vom BACE1 Enzym ( $\beta$ -site APP cleaving enzyme 1) einhergeht. In diesem Zusammenhang ist eine gesteigerte Translation des BACE1 Enzyms unmittelbar an die

Phosphorylierung vom Serin an Position 51 des eukaryotischen Translationsinitiationsfaktors 2 Alpha (eIF2 $\alpha$ ) gebunden. Diese Tatsache wirft die Frage auf, ob eine Runterregulierung von eIF2 $\alpha$  zu einer geringeren Anfallswahrscheinlichkeit durch verminderte Plaquebildung beiträgt und somit den kognitiven Verfall in 5XFAD Mäusen verzögern kann. Dazu untersuchten wir mögliche präventive Effekte von eIF2 $\alpha$  auf die Epileptogenese, indem wir 5XFAD Mäuse mit einer eIF2 $\alpha^{S51A}$  Knock-in Line kreuzten, bei denen, durch eine Substitution von Serin durch Alanin an Position 51 bedingt, eIF2 $\alpha$  nicht mehr phosphoryliert werden kann. Unsere Ergebnisse zeigen einen limitierten präventiven Effekt von eIF2 $\alpha$  auf motorische und kognitive Defizite in 5XFAD Mäusen. Veränderungen im Hippocampus gehen mit elektrophysiologischen Befunden einher, welche nicht-konvulsive Statusformen epileptiformer Aktivität bei 5XFAD Tieren mit eIF2 $\alpha^{S51A}$  Allel belegen. Weiterhin untersuchten wir, wie sich Anfallsaktivität auf die muskarinerge Signalkaskade in 5XFAD Mäusen auswirkt. Wir stellten fest, dass eine verstärkte muskarinerge Signalkaskade sowohl zu neuronaler Dysrhythmie, aber auch zu einer Erhöhung von Atropin sensitiven Typ II Theta beiträgt, die als möglicher Kompensationsmechanismus zu einem dysbalancierten neuronalen System bei Morbus Alzheimer in Betracht gezogen werden kann.

# Abstract

Neuronal networks are strongly connected to voltage-gated  $\text{Ca}^{2+}$  channels which are key elements in mediating hippocampal oscillations and thalamocortical rhythmicity. Among different brain oscillations the  $\text{Ca}_v2.3$  R-type  $\text{Ca}^{2+}$  channel turned out to be responsible for hippocampal theta activity. Theta oscillations occurring at a frequency range of 4-7 Hz represent a specific activity pattern playing a crucial role in cognition, such as memory retrieval. Pharmacologically, theta activity can be differentiated into two different subtypes, atropine resistant type I and atropine sensitive type II. In the hippocampal CA1 region type II theta is mediated by voltage-gated  $\text{Ca}_v2.3$  R-type  $\text{Ca}^{2+}$  channels via the muscarinic signaling cascade. Interestingly, theta oscillations can also be measured during rapid eye movement (REM) sleep indicating that theta rhythms are triggered in a circadian rhythm-dependent manner. Because  $\text{Ca}_v2.3$  R-type  $\text{Ca}^{2+}$  channels are also expressed in the reticular thalamic nucleus (RTN), which is responsible for sleep initiation, it can be hypothesized that the  $\text{Ca}_v2.3$  R-type  $\text{Ca}^{2+}$  channel might be essentially involved in sleep regulation. However, the detailed functional role of  $\text{Ca}_v2.3$  R-type  $\text{Ca}^{2+}$  channels in the thalamocortical network still remains unclear. Therefore, we analyzed  $\text{Ca}_v2.3$  R-type  $\text{Ca}^{2+}$  channels in  $\text{Ca}_v2.3^{-/-}$  mice and controls in spontaneous and artificial, urethane induced sleep, using implantable video-EEG radiotelemetry. Our results illustrate an increased number of sleep transitions and decreased wake duration in  $\text{Ca}_v2.3^{+/+}$  mice, thus confirming the  $\text{Ca}_v2.3$  R-type  $\text{Ca}^{2+}$  channel to be exclusively involved sleep regulation.

Previously,  $\text{Ca}_v2.3^{-/-}$  mice were also reported to exhibit absence seizure susceptibility indicating the  $\text{Ca}_v2.3$  R-type  $\text{Ca}^{2+}$  channel to be related to epileptogenesis. Alterations in brain rhythmicity as well as seizure susceptibility can be promoted by  $\text{A}\beta$  plaque accumulation as occurring in Alzheimer's Disease (AD). Recent studies in mouse models of familial AD (FAD) depict changes in protein synthesis of  $\beta$ -site APP cleaving enzyme 1 (BACE1) to be ultimately responsible for increased generation of  $\text{A}\beta$  plaques. In this regard elevated translation of BACE1 has been associated with increased phosphorylation of the eukaryotic translation initiation factor 2 alpha (eIF2 $\alpha$ ) at serine 51. This fact leads to the question, if decreased levels of phosphorylated eIF2 $\alpha$  could prevent 5xFAD mice from exhibiting enhanced amyloidogenesis and increased amount of seizure activity and therefore delaying cognitive decline. Hence, we analyzed possible preventative effects of eIF2 $\alpha$  on epileptogenesis in Alzheimer's disease by

crossing 5xFAD mice with an eIF2 $\alpha$ <sup>S51A</sup> knock-in mouse line, in which eIF2 $\alpha$  cannot be phosphorylated on the mutant allele according to substitution of serine by alanine at position 51. Our results depict eIF2 $\alpha$ <sup>S51A</sup> to have a limited rescue effect on motor and cognitive deficits in 5XFAD mice. Hippocampal alterations were in line with electrophysiological findings depicting non-convulsive seizure activity in 5XFAD mice carrying the eIF2 $\alpha$ <sup>S51A</sup> allele. Furthermore, we investigated the effects of seizure activity on the muscarinic signaling cascade in the 5XFAD mice. Our results demonstrate that enhanced muscarinic signalling is directly linked to neuronal dysrhythmia and increased amount of atropine sensitive type II theta in 5XFAD mice that might be understood as a compensatory mechanism according to an imbalanced neuronal system in AD.



## Abbreviations

ACE	nucleus of central amygdala
A $\beta$	amyloid- $\beta$
AD	Alzheimer's disease
AFC	absolute fold change
ATF4	activating transcription factor 4
APP	amyloid precursor protein
BACE1	$\beta$ -site APP cleaving enzyme 1
ChAT	rabbit anti-choline acetyltransferase
cGMP	guanosine cyclic monophosphate
CNG	cyclic nucleotide-gated ion channel
CTF	COOH-terminal fragment
DAB	diaminobenzidine
DAG	diacylglycerol
EEG	electroencephalogram
elf2 $\alpha$	eukaryotic translation initiation factor 2 $\alpha$
FAD	familial Alzheimer's disease
GABA <sub>A</sub>	gamma-aminobutyric acid
hAPP	human amyloid precursor protein
HCN	hyperpolarization-activated, cyclic nucleotide-gated cation (channels)
HVA	high-voltage activated
IP3	inositol triphosphate
KO	knock-out
LIA	large irregular activity
LTCS	low-threshold Ca <sup>2+</sup> spike
LTP	long-term potentiation
LVA	low-voltage activated
M1	primary motor cortex
M1/M3	muscarinic M1/M3 receptor
mGLUR1	metabotropic glutamate receptors group I
MS-DBB	medial septum/diagonal band of Broca
NFT	neurofibrillary tangles
NREM	non-rapid eye movement (sleep)

PKC $\delta$	protein kinase C delta type
PLC $\beta$ 1	phospholipase C beta type
PSEN1	presenilin 1
PS	paradoxical sleep
PVDF	polyvinylidene difluoride
qPCR	quantitative Real-time PCR
REM	rapid-eye movement (sleep)
RTN	reticular thalamic nucleus
sAHP	slow afterhyperpolarisation
SK2	small-conductance Ca <sup>2+</sup> -activated K <sup>+</sup> channel type 2
SWD	spike-wave discharge
SWS	slow-wave sleep
TBS	tris-buffered saline
TC	thalamocortical system
TLE	temporal lobe epilepsy
VDB	diagonal band of Broca
VGCC	voltage-gated Ca <sup>2+</sup> channels
WT	wild-type

# Table of Contents

<b>1. Introduction</b> .....	13
1.1 Rhythms of the Brain-Molecular Dissection of Theta Activity .....	13
1.2 The Ca <sub>v</sub> 2.3 R-type Ca <sup>2+</sup> Channel in Rodent Sleep Architecture .....	15
1.3 The functional Role of Theta Activity in Alzheimer`s Disease .....	16
1.4 Aim of the study .....	19
<b>2. Published Studies</b> .....	21
2.1 The Ca <sub>v</sub> 2.3 R-Type Voltage-Gated Ca <sup>2+</sup> Channel in Mouse Sleep Architecture .....	21
2.2 Limited effects of an eIF2 $\alpha$ <sup>S51A</sup> allele on neurological impairments in the 5XFAD mouse model of Alzheimer`s disease .....	49
2.3 Altered muscarinic signalling in 5XFAD mice – Bridging the gap between seizure activity, theta oscillations and Alzheimer`s disease .....	77
<b>3. Discussion</b> .....	111
<b>4. Conclusion</b> .....	117
<b>5. Bibliography</b> .....	119
<b>6. Acknowledgments</b> .....	144
<b>7. Author`s Contribution to Publications</b> .....	145
<b>8. Erklärung</b> .....	147
<b>9. Teilpublikationen</b> .....	148
<b>10. Curriculum Vitae</b> .....	149



# 1. Introduction

## 1.1 Rhythms of the Brain-Molecular Dissection of Theta Activity

In our everyday life communication and interaction with our fellow men seems to be self-evidently indispensable. However, for living and adapting to a constantly changing environment, we rely on the ability to process information from distinct physical dimensions simultaneously. In other words, mastering the complex processing of ongoing behaviour requires high efficiency of neuronal networks. Over the recent years, investigators were making an effort to enrich our knowledge of how populations of neurons contribute to cognitive functions by analysing highly synchronized activity pattern, so-called oscillations. In this regard, oscillations provide the electrophysiological mechanism for coordination of brain regions by streaming the activity of neuronal ensembles to intentional behaviour. However, the detailed mechanisms still remain poorly understood. Recently, it could be shown that the hippocampus plays an important role in central rhythmicity. Being a part of the limbic system combining emotional and spatial information (Bird and Burgess, 2008), the hippocampus exhibits different classes of oscillations, which are connected to particular cognitive states (Buzsaki et al., 1983; Colgin, 2013). Thereby, large irregular activity (LIA) containing sharp waves, marks behavioural automatisms on the one hand. On the other hand the hippocampus exhibits rhythmic pattern of high amplitude emerging as local field potentials from the the hippocampal CA3 and the stratum lacunosum-moleculare of the CA1 region occurring at a frequency range of 4-7 Hz (Buzsaki, 2002; Kahana et al., 1999; Vanderwolf, 1969). These hippocampal theta oscillations are strongly involved in memory consolidation during rapid eye movement sleep (REM), information encoding and exploratory behaviour (Colgin, 2013; Hangya et al., 2009; Kahana et al., 1999; Montgomery and Buzsaki, 2007). Consequently, they can be seen as the “online state” of the hippocampus. Theta activity and can be pharmacologically evoked by stimulation of cholinergic und glutamanergic pathways. According to the sensitivity to certain drug types, theta oscillations can be divided into two different subgroups, type I and type II theta that are also related to certain behavioural modes of the hippocampus (Buzsaki, 2002). Thereby, type I theta or atropine resistant theta requires activation through metabotropic glutamate receptors group I (mGluR1) and remains pharmacologically unaffected to anticholinergic drugs like atropine (Buzsaki, 2002). Atropine resistant theta is physiologically present during locomotion and REM

sleep (Vanderwolf, 1969; Winson, 1974). In contrast, type II theta or atropine sensitive theta occurs during immobility and can be experimentally induced by urethane or specific muscarinic agonists, such as pilocarpine, arecoline or oxotremorine (Buzsaki, 2002). At first glance the pharmacological dissection of theta activity might seem to be trivial. However, it indicates that theta oscillations can be entrained by different excitatory sources in absence of either cholinergic or glutamatergic inputs. In this regard, it has been a question of debate whether hippocampal theta genesis arrives from extrinsic input from the medial septum/diagonal band of Broca (MS-DBB) or can be intrinsically elicited by horizontal cell-interneuron interconnectivity via hyperpolarization-activated and cyclic nucleotide-gated nonselective cation (HCN) channels (Goutagny et al., 2008; Hangya et al., 2009; Manseau et al., 2008). HCN channels interact together with small-conductance  $\text{Ca}^{2+}$ -activated  $\text{K}^+$  channel type 2 (SK2) channels as a functional unit and are responsible for a reprimed  $\text{Ca}^{2+}$  current mediated burst cycle. Furthermore, preliminary studies demonstrate that on the molecular level theta oscillations are mediated by voltage-gated  $\text{Ca}^{2+}$  channels, e.g.  $\text{Ca}_v2.3$  R-type  $\text{Ca}^{2+}$  channels via intracellular muscarinic cascades (Shin et al., 2006; Shin, 2006). Activation of Gαq/11 coupled muscarinic M1/M3 receptors is capable to enhance R-type currents in pyramidal neurons of rat hippocampal CA1 region via the generation of diacylglycerol (DAG) and inositol triphosphate (IP3) followed by phospholipase C beta1 (PLCβ1) and phosphokinase C delta (PKCδ) activation (Tai et al., 2006) while leaving T-type  $\text{Ca}^{2+}$  currents unaffected. These findings were recently supported by the fact that deletion of PLCβ1 leads to absence of type II theta (Shin et al., 2005) underlying the functional importance of  $\text{Ca}_v2.3$   $\text{Ca}^{2+}$  channels and the muscarinic pathway in theta genesis. Although the final signaling pathway of still remains unrevealed, it is not surprising that after muscarinic stimulation enhanced intracellular cytosolic  $\text{Ca}^{2+}$  levels mediated by  $\text{Ca}_v2.3$  R-type  $\text{Ca}^{2+}$  channels can also implicate the activation of CNG channels through increased guanosine cyclic monophosphate (cGMP) levels. Consequently, CNG channels contribute to prolonged membrane potentials with pronounced bursting, that is responsible for exhibition of epileptiform activity (Tai et al., 2006). Hence,  $\text{Ca}_v2.3$  R-type  $\text{Ca}^{2+}$  currents followed by the activation of muscarinic receptors can elicit both, theta as well as seizure activity. Due to this fact, it is indispensable to take secondary effects and functions of the  $\text{Ca}_v2.3$  R-type  $\text{Ca}^{2+}$  channel into account to provide its comprehensive role in neuronal network functioning sufficiently.

## 1.2 The $\text{Ca}_v2.3$ R-type $\text{Ca}^{2+}$ Channel in Rodent Sleep Architecture

To get a global view of the functional role of the voltage-gated calcium channels it is necessary to look closer at intrinsic mechanisms of single neurons and propensity of coupled neuronal networks exhibiting coherent oscillatory states at a variety of spatial extent and frequency. Modulatory processes within neuronal circuits indicate dynamical changes of oscillations providing clues of one or many entire neuronal systems at particular cognitive states. Indeed, it was recently proven that  $\text{Ca}_v2.3$  R-type  $\text{Ca}^{2+}$  channels are key regulators in neuronal excitability by regulating internal  $\text{Ca}^{2+}$  levels (Tao et al., 2008). Increase of internal  $\text{Ca}^{2+}$  levels finally results in afterdepolarisations (Kuzmiski et al., 2005; Metz et al., 2005) and long-lasting plateau potentials via activation of Cyclic nucleotide-gated ion channels (CNG) (Kuzmiski and MacVicar, 2001) that can trigger absence slow wave discharges (SWDs) in the hippocampus (Lakaye et al., 2002). The extraordinary role of  $\text{Ca}_v2.3$  R-type  $\text{Ca}^{2+}$  channels are furthermore supported by the observation that administration of carbachol leads to an enhanced E/R type dependent spiking of CA1 neurons while other channel activity is depressed (Gahwiler and Brown, 1987; Toselli et al., 1989).  $\text{Ca}_v2.3$  R-type  $\text{Ca}^{2+}$  channels are dominantly expressed in dendrites and soma of CA1 neurons but can also be found in the thalamocortical network (Day et al., 1996; Westenbroek et al., 1995). Taking the fact into consideration that  $\text{Ca}_v2.3$  R-type  $\text{Ca}^{2+}$  channels are differentially distributed throughout neuronal entities but are always regulated via muscarinic receptors as a biochemical unit, it is fear to assume that  $\text{Ca}_v2.3$  R-type  $\text{Ca}^{2+}$  channels do not only shape up as key players in hippocampal seizure propagation and epileptogenesis (Lakaye et al., 2002) but might be also crucially involved in mediating thalamocortical rhythmicity as well. By simplifying thalamic rhythmicity, the thalamocortical system (TC) is composed of two different classes of neuronal population, the Reticular thalamic nucleus (RTN) neurons and relay cells, which are capable of switching between different modes of action while receiving input from cortical regions and extrathalamic structures. During high stages of vigilance thalamic neurons exhibit the tonic mode of action at slightly depolarised membrane potentials. Thereby, tonic neuronal activity within thalamic relay cells is due to activating input from deeper brainstem structures and simultaneous inhibition of RTN neurons. These processing mechanisms of peripheral information are finally encoded as action potentials to the cortex during wake state. With decreased input from extrathalamocortical structures sensory gating is abolished and both, relay and RTN

neurons, shift to a rebound burst firing mode of action. On a cellular level different stages of vigilance are linked to activation of specific  $\text{Ca}^{2+}$  channels. Previously, it was shown, that low-voltage activated (LVA)  $\text{Ca}_v3$  T-type  $\text{Ca}^{2+}$  channels which are expressed in thalamic relay cells have been related to thalamic rebound burst firing and the generation of non-rapid eye movement sleep (NREM sleep) (Contreras, 2006). In contrast, burst activity is accomplished by  $\text{Ca}_v2.3$   $\text{Ca}^{2+}$  channels that are highly expressed in the RTN.  $\text{Ca}_v2.3$  mediated  $\text{Ca}^{2+}$  influx into RTN neurons triggers potassium release through activation of a small conductance  $\text{Ca}^{2+}$ -activated potassium channels (SK2). Consequently, SK-mediated K currents repolarize RTN neurons causing repriming of LVA T-type  $\text{Ca}^{2+}$  channels and activation of HCN channels. As a result of the subsequent membrane depolarisation, a low-threshold  $\text{Ca}^{2+}$  spike (LTCS) is generated leading to  $\text{Ca}_v2.3$   $\text{Ca}^{2+}$  channel activation that initiates SK channel opening in a cyclic manner. By the periodic activation of the individual ion channel entities, burst cycles in the RTN are mediated resulting in SWS delta oscillations (Zaman et al., 2011). In accordance to these findings, it was also reported that  $\text{Ca}_v2.3^{-/-}$  mice exhibit absence seizure susceptibility and altered spike-wave discharges by effecting thalamocortical hyperoscillations similar to seizure propagation in the hippocampus (Weiergraber et al., 2008). Hence, it can be strongly suggested, that  $\text{Ca}_v2.3$  R-type  $\text{Ca}^{2+}$  channels are fundamentally pertinent to thalamocortical rhythmicity

### **1.3 The functional Role of Theta Activity in Alzheimer`s Disease**

How can oscillations contribute to a better understanding of cognition and how might they serve as potential biomarkers for the diagnosis of cognitive decline even before the onset of neurodegeneration? To answer these questions it is necessary to investigate the changes and modifications of oscillatory activity, particularly of theta rhythms, as well as their potential relevance to progressive pathophysiology of Alzheimer`s Disease (AD). AD is the most common, irreversible form of dementia that is associated with extensive synaptic loss and disruption of learning and memory skills (Selkoe and Schenk, 2003). Histologically, it is characterized by amyloid- $\beta$  plaques ( $\text{A}\beta$  plaques) and neurofibrillary tangles (NFT) typically occurring in specific brain regions like the hippocampus (Ashe, 2001). Nowadays, it is believed that soluble  $\text{A}\beta$  assemblies which contribute to neurotoxic plaque formation mediating negative effects on learning and memory. However, the whole mechanism behind the disease still remains unclear. Atropine sensitive type II theta is liable to age-dependent neuronal degeneration



resulting in structural reorganization of networks and cognitive decline. Although type II theta is consistently decreased at old age, it could be shown that activation of the muscarinic pathway is able to retard neuronal disruption as a result overexpressed amyloid beta formation in AD (Buttini et al., 2002; Kar et al., 2004; Kar and Quirion, 2004). Hence, theta activity and its underlying molecular structures can contribute to preservation of physiological network functioning. In this regard, transgenic mouse models carrying the mutated human amyloid precursor protein (APP) and presenilin1 (PSEN1) gene, recapitulate a huge range of AD-like phenotypes, attempting to promote our understanding of hippocampal function. In this regard, 5XFAD mice (Tg6799 line, Jackson Laboratories) carry five familial AD mutations, which at high levels of expression have been proved to show the most aggressive phenotype. Therefore 5XFAD mice are widely used to especially mimic histological and cognitive hallmarks of early-onset AD. 5XFAD mice display accumulation of intraneuronal A $\beta$ 42 already at the age of 1.5 months followed by massive neuronal loss (Moon et al., 2012; Oakley et al., 2006). Synaptic degeneration and spatial learning deficits can be detected by around 4 months of age caused by rapidly increasing amount of plaques which spread throughout the hippocampal formation and finally reaching and disrupting cortical areas (Kimura et al., 2007; Oakley et al., 2006). Recently, it was illustrated that impaired LTP in 5XFAD mice (Crouzin et al., 2013) is linked to the expression of the protein synthesis of  $\beta$ -site APP cleaving enzyme 1 (BACE1) that is ultimately required for the generation of A $\beta$  plaques by cleaving the APP to produce A $\beta$ 42 peptides (Ohno et al., 2006; Zhao et al., 2007). Concerning this, it has been a question of debate how disruption of the hippocampal network caused by A $\beta$  plaque accumulations can elicit pharmacologically unprovoked seizures as being present in patients with AD at high prevalence in comparison to elderly individuals (Mendez and Lim, 2003). Although pharmacokinetic changes in neuronal networks occur with aging and may contribute to the incidence of epilepsy in AD, previous studies clearly depict that high levels of A $\beta$  are sufficient to elicit seizures in mice expressing human APP (hAPP) (Palop et al., 2007; Palop and Mucke, 2009; Palop and Mucke, 2010). Furthermore, it could be demonstrated that enhanced translation of BACE1 protease causes increased numbers of A $\beta$  plaques that lead to a reorganisation of neuronal networks, finally resulting in an imbalance of excitation and inhibition. This imbalance can produce hyperexcitability states in the hippocampus and finally facilitate seizures (Metz et al., 2005). Hence, 5XFAD mouse model exhibit seizure like activity. Because the translation of BACE1 is directly linked

to the phosphorylation of eukaryotic translation initiation factor 2 alpha (eIF2 $\alpha$ ), down-regulation of this factor could lead to delayed cognitive decline in AD and preserve 5XFAD mice from developing epileptiform activity. Interestingly, cognitive deficits of these models can be improved by the reduction of endogenous tau protein (Palop and Mucke, 2009; Roberson et al., 2007). In this regard, previous studies give also evidence that amelioration of cognitive skills can be furthermore achieved by theta activity. By comparing wakefulness and REM sleep in which seizures are less frequent to other functional conditions of the hippocampus, it becomes obvious that theta activity can preserve neuronal networks from increased seizing (Colom et al., 2005; Colom, 2006; Miller et al., 1994). The relationship between theta activity and the occurrence of seizures in AD can be explained by the activation of cholinergic and glutaminergic pathways that are required for both oscillation pattern (Gutierrez-Lerma et al., 2013; Palhalmi et al., 2004; Reich et al., 2005). Unlike the previous opinion that A $\beta$  peptides lead to network disruption and changes in theta activity through a general cellular mechanism, it could be shown that type I and II theta are differentially altered by certain A $\beta$  peptide species providing evidence for a specific cellular mechanism (Gutierrez-Lerma et al., 2013) by which theta activity can be shaped. Alterations in theta rhythmicity can either result in increased (Babiloni et al., 2007; Blanchet, 2003; Cummins et al., 2008; Pena-Ortega and Bernal-Pedraza, 2012) or reduced (Cummins et al., 2008) amount of theta activity according to the present stage of cognitive decline in specific mouse models of AD. For this reason it is still challenging to link changes in theta activity to the dynamic neurobiology of AD. Furthermore, it could be also demonstrated that over-production of A $\beta$  does not necessarily need to be related to over-excitation of the hippocampal network. Recent studies by Goutagny et al., 2013 demonstrated that slight changes in the hippocampal theta activity might occur much earlier than recently suggested. Altered theta rhythmicity can even become obvious before histological hallmarks of AD like an advanced manifestation of A $\beta$  accumulation are fully apparent (Goutagny et al., 2013; Goutagny and Krantic, 2013). These findings could facilitate our understanding of theta oscillations as suitable predictors for especially early-onset familial AD in future.

#### 1.4. Aim of the study

The present thesis was aimed to dissect the functional role of the voltage-gated  $\text{Ca}_v2.3$  R-type  $\text{Ca}^{2+}$  channel in sleep architecture and seizure susceptibility in the 5XFAD mouse model of familial AD.

The first study was aimed to declare how  $\text{Ca}_v2.3$  R-type  $\text{Ca}^{2+}$  channels are involved in regulating thalamocortical circuits, thus controlling vigilance and mediating SWS. Motivated by previous results showing that  $\text{Ca}_v2.3$  R-type  $\text{Ca}^{2+}$  channels are responsible for initiation of thalamic rebound burst firing as required for SWS, we investigated  $\text{Ca}_v2.3$  R-type  $\text{Ca}^{2+}$  channels in spontaneous and artificial, urethane induced sleep in  $\text{Ca}_v2.3^{+/+}$  mice and  $\text{Ca}_v2.3^{-/-}$  mice using implantable video-EEG radiotelemetry. By performing time-frequency analysis, we determine alterations in sleep architecture under physiological conditions and sleep deprivation. Furthermore, we used quantitative Realtime PCR to depict any possible changes in thalamic  $\text{Ca}^{2+}$  channel expression.

In the second study we investigated the functional role of non-phosphorylated eIF2 $\alpha$  allele (eIF2 $\alpha^{S51A}$ ) and its possible preventative effect on AD progression and epileptiform activity in 5XFAD mice. Phosphorylated form of eIF2 $\alpha$  is closely related to the BACE1 synthesis which is responsible for A $\beta$  plaque formation, finally leading to elevated seizure susceptibility. Here, we combined electrophysiological together with molecular and behavioural approaches in 5XFAD, 5XFAD- eIF2 $\alpha^{S51A/+}$ , eIF2 $\alpha^{S51A/+}$  and wild type mice to verify, if eIF2 $\alpha^{S51A}$  could improve cognitive performance and delay cognitive decline.

In the third study we attempt to illustrate the functional interdependence between hippocampal theta activity and seizure susceptibility in the 5XFAD mouse model. To answer the question in what extent hippocampal theta oscillations are altered and how seizure activity might contribute to enhanced cognitive decline, we investigated transcriptional alterations in relation to the EEG phenotype of 5XFAD mice.



## 2. Publications

### 2.1 The $\text{Ca}_v2.3$ R-Type Voltage-Gated $\text{Ca}^{2+}$ Channel in Mouse Sleep Architecture

Magdalena Elisabeth Siwek,<sup>1,\*</sup>, Ralf Müller,<sup>2,\*</sup>, Christina Henseler<sup>1</sup>, Karl Broich<sup>1</sup>; Anna Papazoglou,<sup>1</sup>; Marco Weiergräber,<sup>1</sup>

<sup>1</sup>Federal Institute for Drugs and Medical Devices (BfArM), Kurt-Georg-Kiesinger-Allee 3, 53175 Bonn, Germany; <sup>2</sup>Department of Psychiatry and Psychotherapy, University of Cologne, Kerpener Str. 62, 50937 Köln, Germany.

\*These authors contributed equally to the work

**Submitted: April, 2013; Accepted for Publication: December, 2013.**

**Study Objectives:** Voltage-gated  $\text{Ca}^{2+}$  channels (VGCCs) are key elements in mediating thalamocortical rhythmicity. Low-voltage activated (LVA)  $\text{Ca}_v3$  T-type  $\text{Ca}^{2+}$  channels have been related to thalamic rebound burst firing and to generation of non-rapid eye movement (NREM) sleep. High-voltage activated (HVA)  $\text{Ca}_v1$  L-type  $\text{Ca}^{2+}$  channels, on the opposite, favor the tonic mode of action associated with higher levels of vigilance. However, the role of the HVA Non-L-type  $\text{Ca}_v2.3$   $\text{Ca}^{2+}$  channels, which are predominately expressed in the reticular thalamic nucleus (RTN), still remains unclear. Recently,  $\text{Ca}_v2.3^{-/-}$  mice were reported to exhibit altered spike-wave discharge / absence seizure susceptibility supported by the observation that  $\text{Ca}_v2.3$  mediated  $\text{Ca}^{2+}$  influx into RTN neurons can trigger small-conductance  $\text{Ca}^{2+}$  activated  $\text{K}^+$ -channel type 2 (SK2) currents capable of maintaining thalamic burst activity. Based on these studies we investigated the role of  $\text{Ca}_v2.3$  R-type  $\text{Ca}^{2+}$  channels in rodent sleep.

**Methods:** The role of  $\text{Ca}_v2.3$   $\text{Ca}^{2+}$  channels was analyzed in  $\text{Ca}_v2.3^{-/-}$  mice and controls in both spontaneous and artificial, urethane induced sleep, using implantable video-EEG radiotelemetry. Data were analyzed for alterations in sleep architecture using sleep staging software and time-frequency analysis.

**Results:**  $Ca_v2.3$  deficient mice exhibited reduced wake duration and increased slow-wave sleep (SWS). Whereas mean sleep stage durations remained unchanged, the total number of slow-wave sleep epochs was increased in  $Ca_v2.3^{-/-}$  mice. Additional changes were observed for sleep stage transitions and EEG amplitudes. Furthermore, urethane-induced slow-wave sleep mimicked spontaneous sleep results obtained from  $Ca_v2.3$  deficient mice. Quantitative Real-time PCR did not reveal changes in thalamic  $Ca_v3$  T-type  $Ca^{2+}$  channel expression. The detailed mechanisms of SWS increase in  $Ca_v2.3^{-/-}$  mice remain to be determined.

**Conclusions:**  $Ca_v2.3$  R-type  $Ca^{2+}$  channels in the thalamocortical loop and extrathalamocortical circuitries substantially regulate rodent sleep architecture thus representing a novel potential target for pharmacological treatment of sleep disorders in the future.

**Key words:** rapid eye movement (REM), slow-wave sleep (SWS), thalamocortical circuitry, vigilance

## Introduction

Voltage-gated  $\text{Ca}^{2+}$  channels (VGCCs) play key roles in numerous physiological processes, including excitation-contraction and excitation-secretion coupling, neurotransmission and regulation of gene expression (Bers and Weber, 2002; Catterall, 2011; Hofmann et al., 1999; Yang and Berggren, 2005). Both high-voltage activated (HVA) L-type and low-voltage-activated (LVA) T-type  $\text{Ca}^{2+}$  channels were reported to be involved in the regulation of mammalian sleep, due to their functional involvement in thalamocortical and extrathalamocortical rhythmicity (Catterall et al., 2003; Catterall et al., 2005; Jones, 2002; Lopez-Bendito and Molnar, 2003). Thalamocortical relay neurons and reticular thalamic nucleus (RTN) cells harbour the capability to switch between different functional modes, i.e. the tonic, intermediate and burst mode of action. The depolarisation of thalamic relay cells, at least in part, is due to the activating input of deeper brainstem structures, e.g. the reticular formation, and concomitant disinhibition of RTN neurons that project to ventrobasal thalamic relay cells. The tonic firing mode is characteristic of stages of high vigilance. With decreasing activity from deeper activating brain regions, thalamic relay cells re- and hyperpolarize. They pass through the intermediate mode and finally exhibit the rebound burst firing mode of action (Beenhakker and Huguenard, 2009; Llinas and Steriade, 2006; Steriade, 2005). A complex armamentarium of voltage- and ligand-gated ion channels including LVA  $\text{Ca}_v3.1$ - $\text{Ca}_v3.3$  T-type  $\text{Ca}^{2+}$  channels, hyperpolarization and cyclic-nucleotide gated, non-specific cation channels, i.e. HCN2 and HCN4, can trigger low-threshold calcium spikes (LTCSs) with superimposed bursts of conventional  $\text{Na}^+/\text{K}^+$  action potentials (Llinas and Steriade, 2006). Termination of this cycle is mediated by both voltage- and  $\text{Ca}^{2+}$  activated current entries, e.g.  $I_A$  mediated and  $I_{k(\text{Ca})}$ . Rebound burst firing in the thalamocortical circuitry is typical for stages of low vigilance, including slow-wave sleep (SWS). In addition, enhanced oscillatory discharges resulting in rebound burst firing of thalamic relay neurons and RTN cells were shown to play a crucial role in the etiopathogenesis of absence epilepsy (Shin et al., 2006; Shin, 2006). Voltage-gated  $\text{Ca}^{2+}$  channels turned out to be of major relevance in the etiopathogenesis of absence epilepsy and the physiology of sleep due to their unique electrophysiological properties and cellular distribution (Anderson et al., 2005; Astori et al., 2011; Cheong and Shin, 2013; Kim et al., 2001; Lee et al., 2004; Lee and Shin, 2007; Petrenko et al., 2007; Siwek et al., 2012; Talley et al., 2000). Interestingly, recent studies demonstrate that the HVA

Non-L-type  $\text{Ca}_v2.3 \text{ Ca}^{2+}$  channel plays an important role in thalamocortical rhythmicity (Talley et al., 2000; Weiergraber et al., 2006; Weiergraber et al., 2008; Zaman et al., 2011).  $\text{Ca}_v2.3$  R-type  $\text{Ca}^{2+}$  channels are expressed in GABAergic interneurons of the cortex and the RTN (Talley et al., 2000; Weiergraber et al., 2006; Weiergraber et al., 2008). Initial analysis of absence seizure susceptibility in  $\text{Ca}_v2.3^{-/-}$  and control animals revealed that  $\text{Ca}_v2.3 \text{ Ca}^{2+}$  channel affects thalamocortical hyperoscillation and absence seizure architecture (Talley et al., 2000; Weiergraber et al., 2008). In accordance to reports on the absence-preventive effect of Bay K8644- enhanced HVA  $\text{Ca}^{2+}$  current, we speculated that HVA Non-L-type  $\text{Ca}_v2.3$  channels might also favor the tonic mode of action (Talley et al., 2000; Weiergraber et al., 2008). Lately, the role of  $\text{Ca}_v2.3$  R-type  $\text{Ca}^{2+}$  channels in thalamocortical rhythmicity was elaborated in detail on the thalamic level by Zaman et al. (Zaman et al., 2011) using a combination of in-vitro and in-vivo methods. Injection of a hyperpolarizing current in a brain slice approach was capable of triggering a low-threshold  $\text{Ca}^{2+}$  spike with superimposed  $\text{Na}^+$  bursts in RTN neurons from  $\text{Ca}_v2.3^{-/-}$  mice. Interestingly, subsequent oscillatory burst charges were strongly suppressed and slow afterhyperpolarisations (sAHP) reduced. About 51% of HVA  $\text{Ca}^{2+}$  current in RTN neurons turned out to be SNX-482 sensitive and could be dedicated to  $\text{Ca}_v2.3$  R-type  $\text{Ca}^{2+}$  channels. Furthermore,  $\text{Ca}_v2.3$  mediated  $\text{Ca}^{2+}$  influx was shown to interfere with voltage-insensitive SK2 channels that contribute to the generation of  $\text{Ca}^{2+}$ -dependent sAHP. Zaman et al. (Zaman et al., 2011) argued that T-type  $\text{Ca}^{2+}$  channels per se are not sufficient to maintain  $\text{Ca}^{2+}$  levels that can trigger sAHP, the latter however is a prerequisite for repriming T-type  $\text{Ca}^{2+}$  channels and sustained rebound bursting. Consequently,  $\text{Ca}_v2.3^{-/-}$  mice display reduced RTN oscillatory activity and reduced absence seizure susceptibility. Hence, we speculated that  $\text{Ca}_v2.3$  R-type  $\text{Ca}^{2+}$  channels might also affect thalamocortical network oscillation relevant for SWS and overall sleep architecture. To test this hypothesis, we performed analysis of spontaneous sleep, sleep deprivation and pharmacologically induced sleep in  $\text{Ca}_v2.3^{-/-}$  mice and controls using implantable video-EEG radiotelemetry. Our data provide evidence that  $\text{Ca}_v2.3$  R-type channels are functionally relevant for the generation of SWS and modulation of sleep architecture in mice.



## Materials and Methods

### *Study animals*

$Ca_v2.3^{+/-}$  embryos (kindly provided by Richard J. Miller, Department of Neurobiology Pharmacology, and Physiology, The University of Chicago, Chicago (Wilson et al., 2000) were rederived with C57BL/6J mice and maintained with random intra-strain mating obtaining all genotypes. Five  $Ca_v2.3^{+/+}$  (mean body weight:  $27.58 \pm 0.98$  g, mean age:  $13.49 \pm 0.51$  wks, all controls) and five  $Ca_v2.3^{-/-}$  mice (mean body weight:  $31.98 \pm 0.63$  g, mean age:  $17.74 \pm 0.83$  wks, all ♂) have been used for spontaneous and drug-induced sleep analysis. Three  $Ca_v2.3^{+/+}$  (mean body weight:  $29.50 \pm 0.66$  g, mean age:  $13.60 \pm 1.17$  wks, all controls) and three  $Ca_v2.3^{-/-}$  mice (mean body weight:  $31.80 \pm 1.49$  g, mean age:  $12.60 \pm 0.19$  wks, all ♂) were used for sleep deprivation experiments. All mice were housed in groups of 3-4 in clear Macrolon cages type II with ad libitum access to drinking water and standard food pellets. Using ventilated cabinets (Model 9AV125P, Techniplast, Germany), mice were maintained at a temperature of  $21 \pm 2$  °C, 50 – 60% relative humidity, and on a conventional 12 hrs light/dark cycle with the light cycle beginning at 5:00 AM for spontaneous and drug-induced sleep studies. For sleep deprivation experiments a 12 hrs light/dark cycle with the light cycle starting at 8:00 AM was implemented. The animals were strictly adapted to this circadian pattern for 14 days preceding subsequent experimentation. All animal procedures were performed according to guidelines of the German Council on Animal Care and all protocols were approved by the local institutional and national committee on animal care.

### *Radiotelemetric EEG electrode implantation and EEG recordings*

Mice were anesthetized using ketamine/xylazine (100/10 mg/kg ip.) and the radiotelemetry transmitter (TL11M2-F20-EET 2-channel transmitter, Data Science International (DSI), specifications: weight 3.9 g, volume 1.9 cc, input voltage range  $\pm 1.25$  mV, channel bandwidth 1 - 50 Hz) was implanted into a subcutaneous pouch on the back of the animals. The differential EEG electrode was stereotaxically positioned using a computerized 3D stereotaxic StereoDrive<sup>®</sup> (Neurostar, Germany) at the following coordinates: (+)-lead: bregma, -1.5 mm; mediolateral, -3.0 mm (right hemisphere); dorsoventral, 0.0 mm (target region: SB1 barrel field cortex). The reference electrode, i.e. (-)-lead was positioned on the cerebellar cortex: bregma, -6.0

mm; mediolateral, 0.0 mm; dorsoventral, 0.0 mm (**Supplemental Fig. 1**). Electrodes were fixed using glas ionomer cement and the scalp was closed using over and over sutures (Ethilon, 6-0). Electrodes of the second transmitter channel were fixed on the nuchal muscle at a distance of 5 mm and used for EMG recording (**Supplemental Fig. 1**). A detailed description of the procedure is given in Weiergräber et al., 2005. For postoperative pain management animals were administered carprofen (5 mg/kg sc.). Animals were allowed to recover for 10 days prior to subsequent recordings. This recovery period is based on the observation that 10 days post-surgery no difference in physiological parameters between transmitter implanted, non-implanted and sham-operated animals could be detected (Kramer and Kinter, 2003).

### ***Spontaneous sleep recordings***

Following a 10 day recovery period, video-EEGs were recorded 48 hrs continuously using the Dataquest ART 4.2 software (DSI) at a sampling rate of 500 Hz with no a priori filter cut-off. For detailed evaluation of sleep architecture, radiotelemetric EEG data were processed using the Neuroscore 2.1 automated sleep scoring module (DSI).

### ***Sleep deprivation***

Following a 10 day recovery period after transmitter implantation, mice were sleep deprived for 6 hrs starting at 8:00 AM till 2:00 PM. During sleep deprivation period animals were aroused by tapping on the cage and applying tactile stimuli, i.e. gently touching them with a soft brush, for 5 min at an interval of 30 min (Patti et al., 2010). Video-EEGs were recorded prior to, during and post sleep deprivation using the Dataquest ART 4.2 software (DSI) at a sampling rate of 500 Hz with no a priori filter cut-off. For detailed evaluation of sleep architecture, radiotelemetric EEG data were processed using the Neuroscore 2.1 automated sleep scoring module (DSI).

### ***Drugs und pharmacological injection experiments***

Urethane was purchased from Sigma (Germany) and freshly dissolved in 0.9% NaCl prior to the injection.  $Ca_v2.3^{+/+}$  and  $Ca_v2.3^{-/-}$  mice were injected 800 mg/kg body weight ip. at day 13 post transmitter implantation to pharmacologically induce slow-wave sleep. EEGs were recorded and analyzed for 8 hrs after urethane injection.

### ***Analysis of sleep architecture***

Sleep analyses and calculations were performed using Neuroscore 2.1 rodent sleep scoring software (DSI). Three vigilance states, i.e. the wake state (quiet and active), the non-rapid eye movement (NREM) sleep including slow wave sleep (SWS) 1 and SWS 2 and rapid eye movement (REM) sleep (paradoxical sleep, PS) were determined for 10 s epochs. Recording segments containing EEG or EMG artefacts were automatically excluded from analysis. The EMG threshold as an important setting of the automated sleep scoring software was adapted based on the individual level of ECG contamination in the EMG recording. EEG power spectra were computed for 10 s epochs using fast Fourier transformation (sampling rate 250 Hz, Hamming window) and analyzed for selected frequency bands (delta: 0.5 - 4 Hz, theta: 4 - 8 Hz, alpha: 8 - 12 Hz, beta 12 - 24 Hz and gamma 24 - 50 Hz).

### ***EEG data analysis***

Complex EEG analysis was performed for spontaneous 48 hrs sleep recordings at a sampling rate of 500 Hz. In addition, urethane induced artificial SWS was analyzed using 60 min baseline recordings as control and a 180 min recording period following drug exposure. EEG analysis was performed using the complex Morlet wavelet to calculate both frequency and amplitude of oscillations. The *complex Morlet wavelet* is defined by  $\Psi(x) = (\pi b)^{-1/2} \exp(2i\pi cx) \exp(-x^2/b)$ , with  $b$  representing the bandwidth parameter,  $c$  the center frequency and  $i$  the imaginary unit (Muller et al., 2012). This wavelet has often been applied in literature to study EEG data as it guarantees optimal resolution in both frequency and time (Kronland-Martinet et al., 1987; Montgomery and Buzsaki, 2007). In our study the bandwidth parameter and center frequency were both set to 3 in order to particularly weight the frequency resolution to distinguish frequency differences on the 0.1 Hz level, but not to neglect a sufficient time resolution. EEG data were analyzed in the frequency range of 0.5 - 12 Hz with a step size of 0.1 Hz, thus including the typical delta, theta and alpha frequency ranges. For computational reasons, raw EEG data were segregated into 60 min segments. According to segment duration in the Neuroscore<sup>®</sup> sleep module, mean amplitudes for the three frequency bands (delta: 0.5 – 4 Hz; theta: 4 – 8 Hz; alpha: 8 – 12 Hz) were calculated for 10 s non overlapping segments. Every segment was assigned to one of the four vigilance stages, i.e. wake, PS, SWS 1, SWS2 according to the Neuroscore<sup>®</sup> sleep module. Calculated frequency-specific amplitudes were averaged for distinct wake/sleep stages and analyzed for both

the entire 48 hrs recording period and the light/dark cycle. Mean amplitudes for the three frequency bands were statistically analyzed. All calculations were done using custom-made programs in Matlab<sup>®</sup> (The MathWorks Inc., Version R2012b).

***Quantitative Real-time PCR (qPCR)***

To elaborate potential compensating effects of Ca<sub>v</sub>3.1, Ca<sub>v</sub>3.2 and Ca<sub>v</sub>3.3 T-type Ca<sup>2+</sup> channels in Ca<sub>v</sub>2.3<sup>-/-</sup> mice that might account for altered sleep architecture, the expression levels of Ca<sub>v</sub>3 Ca<sup>2+</sup> channels were analyzed using quantitative Real-time PCR (qPCR). Total RNA was extracted from the thalamus of three male mice from each genotype (Ca<sub>v</sub>2.3<sup>+/+</sup>, controls, mean age: 15.86 ± 0.08 wks; Ca<sub>v</sub>2.3<sup>+/-</sup>, all 15 wks; Ca<sub>v</sub>2.3<sup>-/-</sup>, all 15 wks) using RNeasy Lipid Tissue Mini Kit (Qiagen). The cDNA synthesis was carried out using anchored-oligo(dt)18 and hexamer primer in a two-step RT-PCR approach (Transcriptor First Strand cDNA Synthesis Kit, Qiagen) and qPCR reaction protocol was based on Light Cycler 480 SYBR Green I Master (Roche). The qPCR was performed in a Light Cycler 480 System (Roche) thermocycler. The following cycler protocol was used for all primer pairs according to 58,59 (**Tab. 1**): 95°C (10 min, pre-incubation step); 95°C (10s, melting step); 60°C (20s, annealing step); 72°C (30 s, extension step), 35 cycles.

Gene	Forward Sequence	Reverse Sequence	Size (bp)
Ca <sub>v</sub> 3.1	GGCCCCGGTGGTTTTCTTCTACTTG	TGAGCGGTGCGAGCACAC	398
Ca <sub>v</sub> 3.2	TCCCCGTCTACTTCGTCACCTTC	GCGAGAGCATCCTGGACACAGATA	260
Ca <sub>v</sub> 3.3	GCTGCGGCGCCTGAAAAGAA	GCCCATGCACGGACAGCAGACAAT	338
HPRT	GCTGGTGAAAAGGACCTCT	CACAGGACTAGAACACCTGC	249

The specificity of the amplification was checked by melting curve analysis and the products were identified by electrophoresis. Deionized, nuclease-free water (no cDNA) and total RNA samples (without RT) were used as controls. The Ct-values (cycle threshold) were calculated using the LightCycler 480 System software. Fold changes (FC) of Ca<sub>v</sub>3.1, Ca<sub>v</sub>3.2 and Ca<sub>v</sub>3.3 gene expression in Ca<sub>v</sub>2.3<sup>+/-</sup> and Ca<sub>v</sub>2.3<sup>-/-</sup> mice related to controls were calculated according to Schmittgen and Livak (2008).

### ***Statistical analysis***

Statistical analyses concerning sleep architecture, amplitudes, comparisons between groups, also regarding different frequency bands were done with IBM® SPSS® 21 (IBM, Inc.). The Kolmogorov–Smirnov approach was used to test for normal distributions. The two-sample t- test was applied for comparisons between the two groups, i.e.  $Ca_v2.3^{+/+}$  and  $Ca_v2.3^{-/-}$  mice. This procedure was utilized at a p-level of 0.05. All data were plotted as the mean  $\pm$  SEM. Statistical analysis of delta wave amplitude post sleep deprivation was done using repeated measures ANOVA with time factor (within subjects factor, 12 intervals) and group factor (between-subjects factor,  $Ca_v2.3^{+/+}$  and  $Ca_v2.3^{-/-}$ ).

For a detailed analysis of the time factor, pairwise comparisons were done for the within-subjects factor. If necessary, Huynh- Feldt corrections were performed.

## Results

### *Electrocorticographic and electromyographic recordings in control and $Ca_v2.3^{-/-}$ mice*

Control and  $Ca_v2.3^{-/-}$  mice were implanted using a two-channel radiofrequency transmitter allowing simultaneous electrocorticographic (SB1) and nuchal electromyographic recordings (**Fig. 1; Fig. 2**). As reported previously for a different  $Ca_v2.3^{-/-}$  mouse model (Weiergraber et al., 2006), the  $Ca_v2.3$  knock-out model used in this study (Wilson et al., 2000) did not exhibit any type of spontaneous irregular EEG activity that might be indicative of seizure activity (**Fig 1A,B; Fig. 2A,B**).

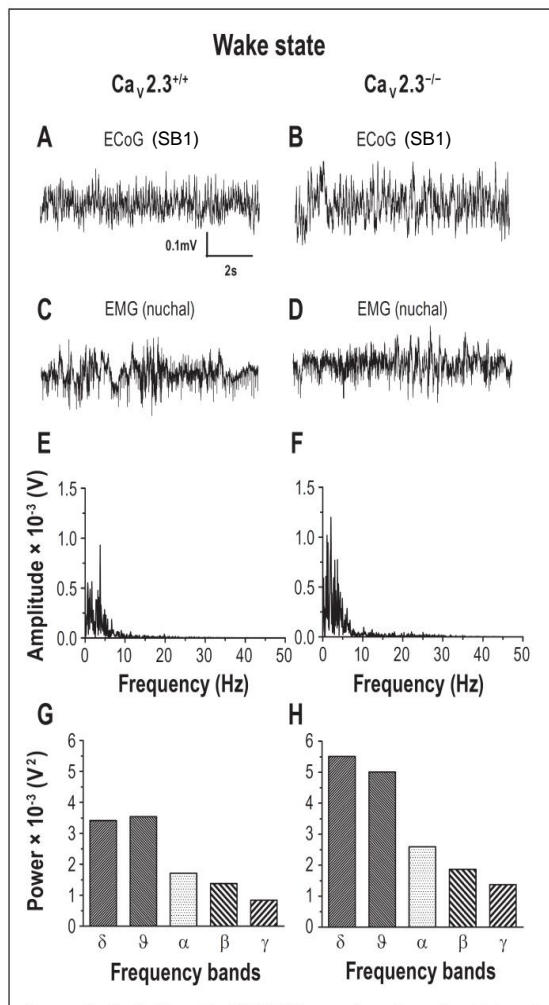


**Figure 1**—Radiotelemetric EEG/EMG recordings from  $Ca_v2.3^{+/+}$  and  $Ca_v2.3^{-/-}$  mice during wake state. Representative 10s ECoG (S1/S2) and nuchal EMGs epochs from  $Ca_v2.3^{+/+}$  (**A, C**) and  $Ca_v2.3^{-/-}$  mice (**B, D**). Frequency characteristics are depicted using the periodogram (**E, F**) and EEG power band function (**G, H**). Representative powerbands point to an increased delta and theta activity in  $Ca_v2.3^{-/-}$  mice (**F, H**) in comparison to  $Ca_v2.3^{+/+}$  controls (**E, G**). Frequencies were defined as follows:  $\delta$  (0.5-4 Hz),  $\theta$  (4-8 Hz),  $\alpha$  (8-12 Hz),  $\beta$  (12- 24 Hz),  $\gamma$  (24-50 Hz).

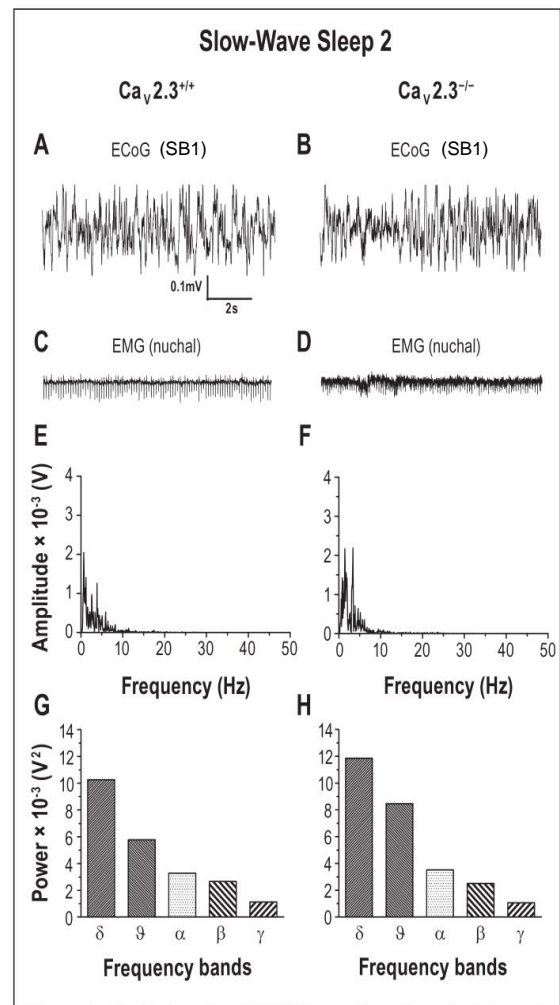


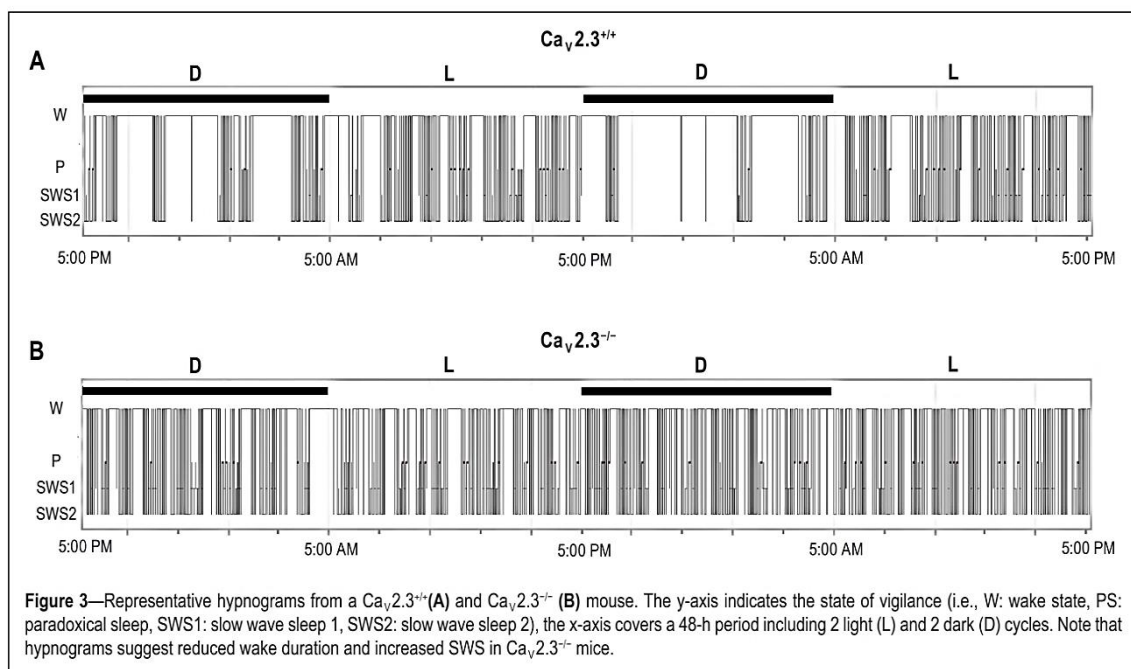
**Figure 2**—Radiotelemetric EEG/EMG recordings from  $Ca_v2.3^{+/+}$  and  $Ca_v2.3^{-/-}$  mice during slow wave sleep 2 (SWS2). Representative 10s ECoG (S1/S2) and nuchal EMGs epochs from  $Ca_v2.3^{+/+}$  (**A, C**) and  $Ca_v2.3^{-/-}$  mice (**B, D**). Note that due to reduced EMG amplitude during SWS, R-spike related ECG contamination becomes apparent. Frequency characteristics are depicted using the periodogram (**E, F**) and EEG power band function (**G, H**). Frequencies were defined as follows:  $\delta$  (0.5-4 Hz),  $\theta$  (4-8 Hz),  $\alpha$  (8-12 Hz),  $\beta$  (12- 24 Hz),  $\gamma$  (24-50 Hz).

Depending on the stage of vigilance, electrocorticographic recording suggest predominance of different frequency bands, i.e. increased theta and delta frequency

activity during SWS2 and less theta and delta, but increased beta activity during the active state. To demonstrate this phenomenon both the periodogram approach and power band analysis was carried out for the active state (**Fig. 1E-H**) and SWS2 state (**Fig. 2E-H**) for both genotypes. Initial power analysis suggests increased theta and delta activity in  $Ca_v2.3^{-/-}$  mice in the wake state (**Fig. 1G,H**; **Fig. 2G,H**). Note that EMG amplitude is dramatically reduced during SWS2 (**Fig. 2C,D**) compared to wake state (**Fig. 1C,D**) leading to the appearance of characteristic ECG-related R-spikes that represent the typical murine heart rate. Technically, ECG contamination is unavoidable in EMG recordings but of no relevance in epidural SB1 recordings (Weiergraber et al., 2006; Weiergraber et al., 2007).

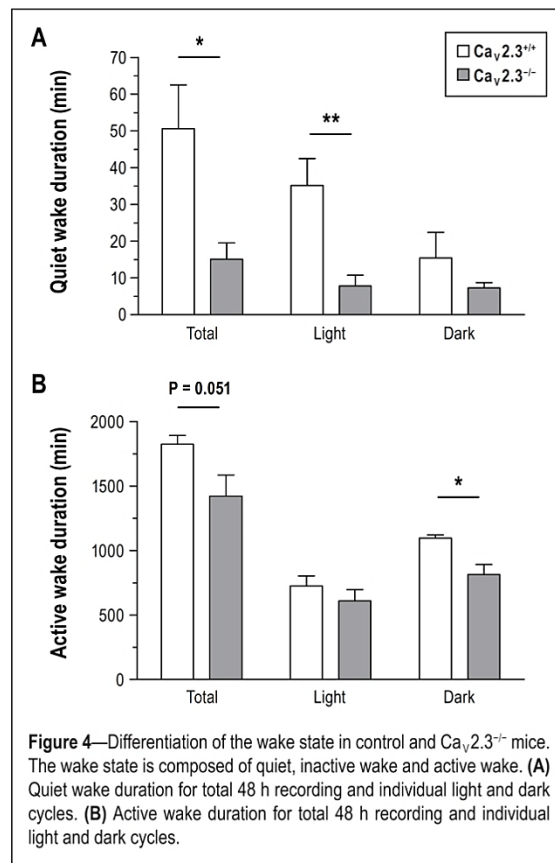
### *Hypnogram*

Representative hypnograms (somnograms) are presented in **Fig. 3** for a total period of 48hrs. Comparison of  $Ca_v2.3^{+/+}$  and  $Ca_v2.3^{-/-}$  hypnograms suggests an alteration in sleep architecture in  $Ca_v2.3^{-/-}$  with increased sleep duration and increased number of sleep stage episodes in knock-out mice (see section below). For precise sleep analysis the Neuroscore<sup>®</sup> sleep module was used which allows for analysis of total duration, mean duration, total number and number of transitions of individual sleep stages.



### *Sleep architecture in control and $Ca_v2.3^{-/-}$ mice*

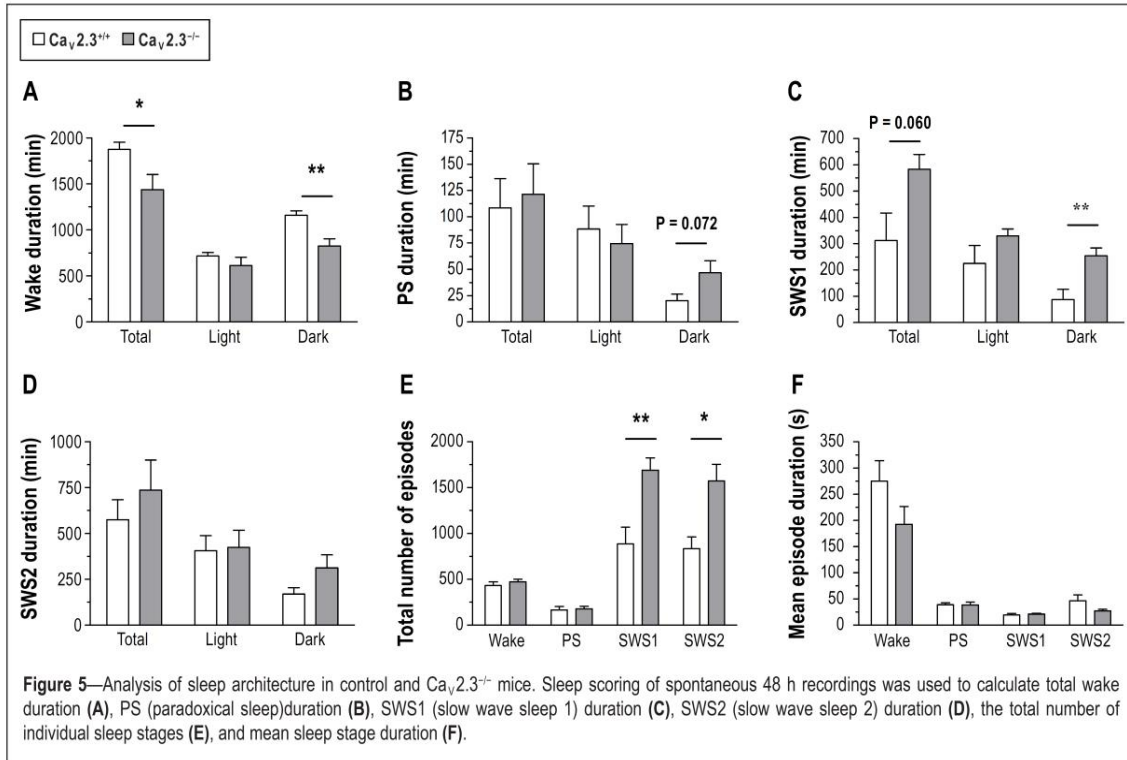
We have analyzed the wake state for quiet, i.e. inactive wake and active wake. In general, the active wake state dramatically predominates in both genotypes. Further analysis of the quiet/active-wake state ratio defined as  $(1 - \text{quiet wake} / \text{active wake}) * 100$  for both light and dark cycle revealed a significant increase of the quiet/active wake ratio in  $Ca_v2.3^{-/-}$  mice compared to controls during light cycle ( $0.989 \pm 0.004$  v.  $0.950 \pm 0.011$ ,  $p = 0.013$ ).  $Ca_v2.3^{-/-}$  showed a clear tendency of reduced quiet wake duration compared to control mice with a significant reduction for the total observation period ( $50.60 \pm 11.91$  min v.  $15.06 \pm 4.45$  min,  $p = 0.038$ ) and the light cycle in specific ( $35.16 \pm 7.26$  min v.  $7.78 \pm 3.01$  min,  $p = 0.008$ , **Fig.4A**).



The same trend was observed for the active wake state during the total recording period ( $1825.72 \pm 66.84$  min v.  $1424.64 \pm 190.81$  min,  $p = 0.051$ ) with significant reduction in  $Ca_v2.3^{-/-}$  mice compared to controls during the dark cycle ( $1097.78 \pm 24.25$  min v.  $813.98 \pm 77.71$  min,  $p = 0.019$ , **Fig. 4B**). Whereas the quiet wake duration was not increased during the dark cycle compared to light cycle, the active wake duration was increased during dark episode compared to light episode in both genotypes ( $Ca_v2.3^{+/+}$ ,



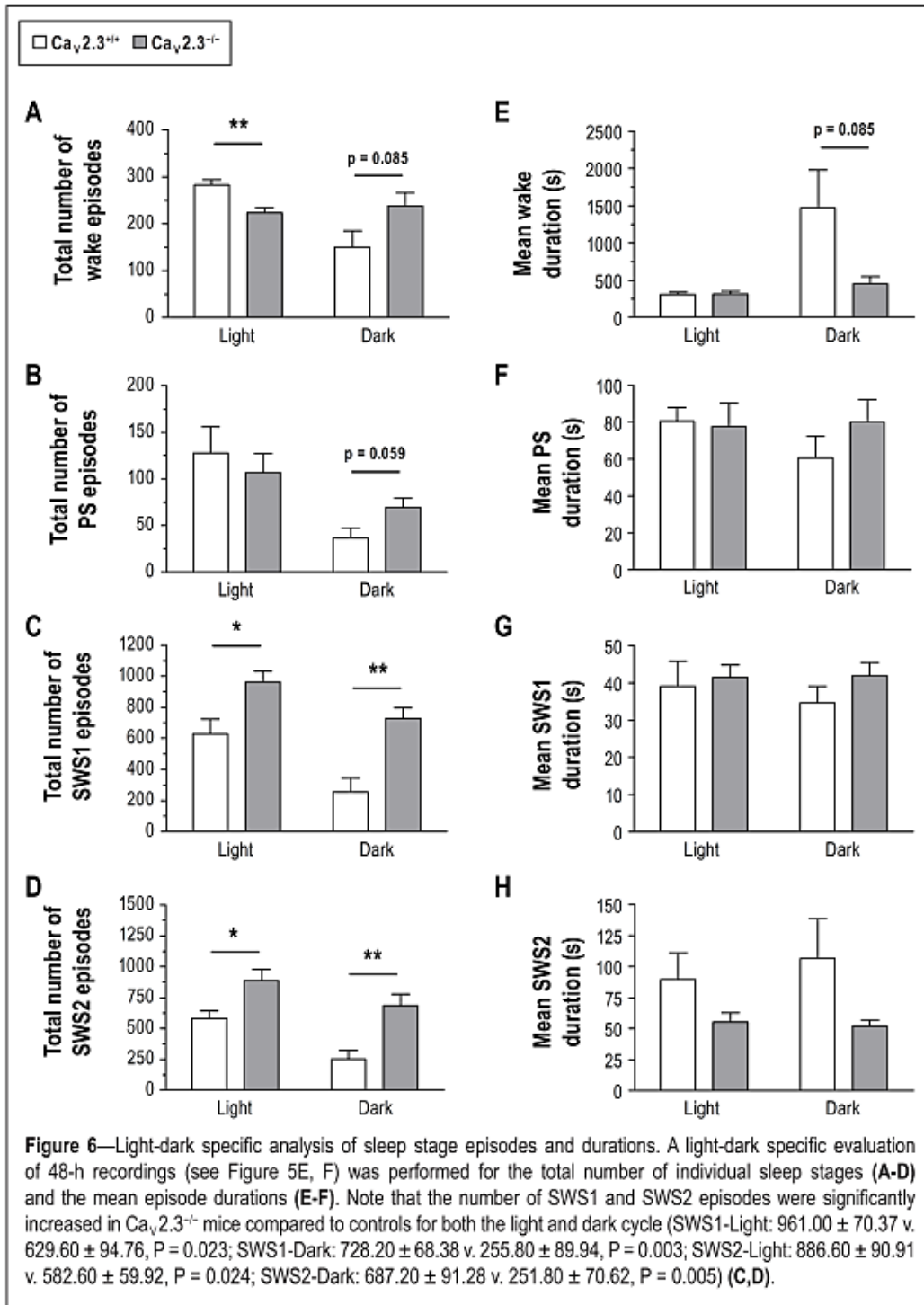
727.94 ± 76.54 min v. 1097.78 ± 24.25 min;  $Ca_v2.3^{-/-}$ , 610.66 ± 87.16 min v. 813.98 ± 77.71 min, **Fig. 4A,B**). Analysis of total wake duration revealed significant reduction in  $Ca_v2.3^{-/-}$  mice versus controls during the dark cycle (826.23 ± 75.69 min v. 1158.93 ± 46.50 min,  $p = 0.006$ ) and the total observational period (1437.90 ± 164.56 min v. 1876.38 ± 75.80 min,  $p = 0.042$ , **Fig. 5A**).



For the paradoxical sleep, a trend for increased PS duration was observed during the dark cycle in  $Ca_v2.3^{-/-}$  mice versus controls (46.80 ± 11.29 min v. 20.27 ± 5.99 min,  $p = 0.072$ , **Fig. 5B**). Interestingly, total SWS1 duration was increased in  $Ca_v2.3^{-/-}$  mice with significant SWS1 increase during the dark cycle (254.03 ± 29.88 min v. 87.23 ± 39.09 min,  $p = 0.009$ , **Fig. 5C**). No difference could be detected regarding mean duration of individual sleep stages during 48 hrs recording (**Fig. 5F**) and for the light and dark cycles in specific (**Fig. 6E-H**).

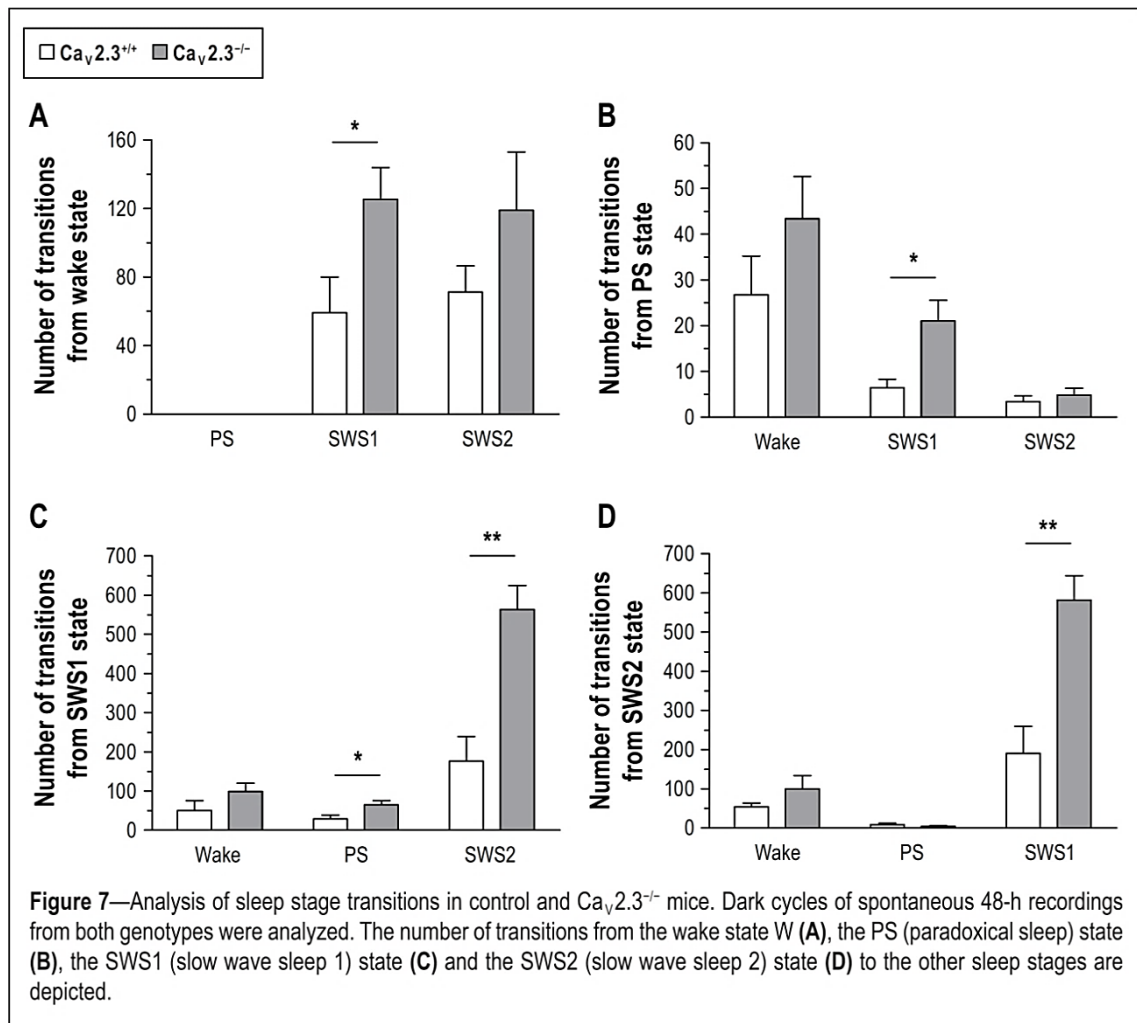
The total number of SWS1 and SWS2 episodes in 48 hrs recording was significantly increased in  $Ca_v2.3^{-/-}$  mice (SWS1, 1689.00 ± 137.13 v. 885.20 ± 183.82,  $p = 0.008$ ; SWS2, 1573.60 ± 180.27 v. 834.20 ± 128.62,  $p = 0.010$ , **Fig. 5E**). This observation also held true for the light and dark cycle specific analysis of SWS1 and SWS2 episode numbers (**Fig. 6C,D**). In addition, a significant difference between both genotypes could be detected for the number of wake episodes during light cycle (282.80 ± 11.46

( $Ca_v2.3^{+/+}$ ) v.  $223.80 \pm 11.18$  ( $Ca_v2.3^{-/-}$ ),  $p = 0.006$ , **Fig. 6A**). In general,  $Ca_v2.3^{+/+}$  mice exhibited a significant reduction of the number of all sleep stage episodes from light to dark



dark cycle, concomitant with an increase in mean wake duration from light to dark cycle ( $p = 0.053$ ). This pattern severely differed from  $Ca_v2.3^{-/-}$  mice, in which the total number and mean duration of individual sleep stages remained largely unaffected by light-dark

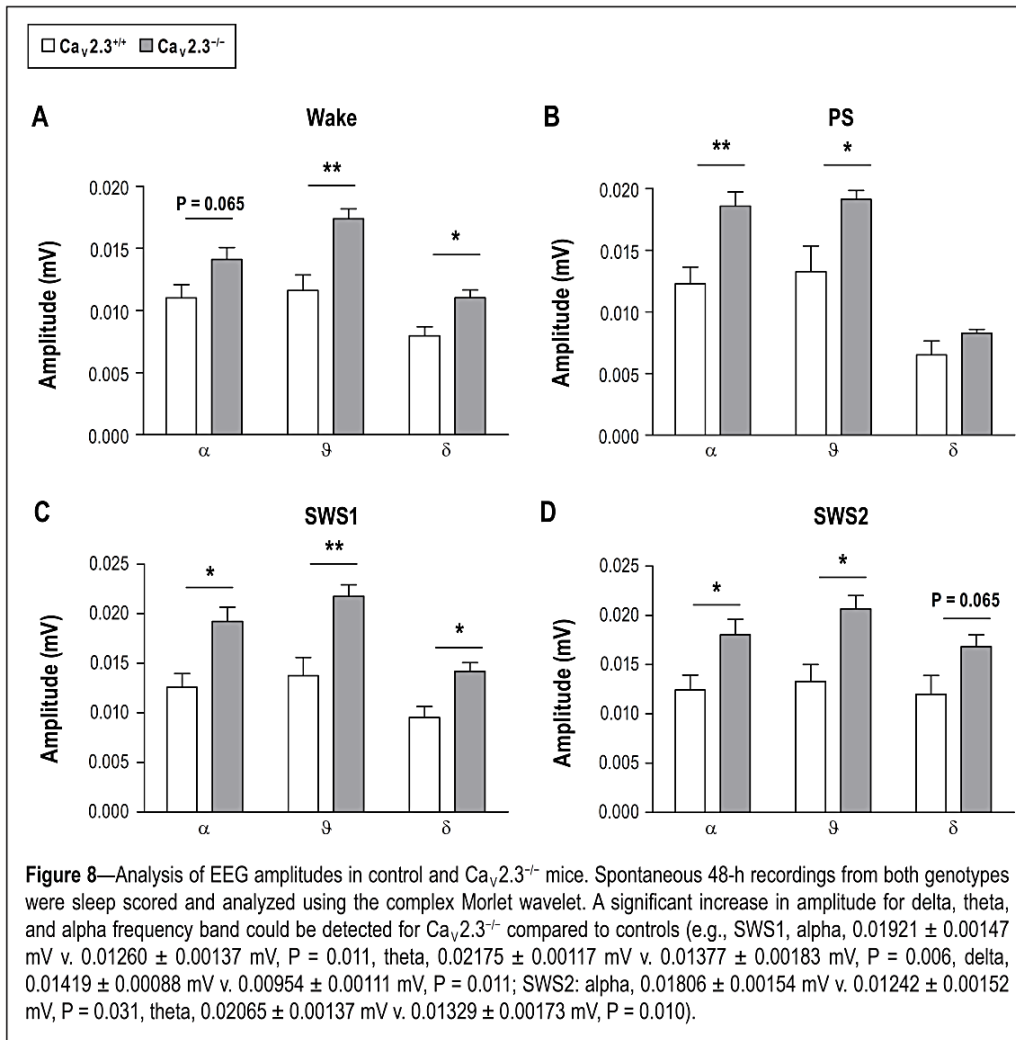
transitions. Particularly, this observation points to a role of  $Ca_v2.3$  R-type  $Ca^{2+}$  channels in modulating sleep architecture via extrathalamocortical structures.



A detailed analysis of sleep transition states for the dark cycle revealed a significant increase in wake-SWS1 transitions and PS-SWS1 transitions in  $Ca_v2.3^{-/-}$  compared to  $Ca_v2.3^{+/+}$  mice (Wake-SWS1:  $125.40 \pm 18.59$  v.  $59.20 \pm 20.82$ ,  $p = 0.045$ ; PS-SWS1:  $21.00 \pm 4.59$  v.  $6.40 \pm 1.86$ ,  $p = 0.019$ , **Fig. 7A,B**).

Moreover, a dramatic increase in SWS1-SWS2 and SWS2-SWS1 transitions was observed in  $Ca_v2.3^{-/-}$  mice (SWS1-SWS2,  $563.00 \pm 61.69$  v.  $176.40 \pm 62.86$ ,  $p = 0.002$ ; SWS2-SWS1,  $581.20 \pm 62.40$  v.  $190.20 \pm 69.01$ ,  $p = 0.003$ , **Fig. 7C,D**) stressing the aforementioned alterations that became apparent in the hypnograms (**Fig. 3**; dark cycle). Though most changes were observed during the dark cycle as described above, significant alterations in SWS1-SWS2 and SWS2-SWS1 transitions were also observed

during the light cycle and total 48 hrs recording period for  $Ca_v2.3^{+/+}$  and  $Ca_v2.3^{-/-}$  mice (light cycle: SWS1- SWS2,  $437.00 \pm 69.09$  v.  $771.40 \pm 76.56$ ,  $p = 0.012$ ; SWS2-SWS1,  $451.20 \pm 72.96$  v.  $805.00 \pm 82.55$ ,  $p = 0.012$ ; 48 hrs: SWS1-SWS2,  $613.80 \pm 131.56$  v.  $1334.60 \pm 136.92$ ,  $p = 0.005$ , SWS2-SWS1,  $641.40 \pm 140.74$  v.  $1386.60 \pm 144.07$ ,  $p = 0.006$ ). These findings indicate that ablation of the  $Ca_v2.3$  voltage-gated  $Ca^{2+}$  channel results in complex alteration of sleep architecture. The individual sleep stages were systematically analyzed for changes in frequency band amplitude (**Fig. 8**). Interestingly, it turned out that in most cases a significant increase in amplitude for delta, theta and alpha frequency band could be detected for  $Ca_v2.3^{-/-}$  compared to controls (**Fig. 8A-D**).

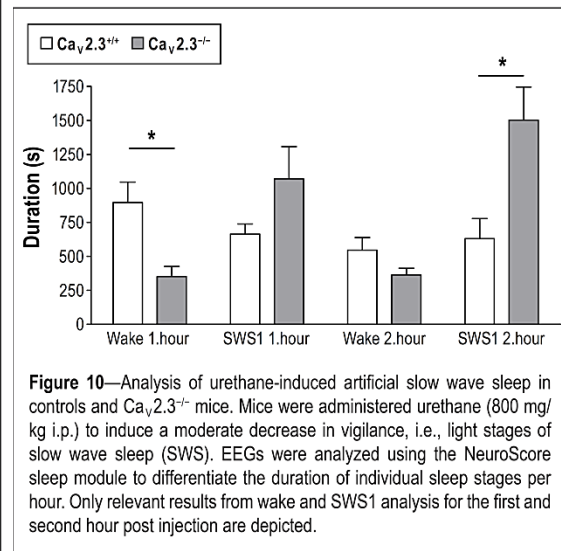
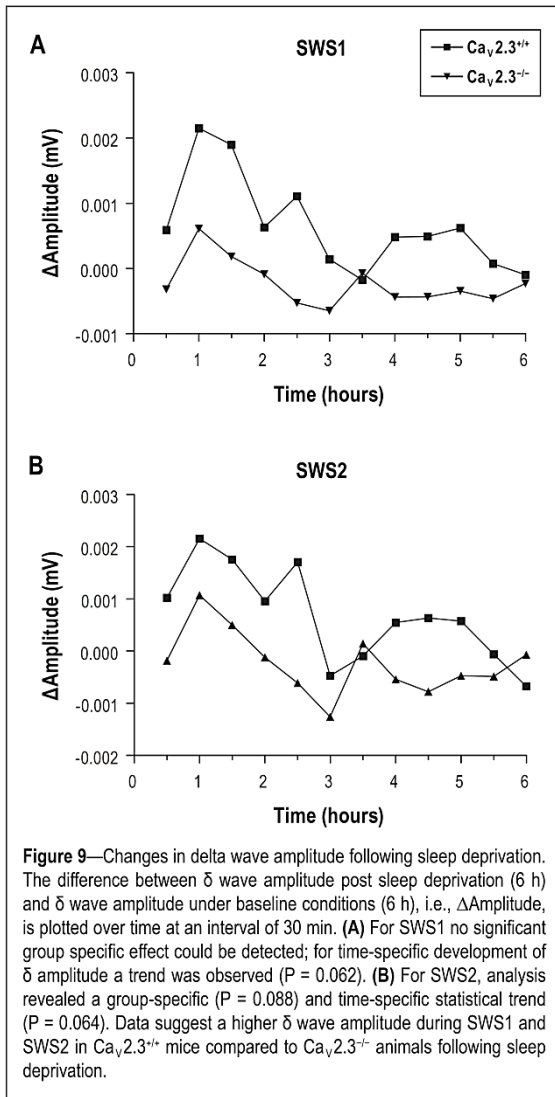


This phenomenon was also observed in the light and dark periods (data not shown). This observation points to an increased degree of neuronal synchronisation in  $Ca_v2.3^{-/-}$  mice the physiological reason of which however remains to be elucidated.

### *Sleep deprivation in control and $Ca_v2.3^{-/-}$ mice*

Following spontaneous sleep recordings we performed sleep deprivation experiments to identify potential SWS rebound mechanisms upon sleep recuperation. As this recuperation can occur immediately after sleep deprivation, with delay of some hours or be totally lacking depending on mouse strain and transgenic lines used, a total duration of 6 hrs (2:00 PM – 8:00 PM, light cycle) was used for analysis of sleep parameters. Although mean values for wake-, SWS1- and SWS2 duration (**Supplemental Fig. 2A,C,D**) display the same tendency as observed in spontaneous 48 hrs sleep analysis (**Fig. 5A,C,D**), no significant difference was observed following sleep deprivation between both genotypes. The same holds true for analysis of transition states (**Supplemental Fig. 3**).

It should be noted that more rigorous sleep deprivation procedures were not applied as  $Ca_v2.3^{-/-}$  mice were reported to exhibit increased levels of anxiety based on functional expression of  $Ca_v2.3$  in the amygdala (Lee et al., 2002). Given the complex reciprocal connections between the amygdala, the limbic system and brainstem structures involved in sleep regulation it seemed mandatory to use a gentle sleep deprivation approach to avoid any potential interference between anxiety and sleep behaviour. This potential bias in physiological, i.e. sleep-deprivation based SWS provocation was avoided by using a pharmacological approach in SWS induction (see below). In addition, we performed amplitude analysis of the  $\delta$  frequency band of SWS1 and SWS2 episodes for the 6 hrs post sleep deprivation period in both genotypes. Changes in delta amplitude,  $\Delta$ Amplitude (mV), i.e. [EEG-Amplitude (post sleep deprivation, 30 minutes intervals) – EEG-Amplitude (average baseline, 6 hrs)], was calculated and is displayed in **Fig. 9**. Statistical analysis revealed no significant difference between both genotypes. However, a group-specific ( $p = 0.088$ ) and time-specific ( $p = 0.064$ ) statistical trend was observed for SWS2 suggesting a higher delta amplitude following sleep deprivation in  $Ca_v2.3^{+/+}$  mice compared to  $Ca_v2.3^{-/-}$  animals. For SWS1, a time-specific trend ( $p = 0.062$ ), but not a group – specific one ( $p = 0.118$ ) was observed. This finding might suggest that sleep deprivation provoked TC hyperoscillation is less in  $Ca_v2.3^{-/-}$  mice compared to controls which is in line with results reported by Zaman et al., 2011.



### Urethane-induced artificial slow-wave sleep

Following analysis of spontaneous sleep in control and  $Ca_v2.3^{-/-}$  mice we pharmacologically induced SWS using urethane (800 mg/kg ip.). Pharmacodynamically, urethane is a multi-target drug that serves i.a. as antagonist on NMDA receptors (Dalo and Hackman, 2013; Hara and Harris, 2002). Simultaneous video-EEG-EMG recordings were performed 1 h prior to injection, up to 8 hrs post injection and analyzed using the Neuroscore<sup>®</sup> sleep module. Individual sleep stages were quantified for one hour intervals. Statistical analysis revealed significant reduction of wake duration in  $Ca_v2.3^{-/-}$  mice compared to controls within the first hour post injection ( $352.00 \pm 73.38$  s v.  $896.00 \pm 150.59$  s,  $p = 0.012$ ) and significant increase of SWS1 duration in  $Ca_v2.3^{-/-}$  mice during the second hour post urethane injection ( $1502.00$

$\pm 243.83$  s v.  $630.00 \pm 148.09$  s,  $p = 0.016$ , **Fig. 10**). These findings strongly support our results obtained from spontaneous sleep analysis. In addition, there is a tendency that wake duration in  $Ca_v2.3^{+/+}$  mice is reduced following urethane injection (1<sup>st</sup> – 2<sup>nd</sup> hr), whereas SWS1 duration remained constant. Interestingly,  $Ca_v2.3^{-/-}$  mice exhibited the opposite behaviour with constant wake duration but increase in SWS1.

***Thalamic expression pattern of  $Ca_v3$  T-type  $Ca^{2+}$  channels in controls and  $Ca_v2.3^{-/-}$  mice***

The expression levels of  $Ca_v3.1$ ,  $Ca_v3.2$ ,  $Ca_v3.3$  T-type  $Ca^{2+}$  channels in  $Ca_v2.3^{+/+}$  and  $Ca_v2.3^{-/-}$  mice were analysed and compared to those of  $Ca_v2.3^{+/+}$  animals based on the procedure of Schmittgen and Livak (2008) (**Supplemental Fig. 4; Tab. 1,2**).

**Table 2**—Fold changes in gene expression of  $Ca_v2.3^{+/+}$  and  $Ca_v2.3^{-/-}$  mice compared to  $Ca_v2.3^{+/+}$

<b>Gene</b>	<b><math>Ca_v2.3^{+/+}</math> mice</b>	<b><math>Ca_v2.3^{-/-}</math> mice</b>
$Ca_v3.1$	1,1545	-1,1225
$Ca_v3.2$	-1,0057	-1,0772
$Ca_v3.3$	-1,0272	-1,0561

Fold changes of  $Ca_v3$  T-type  $Ca^{2+}$  channels exhibit no significant difference between controls,  $Ca_v2.3^{+/+}$  and  $Ca_v2.3^{-/-}$  mice. These findings demonstrate that no thalamic alteration in  $Ca_v3.1-3.3$  T-type  $Ca^{2+}$  channel expression can account for altered sleep architecture in  $Ca_v2.3^{-/-}$  mice.

## Discussion

Our study demonstrates that  $\text{Ca}_v2.3$  R-type  $\text{Ca}^{2+}$  channels modulate fundamental sleep parameters in rodents in a light-dark cycle dependent manner. Major alterations were detected for quiet and active wake duration, SWS1 duration and total number of sleep episodes. Specifically, wake duration was decreased compared to controls with significant increase in SWS 1. Sleep analysis further pointed to an alteration of sleep architecture in  $\text{Ca}_v2.3^{-/-}$  mice due to aberration in sleep stage transitions. Interestingly, the most severe changes were observed during the dark cycle. Pharmacologically induced SWS following urethane administration clearly supported sleep scoring results from spontaneous 48 hrs sleep recordings. How can  $\text{Ca}_v2.3$  VGCCs exert such a tremendous impact on sleep regulation? In a discussion on this issue one has to differentiate between thalamocortical and extrathalamocortical mechanisms. In a recent study on TC rhythmicity, Zaman et al., 2011 showed that there is a clear functional interdependence between  $\text{Ca}_v2.3$  R-type  $\text{Ca}^{2+}$  channels, small-conductance  $\text{Ca}^{2+}$ -activated  $\text{K}^+$  channels (SK) and T-type  $\text{Ca}^{2+}$  channels that build-up functional microdomains in RTN neurons. Interestingly,  $\text{Ca}_v2.3$  mediated  $\text{Ca}^{2+}$  influx is capable of activating SK channels which results in re- and hyperpolarisation of the cell membrane causing repriming of T-type  $\text{Ca}^{2+}$ -channels and activation of HCN channels. Thus,  $\text{Ca}_v2.3$  R-type  $\text{Ca}^{2+}$  channels seem to actively promote and sustain rebound burst firing in RTN neurons. Electrophysiological data from the RTN of  $\text{Ca}_v2.3^{-/-}$  mice clearly demonstrated an impairment of reticular thalamic bursting which was supposed to result in reduced SWD activity triggered by  $\gamma$ -hydroxybutyrate administration (Zaman et al., 2011). This functional scenario of  $\text{Ca}_v2.3$  mediated SK2 activation has previously been described in the CA1 region as a mechanism to induce AHPs that might serve as a negative feedback in regulating synaptic activity and plasticity in dendritic spines (Bloodgood and Sabatini, 2007; Yasuda et al., 2003). Based on the studies of Zaman et al., 2011 one might speculate that ablation of  $\text{Ca}_v2.3$  R-type  $\text{Ca}^{2+}$  channels results in decreased slow wave sleep. It should be noted that anaesthetic sensitivities to propofol and halothane were shown to be decreased in  $\text{Ca}_v2.3^{-/-}$  mice probably due to different pharmacodynamics profiles compared to urethane (Takei et al., 2003). Joksovic et al. (2009) reported that presynaptic  $\text{Ca}_v2.3$  R-type  $\text{Ca}^{2+}$  channels support inhibitory gamma-aminobutyric acid<sub>A</sub> ( $\text{GABA}_A$ ) transmission in RTN neurons and are inhibited by



isoflurane. Recombinant and native T-type  $\text{Ca}^{2+}$  channels are also potently inhibited by volatile anesthetics as well, including isoflurane (Joksovic et al., 2005; Todorovic et al., 2000). Joksovic et al. (2009) concluded that it is difficult to predict the consequences that an inhibition of  $\text{Ca}_v2.3$  R-type  $\text{Ca}^{2+}$  channels and IPSCs in the RTN might have on TC rhythmicity. We previously found that  $\text{Ca}_v2.3^{-/-}$  exhibited a decrease in the duration of suppression episodes in the EEG following isoflurane anesthesia (Joksovic et al., 2009) which is in line with data from Zaman et al., 2011 assuming that  $\text{Ca}_v2.3$  channels might play a role in deep sleep / deep anesthesia. However, urethane results from our present study do not support this view. This might be due to the different pharmacodynamic profile of urethane and the fact that urethane at a dose of 800 mg/kg ip. induces light SWS but not deep anesthesia. Interestingly, our experiments show a non-significant trend of higher delta amplitude in  $\text{Ca}_v2.3^{+/+}$  mice compared to  $\text{Ca}_v2.3^{-/-}$  animals following sleep deprivation, suggesting a potential role of  $\text{Ca}_v2.3$  in synchronisation of TC rhythmicity (Zaman et al., 2011) . In order to get an integrative view of  $\text{Ca}_v2.3$  in sleep modulation, it is worthwhile to have a short glance at T-Type  $\text{Ca}^{2+}$  channels in the TC system as well. Within the last decade, the functional involvement of T-Type  $\text{Ca}^{2+}$  channels in rodent sleep architecture has been elaborated in detail, leading to a “ $\text{Ca}^{2+}$  channel model of thalamocortical rhythmicity”. T-type  $\text{Ca}^{2+}$  channels are differentially distributed throughout the thalamus.  $\text{Ca}_v3.1$  channels are expressed in thalamic relay cells whereas  $\text{Ca}_v3.2$  and  $\text{Ca}_v3.3$  channels are expressed in RTN neurons (Talley et al., 1999). Gene ablation studies on  $\text{Ca}_v3.1^{-/-}$  mice showed that lack of  $\text{Ca}_v3.1$  mediated  $\text{Ca}^{2+}$  influx in thalamic relay cells results in lack of burst firing activity due to impaired low-threshold  $\text{Ca}^{2+}$  spike activity (Lee et al., 2004). However, region specific, i.e. cortical, not thalamic  $\text{Ca}_v3.1$  deletion did not result in altered sleep (Anderson et al., 2005). Generalized  $\text{Ca}_v3.1$  ablation was capable of rescuing multiple  $\text{Ca}_v2.1$  mouse mutants exhibiting SWD activity (Song et al., 2004; Zhang et al., 2002) and SWDs were also shown to be accelerated upon thalamic  $\text{Ca}_v3.1$  overexpression (Ernst and Noebels, 2009). SWD are characteristic of absence like seizure activity which is supposed to be a pathophysiological aberration of SWS. Finally, these findings evolved into a well-described model of  $\text{Ca}_v3.1$  T-type  $\text{Ca}^{2+}$  channels in regulating thalamocortical rhythmicity. Based on this, it might be speculated that ablation of  $\text{Ca}_v3.2$  and  $\text{Ca}_v3.3$  in the RTN might result in a phenotype comparable to that of

Ca<sub>v</sub>3.1<sup>-/-</sup> mice (Cheong and Shin, 2013). However, although effects of Ca<sub>v</sub>3.3 ablation on sleep spindles have been described, we are still lacking detailed sleep analysis in Ca<sub>v</sub>3.2 and Ca<sub>v</sub>3.3 knock-out mice. The model might predict that ablation of Ca<sub>v</sub>3.2 and Ca<sub>v</sub>3.3 results in impaired SWS, however, it was recently reported from a patent application that pharmacological blockade of Ca<sub>v</sub>3.2 channels can result in enhanced rather than impaired sleep, the reason of which remains to be determined. Moreover, transition rates and sleep architecture were altered (Lee and Shin, 2007). The latter findings strongly suggest that interpretation of sleep architecture in transgenic mice cannot be restricted to the thalamocortical network itself, or thalamic nuclei in specific. Like Ca<sub>v</sub>3.2 and Ca<sub>v</sub>3.3 channels, Ca<sub>v</sub>2.3 channels are expressed in the RTN, but not thalamic relay neurons. In addition, Ca<sub>v</sub>2.3 transcripts are present in cortical interneurons. Moreover, Ca<sub>v</sub>2.3 channels are expressed in a number of extrathalamocortical structures, such as the mesopontine REM-NREM modulators (i.e. the locus coeruleus, the dorsal raphe nuclei, the pedunculopontine and the laterodorsal tegmental nuclei), the diencephalic sleep onset controllers (i.e. hypothalamic nuclei including the ventrolateral/lateral preoptic region and the tuberomammillary basal forebrain), the cerebellum, the basal ganglia and the hippocampus (Weiergraber et al., 2006; Weiergraber et al., 2007; Weiergraber et al., 2008; Zaman et al., 2011). These structures are known to project to the thalamocortical circuitry and substantially modify its activity via different neuromodulators, e.g. noradrenalin, histamine, serotonin (5-HT) and acetylcholine (Deransart et al., 1998; Khosravani and Zamponi, 2006; Manning et al., 2003; Pace-Schott and Hobson, 2002) (**Fig. 11**). The suprachiasmatic nucleus, which is involved in the regulation of the circadian rhythm and also in sleep architecture, is also modulated by Ca<sub>v</sub>2.3 channels (Merica and Fortune, 2011; Wurts and Edgar, 2000). Both, suprachiasmatic AHP and plateau potentials were reported to be triggered by Ca<sub>v</sub>2.3 channels (Cloues and Sather, 2003; Pierson et al., 2005). This aspect is even more striking as sleep changes in Ca<sub>v</sub>2.3<sup>-/-</sup> mice seem to be dependent on light- dark cycles. Special attention has to be paid to the role of the amygdala in sleep regulation. The central nucleus of the amygdala (ACE) has numerous neuroanatomical connections to the basal forebrain, hypothalamus and brainstem thus substantially modulating sleep architecture (Jha et al., 2005). Within the ACE individual neuronal cell entities, i.e. Wake-ON, REM-ON and NREM-ON neurons have been identified that are functionally distinct from each other and exhibit characteristic firing patterns (Jha et al., 2005).

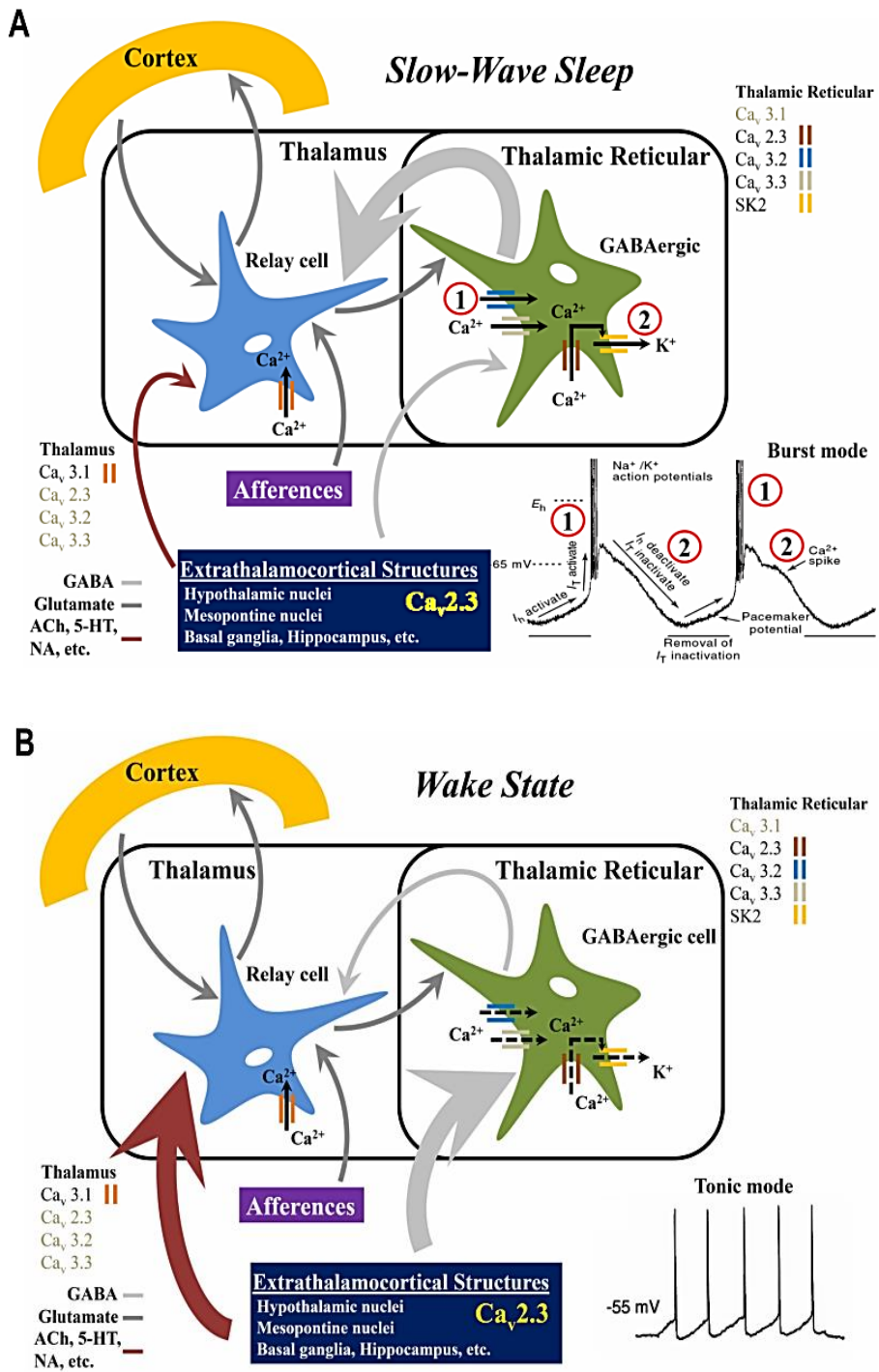


**Figure 11**—Voltage-gated Ca<sup>2+</sup> channels in regulating thalamocortical rhythmicity and different stages of vigilance. Voltage-gated Ca<sup>2+</sup> channel entities are differentially distributed throughout the thalamic relay and reticular nucleus. Genetic ablation studies suggest that T-type Ca<sup>2+</sup> channels play a major role in regulating oscillatory activity in the thalamocortical system (A). During high stages of vigilance, i.e. wake state, strong excitatory input from the brain stem to relay cells and reduced inhibitory input to RTN neurons promotes the thalamic tonic mode of action (B). However, decreasing brain stem activity associated with low stages of vigilance favors rebound burst firing in RTN and relay cells thus promoting the burst mode of action. Note that a number of extra-thalamocortical structures using different neurotransmitter systems and expressing Ca<sub>v</sub>2.3 Ca<sup>2+</sup> channels project to the thalamocortical circuitry and are likely to modulate the tonic-burst activity balance.

Interestingly,  $\text{Ca}_v2.3$  plays a major role in the amygdala physiology. Lee et al (2002) analyzed the molecular basis of R-type  $\text{Ca}^{2+}$  channels in ACE neurons proving that  $\text{Ca}_v2.3$  underlies R-type  $\text{Ca}^{2+}$  currents in ACE neurons. In 40 % of ACE neurons an extremely high amount of  $\text{Ca}_v2.3$  R-type based  $\text{Ca}^{2+}$  current was observed. Importantly, deletion of  $\text{Ca}_v2.3$  did not change expression of other VGCCs in ACE neurons. Thus, it is highly likely that R-type channel currents are substantially involved in the regulation of ACE neuronal excitability. Yet, it is not known what the functional consequences of  $\text{Ca}_v2.3$  based R-type  $\text{Ca}^{2+}$  currents in Wake-ON, REM-ON and NREM-ON ACE neurons are and how complex G-protein coupled neurotransmitter receptors are involved in modulating their activity. However, these findings illustrate that interpretation of sleep data in  $\text{Ca}_v2.3^{-/-}$  mice needs to consider more than RTN physiology and that altered extrathalamocortical input is likely to modulate thalamocortical oscillations in  $\text{Ca}_v2.3^{-/-}$  mice. It could further be speculated that compensatory alterations, particularly in T-type  $\text{Ca}^{2+}$  channel expression might be related to altered sleep architecture in  $\text{Ca}_v2.3^{-/-}$  mice. Thus, we performed qPCR for  $\text{Ca}_v3.1-3.3$  using thalamic RNA preparations from  $\text{Ca}_v2.3^{+/+}$ ,  $\text{Ca}_v2.3^{+/-}$  and  $\text{Ca}_v2.3^{-/-}$  mice. No significant up- or down-regulation of  $\text{Ca}_v3$  T-type  $\text{Ca}^{2+}$  channels could be detected. These findings further underline that sleep alterations in  $\text{Ca}_v2.3$  deficient mice are directly related to  $\text{Ca}_v2.3$  ablation itself. This of course does not exclude other potential changes in gene expression. Our studies demonstrate for the first time that  $\text{Ca}_v2.3$  R-type  $\text{Ca}^{2+}$  channels substantially modulate mammalian sleep architecture. Further studies are necessary to elucidate the pathophysiological implications of  $\text{Ca}_v2.3$   $\text{Ca}^{2+}$  channels in the thalamocortical system and extrathalamocortical modulators and their potential role in sleep disorders.

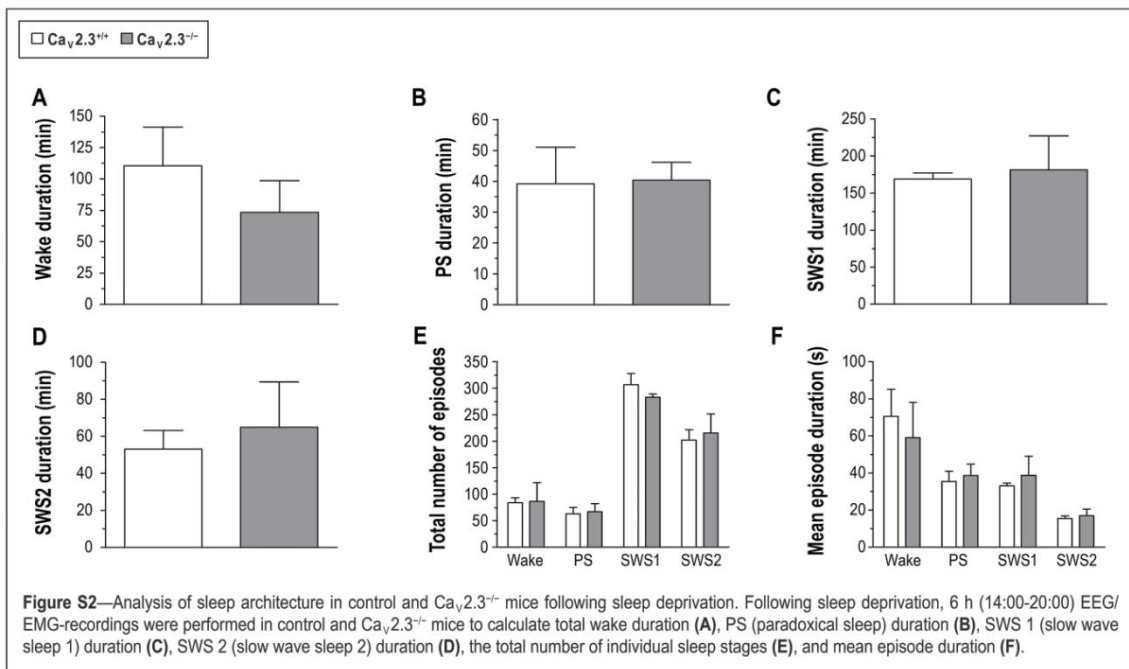
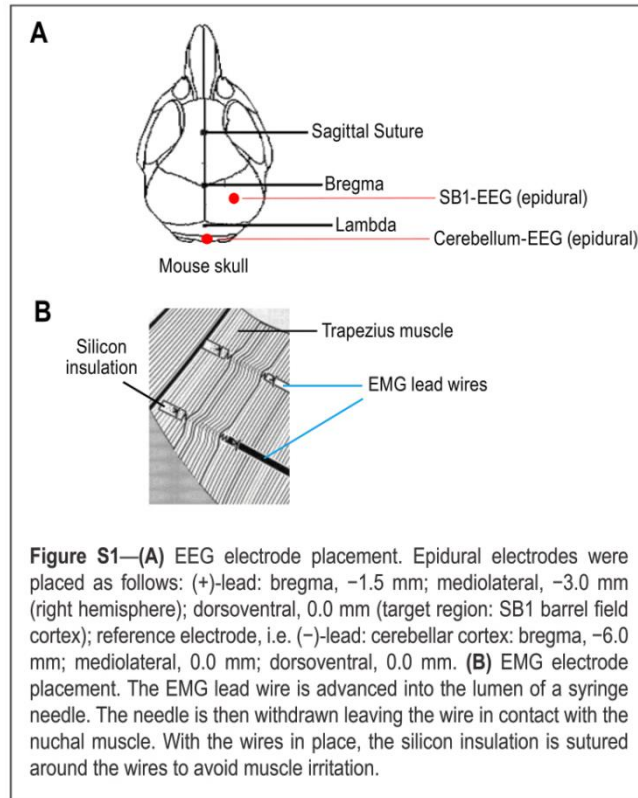
## **Acknowledgments**

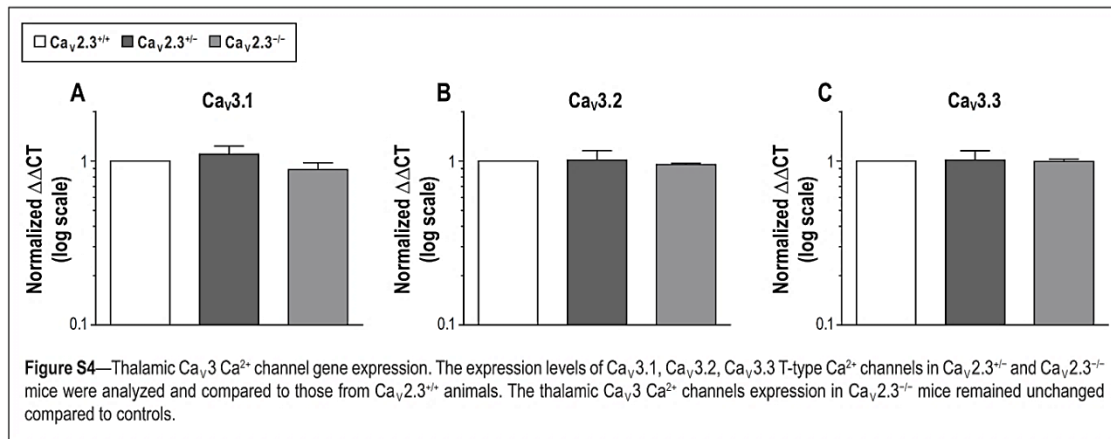
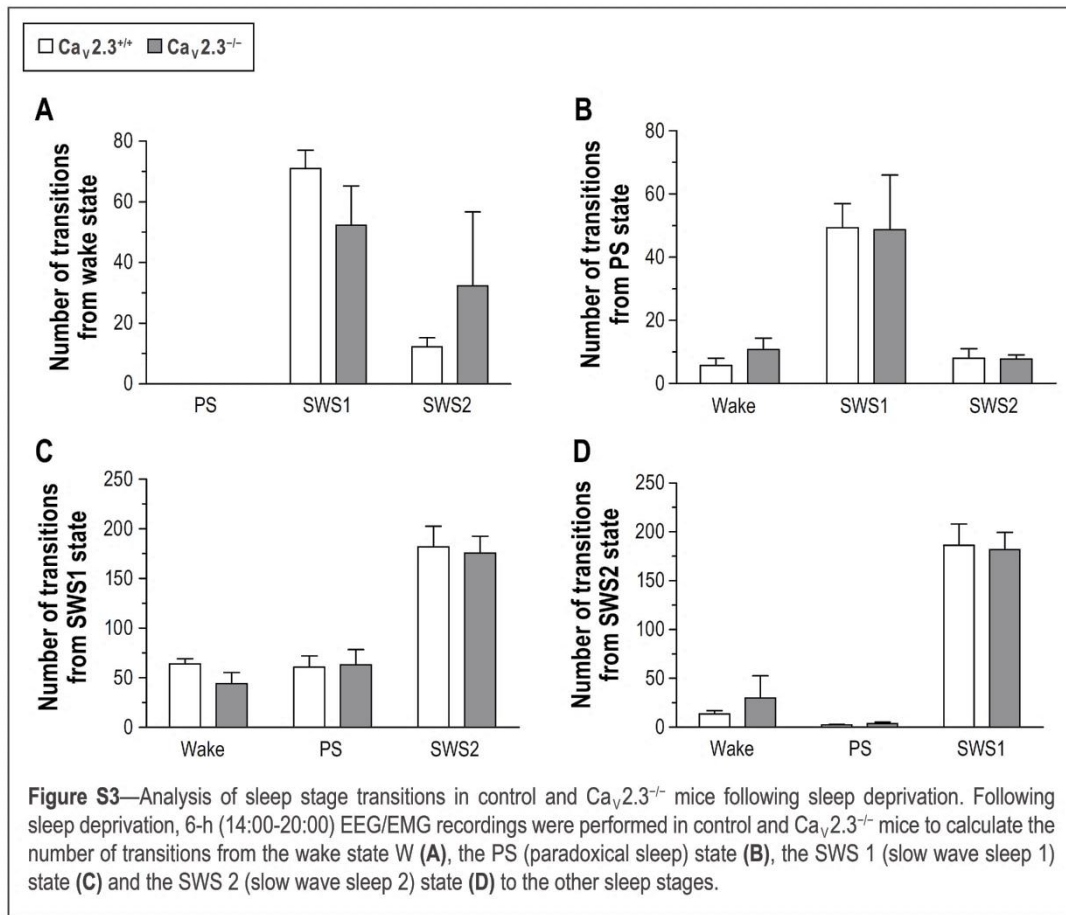
The authors are grateful to Richard J. Miller (Department of Neurobiology Pharmacology, and Physiology, The University of Chicago) for providing  $Ca_v2.3^{+/-}$  embryos. The authors would also like to thank YlvaMende (DZNE) and MichaelaMoehring (DZNE) for assistance in animal breeding and animal health care. This work was financially supported by the Federal Institute for Drugs and Medical Devices (Bundesinstitut für Arzneimittel und Medizinprodukte, BfArM, Germany).

## **Conflict of interest**

The authors confirm that there are no conflicts of interests.

# Supplement









## 2.2 Limited effects of an eIF2 $\alpha$ <sup>S51A</sup> allele on neurological impairments in the 5XFAD mouse model of Alzheimer's disease

Katharina Paesler<sup>1</sup>, Moritz M. Hettich<sup>1</sup>, Kan Xie<sup>1</sup>, Magdalena E. Siwek<sup>2</sup>, Devon P. Ryan<sup>1</sup>, Susanne Schröder<sup>1</sup>, Anna Papazoglou<sup>2</sup>, Karl Broich<sup>2</sup>, Ralf Müller<sup>3</sup>, Astrid Becker<sup>4</sup>, Alexander Garthe<sup>5</sup>, Gerd Kempermann<sup>5</sup>, Marco Weiergräber<sup>2</sup>, and Dan Ehninger<sup>1</sup>

<sup>1</sup>German Center for Neurodegenerative Diseases (DZNE), Ludwig-Erhard-Allee 2, 53175 Bonn, Germany; <sup>2</sup>Federal Institute for Drugs and Medical Devices (BfArM), Kurt-Georg-Kiesinger-Allee 3, 53175 Bonn, Germany; <sup>3</sup>Department of Psychiatry and Psychotherapy, University of Cologne, Kerpener Str. 62, 50937 Köln, Germany; <sup>4</sup>Institute of Molecular Psychiatry, University of Bonn, Sigmund-Freud-Str. 25, 53125 Bonn, Germany; <sup>5</sup>German Center for Neurodegenerative Diseases (DZNE), Fetscherstraße 105, 01307 Dresden, Germany.

**Submitted: October, 2013; In Revision**

### Abstract

Alzheimer's disease (AD) has been associated with increased phosphorylation of the translation initiation factor eIF2 $\alpha$  at serine 51. Increased phosphorylation of eIF2 $\alpha$  causes global repression of protein synthesis, while stimulating the expression of specific transcripts, such as those encoding activating transcription factor 4 (ATF4) and  $\beta$ -site APP cleaving enzyme 1 (BACE1). Increased expression of ATF4 may inhibit synaptic plasticity, learning and memory, whereas elevated BACE1 levels may promote amyloid- $\beta$  (A $\beta$ ) generation and therefore favor amyloid accumulation in the brain. To analyze if increased levels of phosphorylated eIF2 $\alpha$  indeed promote learning and memory impairments and/or amyloidogenesis in a mouse model of Alzheimer's disease, we crossed 5XFAD transgenic mice with an eIF2 $\alpha$ <sup>S51A</sup> knock-in line that expresses the non-phosphorylatable eIF2 $\alpha$  variant eIF2 $\alpha$ <sup>S51A</sup>. Behavioural assessment of the resulting mice revealed motor and cognitive deficits in 5XFAD mice that were, for the most part, not restored by the eIF2 $\alpha$ <sup>S51A</sup> allele. The eIF2 $\alpha$ <sup>S51A</sup> allele, however, appeared to have a rescue effect on hyperactivity in the 5XFAD model, the mechanistic underpinnings of which deserve further attention in future studies. Telemetric intracranial EEG recordings revealed seizures in both groups with the 5XFAD transgene, indicating that the eIF2 $\alpha$ <sup>S51A</sup> allele had no measureable effect on epileptic activity in this model. Transcriptome analyses showed clear transcriptional alterations in 5XFAD hippocampus that were not corrected by the eIF2 $\alpha$ <sup>S51A</sup> allele. In contrast to prior studies, our immunoblot analyses did not reveal increased levels of p-eIF2 $\alpha$  and BACE1 in the

hippocampus of 5XFAD mice, suggesting that elevated p-eIF2 $\alpha$  levels are not a universal feature of Alzheimer's disease models.

Collectively, our data indicate that 5XFAD-related pathologies do not necessarily require hyperphosphorylation of eIF2 $\alpha$  to emerge; they also show that heterozygosity for the non-phosphorylatable eIF2 $\alpha$ <sup>S51A</sup> allele has limited effects on 5XFAD-related disease manifestations.

## Introduction

Alzheimer's disease is associated with progressive cognitive and neurological impairments. Synaptic dysfunction downstream of toxic amyloid species is thought to play a major role in altered brain function and cognitive impairments in Alzheimer's disease (Palop and Mucke, 2010). A growing body of literature suggests that translational regulatory mechanisms are disrupted in Alzheimer's disease (Ding et al., 2005; Gamliel et al., 2002; Langstrom et al., 1989). More specifically, Alzheimer's disease has been associated with elevated phosphorylation levels of the eukaryotic translation initiation factor 2 $\alpha$  (eIF2 $\alpha$ ) (Chang et al., 2002; Choi et al., 2007; Kim et al., 2007; O'Connor et al., 2008). eIF2 $\alpha$  is phosphorylated in the context of cellular stress responses, such as the unfolded protein response; increased eIF2 $\alpha$  phosphorylation then leads to a general inhibition of protein synthesis (Harding et al., 1999). In addition, elevated eIF2 $\alpha$  phosphorylation favors the translational expression of certain mRNAs, such as the ones encoding for the transcription factor ATF4 (Blais et al., 2004). *De novo* protein synthesis is well known to play important roles in the establishment of long-lasting synaptic plasticity and the formation of long-term memory (Costa-Mattioli et al., 2009; Klann and Dever, 2004). Hyperphosphorylation of eIF2 $\alpha$  may interfere with protein synthesis-dependent forms of plasticity and memory formation by inhibiting *de novo* protein synthesis (Costa-Mattioli et al., 2005). Additionally, eIF2 $\alpha$  hyperphosphorylation may perturb synaptic plasticity and memory formation by suppressing CREB-dependent gene expression via upregulation of ATF4 (Costa-Mattioli et al., 2005). These considerations suggest that p-eIF2 $\alpha$ -mediated translational and transcriptional effects may contribute to altered plasticity and cognitive dysfunction in Alzheimer's disease. Indeed, it was reported recently that the genetic removal of either of two different eIF2 $\alpha$  kinases (Perk and Gcn2, respectively) restores plasticity and memory impairments in an APP/PS1 mouse model of Alzheimer's disease (Ma et al., 2013). We, here, set out to explore the role of eIF2 $\alpha$  phosphorylation in Alzheimer's pathogenesis by crossing the 5XFAD mouse model (Oakley et al., 2006) with an eIF2 $\alpha$ <sup>S51A</sup> knock-in line (Scheuner et al., 2001), in which eIF2 $\alpha$  cannot be phosphorylated on the mutant allele due to substitution of serine at residue 51 by alanine. We analyzed the effects of the eIF2 $\alpha$ <sup>S51A</sup> allele on cognitive impairments, as well as general disease progression seen in 5XFAD animals.

## Material and Methods

### *Animals*

5XFAD mice (genetic background: B6/SJL) overexpress mutant forms of human *APP* (the Swedish mutation: K670N, M671L; the Florida mutation: I716V; the London mutation: V717I) and mutant *PSEN1* (M146L, L286V) (Oakley et al., 2006).  $eIF2\alpha^{+/S51A}$  mice (genetic background: C57BL/6J) were generated as previously described (Scheuner et al., 2001). 5XFAD mice were crossed with  $eIF2\alpha^{+/S51A}$  mice, yielding animals of four different genotypes: wild-type, 5XFAD, 5XFAD; $eIF2\alpha^{+/S51A}$ ,  $eIF2\alpha^{+/S51A}$ . Our studies were performed using heterozygous  $eIF2\alpha^{S51A}$  mutant mice because homozygous  $eIF2\alpha^{S51A}$  mutants die shortly after birth (Scheuner et al., 2001) and are therefore not suitable to address the aims of the present paper. One cohort of animals was generated for behavioural and neurological assessments. Tests were conducted in the following order / at the following age of the animals: open field (8 months, 11 months), wire hang test (10-11 months), tail suspension test (10-11 months), Morris water maze (12 months), contextual fear conditioning (13-14 months). Ages of animals used for electrophysiological, biochemical and gene expression analyses are provided in the respective sections below (see below). The present study was approved by 'Landesamt für Natur, Umwelt und Verbraucherschutz Nordrhein-Westfalen' (Recklinghausen, Germany).

### *Tail suspension test*

Assessment of pathological hindlimb clasping was performed using the tail suspension test. Hindlimb movements in the test were assigned to one of the four following categories: 1 = normal hindlimb movements, 2 = intermittent clasping of one hindlimb, 3 = intermittent clasping of both hindlimbs, 4 = enduring clasping of both hindlimbs. Statistical analysis was performed by ordered logistic regression with the factors of "5XFAD genotype" (5XFAD transgenes present vs. absent) and " $eIF2\alpha$  genotype" ( $eIF2\alpha^{+/S51A}$  vs.  $eIF2\alpha^{+/+}$ ).

### *Wire hang test*

Mice were placed on a wire cage lid, which was turned upside down and positioned about 25 cm above an empty cage. Latency to fall was recorded with a maximum duration of 10 min. Mice received one trial per day over a period of 3 days (latencies

were averaged across these trials). Statistical analysis was performed using two-way ANOVA with the between-subject factors “5XFAD genotype” (5XFAD transgenes present vs. absent) and “eIF2 $\alpha$  genotype” (eIF2 $\alpha$ <sup>+S51A</sup> vs. eIF2 $\alpha$ <sup>+/+</sup>).

### ***Open field***

To assess motor activity in a novel environment, mice were placed in an open field (27.5 cm x 27.5 cm x 20 cm) for 20 min on each of 3 consecutive days. The distance travelled was recorded using the EthoVision XT video tracking system (Noldus, Wageningen, the Netherlands) and an average across all 3 sessions was calculated for each animal. Statistical analysis was performed using two-way ANOVA with the between-subject factors “5XFAD genotype” (5XFAD transgenes present vs. absent) and “eIF2 $\alpha$  genotype” (eIF2 $\alpha$ <sup>+S51A</sup> vs. eIF2 $\alpha$ <sup>+/+</sup>).

### ***Morris water maze***

Mice were trained on a hidden version of the Morris water maze ( $\varnothing$  135 cm). In this task animals learned to find an escape platform ( $\varnothing$  10 cm) hidden underneath the water surface in a constant location of the pool. Mice received 6 training trials per day for 7 consecutive days. Training trials were completed when the animal had reached the escape platform or when 60 s were elapsed, whichever came first. During training trials, animals were started from randomly alternating starting positions. If animals did not manage to get on the escape platform within 60 s, they were gently guided to the escape platform. There was a 15 s post-trial period on the escape platform. To test how well the animals had learned the position of the escape platform, we gave a probe trial at the end of training day 7. During the probe trial the platform was removed from the pool and the swim pattern was analyzed (with respect to quadrant occupancy and target crossings). After completion of the 7 days of hidden training, we gave one day of cued training (6 trials), during which the platform position was indicated by a visible cue. Swim patterns of mice were recorded using the EthoVision XT video tracking system (Noldus, Wageningen, the Netherlands). Time spent in quadrants and target crossings were analyzed using the built-in features of the software. Further analyses were done based on the raw time-tagged xy-coordinates using Matlab (The Mathworks). Search strategies were classified according to parameters described in our previous study (Garthe et al., 2009), originally based on (Balschun et al., 2003). Search strategies were defined by no more than two quantitative parameters that were chosen to reflect the

unique abstract properties of a given strategy and that were not dependent on the specific pool dimensions used. Statistical analysis of the groups was done by three-way repeated-measures ANOVA with the between-subject factors “5XFAD genotype” (5XFAD transgenes present vs. absent) and “eIF2 $\alpha$  genotype” (eIF2 $\alpha$ <sup>+S51A</sup> vs. eIF2 $\alpha$ <sup>+/+</sup>) and one of the following within-subjects factors: training trials (for the analysis of the escape latency curves), quadrants (for the analysis of probe trial data, i.e. target crossings and quadrant occupancy, respectively).

### ***Contextual fear conditioning***

Mice were placed in a conditioning chamber (Med Associates, St. Albans, Vermont, USA) for 3 min and received foot shocks (0.75 mA, 2 s) after minutes 1 and 2. One day later, for testing, mice were again placed in the conditioning chamber for a period of 3 min. Freezing behaviour, as well as activity levels during the baseline (i.e., first minute on the training day) and the test were recorded and analysed using Video Fear Conditioning software (Med Associates, St. Albans, Vermont, USA). Due to differences in baseline activity levels between groups (data not shown), we do not report freezing scores, but report activity suppression ratios instead, which were calculated as follows:  $\text{activity}_{\text{test}} / (\text{activity}_{\text{baseline}} + \text{activity}_{\text{test}})$ . Statistical comparison of the groups was performed by two-way ANOVA with the between-subject factors “5XFAD genotype” (5XFAD transgenes present vs. absent) and “eIF2 $\alpha$  genotype” (eIF2 $\alpha$ <sup>+S51A</sup> vs. eIF2 $\alpha$ <sup>+/+</sup>).

### ***Radiotelemetric EEG recordings***

Mice (>10 months of age) were anesthetized by intraperitoneal injection containing ketamine (KetanestR, Parke-Davis/Pfizer, Germany) / xylazine (RompunR 2%, Bayer Vital, Germany) at 100/10mg/kg. For measuring of the electroencephalogram (EEG), TL11M2-F20-EET 2-channel transmitters (technical specification: 3.9 g, 1.9 cc; Data Science International (DSI), USA) were implanted into a subcutaneous pouch on the back of the animals. The first channel was used to target the primary motor cortex region (M1). A differential epidural electrode was placed at the following stereotaxic coordinates: (M1)-lead bregma +1 mm, lateral of bregma 1.5 mm (left hemisphere). For deep brain recordings targeting the hippocampal CA1 region, the differential electrode of channel 2 was positioned as follows: (CA1)-lead, bregma -2 mm, lateral of bregma 1.5 mm (right hemisphere), dorsoventral (depth) 1.5 mm. For both channels, epidural reference electrodes were placed at: bregma -6 mm, lateral of bregma 1 mm (left

hemisphere) and bregma -6 mm, lateral of bregma 1 mm (right hemisphere). Electrodes were fixed at the neurocranium using glass ionomer cement (Kent Express, UK), and the scalp was closed using over and over sutures (Ethilon, 6-0). A detailed description of the implantation procedure is provided elsewhere (Weiergraber et al., 2005). For post-operative pain management carprofen (5 mg/kg; Rimadyl, Pfizer, Germany) was administered subcutaneously to the animals. Following a 10-day recovery period, simultaneous video-EEG recordings from the motor cortex (M1) and the hippocampal CA1 region were performed for 48 h using Dataquest ART 4.2 software (DSI) at a sampling rate of 500 Hz with no *a priori* filter cut-off. For further analyses, data were processed using Neuroscore<sup>®</sup> 2.1 (DSI). Seizure analyses and calculations were performed using Neuroscore Spike Train Detector, i.e. a seizure detection module. Seizure protocols contained total number of episodes and spikes, spike frequency, total spike train duration, shortest and longest spike train duration.

### ***Histology and immunostaining***

Mice (13 months old) were anaesthetized by intraperitoneal injection of ketamine (100 mg/kg) and xylazine (7 mg/kg). For perfusion, the bloodstream was rinsed with sterile 0.9% sodium chloride and organs were fixed using 4% paraformaldehyde (PFA) in phosphate buffered saline (PBS). Brains were dissected and post-fixed in 4% PFA in PBS overnight at 4°C and dehydrated in 30% sucrose in PBS at 4°C. Coronal brain sections of 40 µm thickness were cut using a sliding microtome (Leica, Wetzlar, Germany) and were stored in cryoprotectant buffer (0.05 M phosphate buffer, 25% glycerol and 25% ethylene glycol) at -20°C. Brain sections spaced 240 µm apart were transferred into Tris-buffered saline (TBS), washed twice for 5 min each and incubated in 0.6% H<sub>2</sub>O<sub>2</sub> in TBS for 30 min. Sections were then washed three times in TBS for 5 min. For blocking, sections were incubated for 30 min in TBS-plus (TBS, 0.1% Triton X-100 and 3% donkey serum). Next, sections were incubated with primary antibody (rabbit anti-choline acetyltransferase (ChAT), 1:100, Millipore, Darmstadt, Germany) in TBS-plus for 48 h at 4°C, washed twice in TBS for 5 min and blocked in TBS-plus for 45 min. This was followed by a 1-hour incubation step (at room temperature) in TBS-plus containing biotin-conjugated secondary antibody (donkey anti-rabbit, 1:500, Jackson ImmunoResearch Laboratories, West Grove, Pennsylvania, USA). Sections were then washed three times in TBS for 5 min and incubated in 3,3'-Diaminobenzidine (DAB) for 2 min using the DAB Substrate Kit (Roche, Mannheim, Germany). To stop

the peroxidase reaction, sections were washed in tap water and TBS. Next, sections were mounted on glass slides, dehydrated in an ascending series of alcohol (twice 70%, once 96%, twice 100% Ethanol), cleared in xylene and covered with a coverslip. Stereological analysis of brain sections was performed using a bright field microscope Eclipse 90i (Nikon, Düsseldorf, Germany). Immunoreactive neurons within the medial septum (MS) and vertical limb of the diagonal band of Broca (VDB) were quantified using the software Stereo Investigator (MBF Bioscience, Magdeburg, Germany). Statistical analysis was performed via two-way ANOVA with the between-subject factors “5XFAD genotype” (5XFAD transgenes present vs. absent) and “eIF2 $\alpha$  genotype” (eIF2 $\alpha$ <sup>+S51A</sup> vs. eIF2 $\alpha$ <sup>+/+</sup>).

### ***Immunoblot analysis***

Hippocampal samples were taken from 14- to 15-month-old mice after cervical dislocation and snap-frozen in liquid nitrogen. Each sample was homogenized in 250  $\mu$ l lysis buffer containing RIPA buffer, Phospho-Stop (Roche, Mannheim, Germany), Protease-Inhibitor (Roche, Mannheim, Germany), 50 mM sodium fluoride and 5 mM sodium orthovanadate and incubated on a rotator for 30 min at 4°C. Samples were centrifuged at 14000 rpm for 15 min at 4°C. Protein concentration was determined using the Pierce BCA protein assay kit (Thermo Fisher Scientific, Bonn, Germany). If not stated otherwise, 15  $\mu$ g protein was loaded on 10% tris glycine gels (APP, BACE1, ChAT, eIF2 $\alpha$ ) or 16% tris tricine gels (CTF) for PAGE. Proteins were transferred onto a polyvinylidene difluoride (PVDF) membrane and incubated in TBS with 10% Western Blocking Reagent (Roche, Mannheim, Germany) for 1 h. Incubation of PVDF membrane in primary antibody (rabbit anti-eIF2 $\alpha$ , 1:2000, Cell Signaling, Danvers, Massachusetts, USA; rabbit anti-p-eIF2 $\alpha$ , 1:2000, Cell Signaling, Danvers, Massachusetts, USA; rabbit anti-APP, 1:1000, Cell Signaling, Danvers, Massachusetts, USA; rabbit anti-CTF, 1:1000, Sigma-Aldrich, Taufkirchen, Germany; rabbit anti-BACE1, 1:1000, Abcam, Cambridge, UK; goat anti-ChAT, 1:1000, Millipore, Darmstadt, Germany; mouse anti Beta Amyloid, clone 6E10, 1:1000, Covance, Princeton, NJ, USA; mouse anti- $\alpha$ -tubulin, 1:20000, Abcam, Cambridge, UK; mouse anti- $\beta$ -actin, 1:5000, MP Biomedicals, Solon, Ohio, USA) in TBS with 5% Western Blocking Reagent was carried out overnight at 4°C. After multiple washing steps in TBS with 0.1% Tween-20, membranes were incubated in horseradish peroxidase-conjugated secondary antibody (donkey anti-rabbit IgG, 1:1000, Jackson



ImmunoResearch Laboratories, West Grove, Pennsylvania, USA; donkey anti-mouse IgG, 1:1000, Jackson ImmunoResearch Laboratories, West Grove, Pennsylvania, USA; donkey anti-goat IgG, 1:10000, Jackson ImmunoResearch Laboratories, West Grove, Pennsylvania, USA) in TBS with 5% Western Blocking Reagent (for 1 h at room temperature or overnight at 4°C). Next, membranes were washed several times in TBS with 0.1% Tween-20. Immunosignals were detected using enhanced chemiluminescence (Amersham ECL Western Blotting Detection Reagents, GE Healthcare, Munich, Germany or SuperSignal West Femto Maximum Sensitivity Substrate, Thermo Fisher Scientific, Bonn, Germany) and were quantified using a Chemidoc XRS imager (Bio-Rad, Munich, Germany). Densitometric analysis was performed using Image Lab software (Bio-Rad, Munich, Germany). Proteins were normalized to  $\alpha$ -tubulin or  $\beta$ -actin, phosphorylated proteins were normalized to their respective total proteins. eIF2 $\alpha$  and p-eIF2 $\alpha$  were detected on different blots together with the respective loading controls. Statistical analysis was accomplished by t-test or two-way ANOVA with the between-subject factors “5XFAD genotype” (5XFAD transgenes present vs. absent) and “eIF2 $\alpha$  genotype” (eIF2 $\alpha$ <sup>+S51A</sup> vs. eIF2 $\alpha$ <sup>+/+</sup>), as appropriate.

#### ***Amyloid beta enzyme-linked immunosorbent assays***

Hippocampal homogenates in RIPA buffer (as described above) were used for quantitative analysis of the two abundant species of Amyloid  $\beta$  (A $\beta$ ), A $\beta$ 40 and A $\beta$ 42, using ELISA kits (Life Technologies, Carlsbad, CA, USA) according to manufacturer’s instructions. Amounts of A $\beta$  peptides were subsequently normalized to protein concentration of each respective sample.

#### ***RNA extraction and Affymetrix microarray procedures***

Microarray experiments were carried out using Mouse Exon ST arrays (Affymetrix). Total RNA (250 ng) with integrity numbers about 10 of 14- to 15-month-old mice was used as starting material. Arrays were washed and stained according to the manufacturer’s recommendations. Labeled and purified cDNA was fragmented (5.5  $\mu$ g) and subsequently hybridized to the arrays before scanning in a GeneChip 3000 7G scanner (Affymetrix). Normalization to the median of all samples, background correction as well as statistical analysis was performed with GeneSpringGX software (Agilent technologies). An implemented GC-RMA algorithm was applied on all chips to summarize probe level information. Microarray data were analyzed using unpaired t-

tests. An uncorrected significance level  $p < 0.05$  was adopted in all instances. Differentially regulated transcripts with a fold change (FC) greater than 1.6 were then subjected to hierarchical clustering analysis in order to visualize gene expression changes across groups. Array data are available in the GEO database under GSE50521. DAVID (Huang et al., 2009) was used to carry out gene ontology enrichment analyses in the gene set differentially expressed between 5XFAD and wild-type controls.

### ***Statistical analyses***

Statistical analyses were performed as described above.  $P < 0.05$  was considered statistically significant.

## Results

In order to test if increased eIF2 $\alpha$  phosphorylation contributes to cognitive dysfunction and disease progression in 5XFAD mice, we crossed these mice with an eIF2 $\alpha$ <sup>S51A</sup> knock-in line (Scheuner et al., 2001), in which eIF2 $\alpha$  cannot be phosphorylated on one allele due to substitution of serine at residue 51 by alanine. We performed Western blot analyses to measure the abundance of p-eIF2 $\alpha$  (i.e., eIF2 $\alpha$  phosphorylated at serine 51), total eIF2 $\alpha$ , BACE1, APP and APP cleavage products in lysates prepared from hippocampal tissue of 5XFAD, 5XFAD;eIF2 $\alpha$ <sup>+S51A</sup>, eIF2 $\alpha$ <sup>+S51A</sup> animals as well as wild-type controls. Unexpectedly, our analyses showed no significant effect of the 5XFAD transgenes on p-eIF2 $\alpha$  levels (**Figure 1A**; two-way ANOVA with between-subjects factors 5XFAD genotype and eIF2 $\alpha$  genotype, effect of 5XFAD genotype,  $p = 0.15$ ). Consistent with previously published work (O'Connor et al., 2008), the 5XFAD transgenes affected total eIF2 $\alpha$  levels with slightly increased eIF2 $\alpha$  abundance in animals bearing the 5XFAD transgenes (**Figure 1A**; two-way ANOVA with between-subjects factors 5XFAD genotype and eIF2 $\alpha$  genotype, effect of 5XFAD genotype,  $p = 0.01$ ). The eIF2 $\alpha$  phosphorylation status did not differ significantly between heterozygous carriers of the eIF2 $\alpha$ <sup>S51A</sup> mutation and animals carrying two wild-type eIF2 $\alpha$  alleles (**Figure 1A**; two-way ANOVA with between-subjects factors 5XFAD genotype and eIF2 $\alpha$  genotype, effect of eIF2 $\alpha$  genotype,  $p = 0.62$ ), which is in line with published data (Scheuner et al., 2001), and indicates that the heterozygous eIF2 $\alpha$ <sup>S51A</sup> mutation is not sufficient, at least under basal conditions, to reduce p-eIF2 $\alpha$  abundance (unlike the eIF2 $\alpha$ <sup>S51A</sup> mutation in the homozygous state that leads to the expected abolishment of eIF2 $\alpha$  phosphorylation (Scheuner et al., 2001). These biochemical findings suggest that an excessive eIF2 $\alpha$  phosphorylation is not a universal feature of Alzheimer's disease mouse models, such as 5XFAD mice, and they also indicate that the heterozygous eIF2 $\alpha$ <sup>S51A</sup> mutation is not sufficient to suppress hippocampal eIF2 $\alpha$  phosphorylation, at least under basal conditions. Further Western blot analyses showed no clear effects of the eIF2 $\alpha$ <sup>S51A</sup> mutation on the abundance of total APP (**Figure 1B**; two-way ANOVA with between-subjects factors 5XFAD genotype and eIF2 $\alpha$  genotype, effect of eIF2 $\alpha$  genotype,  $p = 0.31$ ), human APP (**Figure 1B**; t-test, 5XFAD vs. 5XFAD;eIF2 $\alpha$ <sup>+S51A</sup>,  $p = 0.97$ ), and APP cleavage products (**Figure 1C**;  $\alpha$ -CTF, t-test, 5XFAD vs. 5XFAD;eIF2 $\alpha$ <sup>+S51A</sup>,  $p = 0.66$ ;  $\beta$ -CTF, t-test, 5XFAD vs. 5XFAD;eIF2 $\alpha$ <sup>+S51A</sup>,  $p = 0.39$ ). ELISA analyses showed no group differences regarding

hippocampal A $\beta$ 40 and A $\beta$ 42 concentrations (**Figure 1D**; A $\beta$ 40, t-test, 5XFAD vs. 5XFAD; eIF2 $\alpha$ <sup>+S51A</sup>,  $p = 0.90$ ; A $\beta$ 42, t-test, 5XFAD vs. 5XFAD; eIF2 $\alpha$ <sup>+S51A</sup>,  $p = 0.30$ ). Western blot analyses of BACE1 abundance also showed no discernable difference between groups (**Figure 1E**; two-way ANOVA with between-subjects factors 5XFAD genotype and eIF2 $\alpha$  genotype, effect of 5XFAD genotype,  $p = 0.77$ ; effect of eIF2 $\alpha$  genotype,  $p = 0.81$ ; 5XFAD x eIF2 $\alpha$  interaction,  $p = 0.75$ ). In line with these biochemistry results, our behavioural, electrophysiological and gene expression analyses revealed limited effects of the eIF2 $\alpha$ <sup>S51A</sup> allele on disease phenotypes present in 5XFAD mice, as outlined below. In brief, the eIF2 $\alpha$ <sup>S51A</sup> allele did not appear to ameliorate pathological hindlimb claspings in 5XFAD mice (**Figure 2A**; ordered logistic regression, effect of 5XFAD transgenes,  $p < 0.0001$ ; effect of eIF2 $\alpha$  genotype  $p = 0.941$ ; 5XFAD genotype x eIF2 $\alpha$  genotype interaction,  $p = 0.081$ ), nor was there any apparent effect on motor impairments as measured in the wire hang test (**Figure 2B**; two-way ANOVA with between-subjects factors 5XFAD genotype and eIF2 $\alpha$  genotype, effect of 5XFAD genotype,  $p < 0.0001$ ; effect of eIF2 $\alpha$  genotype,  $p = 0.56$ ; 5XFAD x eIF2 $\alpha$  interaction,  $p = 0.87$ ). We analyzed learning and memory using a context fear conditioning paradigm (**Figure 2C**) and the Morris water maze (**Figure 2D-G**). In context fear conditioning, 5XFAD mice showed higher activity suppression scores upon testing, indicative of associative learning impairments in these animals (**Figure 2C**; two-way ANOVA with between-subjects factors 5XFAD genotype and eIF2 $\alpha$  genotype, effect of 5XFAD genotype,  $p = 0.0003$ ), that were not influenced by the eIF2 $\alpha$ <sup>S51A</sup> allele in any obvious way (**Figure 2C**; two-way ANOVA with between-subjects factors 5XFAD genotype and eIF2 $\alpha$  genotype, effect of eIF2 $\alpha$  genotype,  $p = 0.94$ ; 5XFAD x eIF2 $\alpha$  interaction,  $p = 0.87$ ). In the Morris water maze, 5XFAD animals showed substantially higher escape latencies during training trials than controls (**Figure 2D**; three-way repeated-measures ANOVA with 5XFAD genotype and eIF2 $\alpha$  genotype as between-subjects factors and training trial as within-subjects factor, effect of 5XFAD transgenes,  $p < 0.0001$ ; effect of eIF2 $\alpha$  genotype,  $p = 0.76$ ; 5XFAD x eIF2 $\alpha$  interaction,  $p = 0.67$ ), as well as a reduced number of target crossings during the probe trial given after completion of training (**Figure 2F**; three-way repeated-measures ANOVA with 5XFAD genotype and eIF2 $\alpha$  genotype as between-subjects factors and quadrant as within-subjects factor, 5XFAD genotype x quadrant interaction,  $p = 0.03$ ; eIF2 $\alpha$  genotype x quadrant interaction:  $p = 0.89$ ; eIF2 $\alpha$  genotype x 5XFAD genotype x quadrant interaction:  $p = 0.58$ ). An extended strategy analysis, in the context of which

behaviours during the training trials were classified into increasingly hippocampus-dependent (directed search, focal search, direct swimming), as well as primarily hippocampus-independent (chaining, scanning, random search, thigmotaxis) search categories, revealed an excessive use of less hippocampus-dependent strategies in animals with the 5XFAD transgenes (**Figure 2G**). The eIF2 $\alpha$ <sup>S51A</sup> allele had no obvious modulatory effect on any of these 5XFAD water maze phenotypes (**Figure 2D-G**). Our behavioural analyses did, however, reveal one neurobehavioural 5XFAD phenotype that appeared to be restored by the eIF2 $\alpha$ <sup>S51A</sup> allele (**Figure 2H,I**). 5XFAD animals showed pronounced motor hyperactivity in an open field assay (two-way ANOVA with 5XFAD genotype and eIF2 $\alpha$  genotype as between-subjects factors, effect of 5XFAD genotype,  $p = 0.02$  and  $0.0003$ , respectively). 5XFAD-related hyperactivity appeared to be reduced in animals carrying the eIF2 $\alpha$ <sup>S51A</sup> allele (two-way ANOVA with 5XFAD genotype and eIF2 $\alpha$  genotype as between-subjects factors, 5XFAD x eIF2 $\alpha$  genotype,  $p = 0.06$  for panel H and  $p = 0.07$  for panel I). The neurobiology underlying this possible eIF2 $\alpha$ <sup>S51A</sup>-mediated rescue of 5XFAD-related hyperactivity remains to be elucidated. Here, we considered one possibility and that is that the eIF2 $\alpha$ <sup>S51A</sup> allele modifies the degeneration of the cholinergic system in 5XFAD animals, which may contribute to hyperactive behaviours in AD mouse models (Bellucci et al., 2006; Boncristiano et al., 2002; Christensen et al., 2010; Devi and Ohno, 2010; Perez et al., 2007). Initial stereological cell countings showed neither a significant effect of the 5XFAD transgenes (two-way ANOVA with 5XFAD genotype and eIF2 $\alpha$  genotype as between-subjects factors, effect of 5XFAD genotype,  $p = 0.74$ ) nor an effect of the eIF2 $\alpha$ <sup>S51A</sup> allele (two-way ANOVA with 5XFAD genotype and eIF2 $\alpha$  genotype as between-subjects factors, effect of eIF2 $\alpha$  genotype,  $p = 0.32$ ) on the number of ChAT-positive neurons in the basal forebrain (**Supplementary Figure 1**). Western blot analyses of ChAT abundance in the hippocampus, one of the target areas that basal forebrain cholinergic neurons project into, however, revealed lower ChAT levels in animals carrying the 5XFAD transgenes (**Supplementary Figure 1**; two-way ANOVA with 5XFAD genotype and eIF2 $\alpha$  genotype as between-subjects factors, effect of 5XFAD genotype,  $p = 0.002$ ). The eIF2 $\alpha$ <sup>S51A</sup> allele had no apparent effect on hippocampal ChAT expression (two-way ANOVA with 5XFAD genotype and eIF2 $\alpha$  genotype as between-subjects factors, effect of eIF2 $\alpha$  genotype,  $p = 0.49$ ) and also showed no significant interaction with the 5XFAD genotype (two-way ANOVA with 5XFAD genotype and eIF2 $\alpha$  genotype as between-subjects factors, 5XFAD x eIF2 $\alpha$

genotype interaction,  $p = 0.78$ ), indicating that the  $eIF2\alpha^{S51A}$  allele did not protect against the hippocampal ChAT loss in 5XFAD mice. Network hyperexcitability and seizures are important features of animal models of Alzheimer's disease (Palop and Mucke, 2009; Verret et al., 2012). We performed electrocorticographic (M1) and deep intrahippocampal CA1 EEG recordings in 5XFAD animals crossed into the  $eIF2\alpha^{S51A}$  background (**Figure 3**). Qualitative and quantitative seizure analysis using Neuroscore Seizure Module (DSI) revealed that animals of all genotypes with the exception of wild-type animals exhibited seizure activity in the M1 recording, although ictal discharges were not seen in the deep, intrahippocampal CA1 recording (in none of the groups; not shown). Video analysis revealed that none of the cortical seizures was associated with motoric exacerbation. Thus, we observed predominantly non-convulsive seizure activity in 5XFAD mice.  $eIF2\alpha^{+/S51A}$  mice showed non-convulsive seizure activity as well and introduction of the  $eIF2\alpha^{S51A}$  mutation in 5XFAD mice did not appear to modify the epileptic phenotype in any apparent way. Alzheimer's disease is associated with considerable transcriptional alterations in key brain areas (Blalock et al., 2004; Colangelo et al., 2002; Liang et al., 2008; Loring et al., 2001). Microarray analyses performed on hippocampal tissue of 5XFAD animals crossed into the  $eIF2\alpha^{S51A}$  background revealed a number of 5XFAD-related transcriptional alterations: Statistical analysis applying an uncorrected significance level of  $p < 0.05$ , revealed 1421 transcripts differentially regulated between 5XFAD mice and wild-type controls. Of these transcripts, we highlight a set of 139 genes with a fold change greater than  $\pm 1.6$  (**Supplementary Figure 2**). Gene ontology analysis of these 139 candidate genes showed a substantial enrichment of immune-response related genes in this gene set (**Supplementary Table 1**), which is in agreement with considerable inflammatory and immunological alterations observed in the context of late-stage cerebral amyloidosis. Comparison of the expression patterns of 5XFAD and 5XFAD; $eIF2\alpha^{+/S51A}$  animals revealed a striking 98.56% congruence. Only 2 out of the 139 selected candidate genes differed in their expression pattern between 5XFAD and 5XFAD; $eIF2\alpha^{+/S51A}$  (H2-Aa (histocompatibility 2, class II antigen A) and Cd74 (HLA class II histocompatibility antigen gamma), indicating that the  $eIF2\alpha^{S51A}$  mutation only very slightly modified the hippocampal transcriptional changes induced by the 5XFAD transgenes.

## Discussion

In this study, we assessed the effects of a non-phosphorylatable eIF2 $\alpha$  allele (eIF2 $\alpha^{S51A}$ ) on disease progression in the 5XFAD mouse model of familial AD. While profound pathology was evident in 5XFAD mice, these abnormalities remained mostly unmodified by the heterozygous eIF2 $\alpha^{S51A}$  mutation. This was the case for a wide range of molecular (APP expression and processing; gene expression), electrophysiological (EEG) and neurobehavioural (motor impairments; learning and memory impairments) features of the model. In contrast to previously published elevated p-eIF2 $\alpha$  levels in the whole brain of 5XFAD mice (Devi and Ohno, 2010; O'Connor et al., 2008), we did not observe changes in hippocampal p-eIF2 $\alpha$  levels in 5XFAD and 5XFAD;eIF2 $\alpha^{+/S51A}$  mice. Also, hippocampal BACE1 expression levels did not differ between the groups of mice used in the present study. We currently do not know the factors that might account for these discrepant findings. Possibilities that need to be formally addressed in future studies include differences in genetic background, on which the 5XFAD mutations were kept, as well as differences in the brain areas examined (whole brain in previous reports (Devi and Ohno, 2010; O'Connor et al., 2008) versus hippocampus in the present study). Ma *et al.* recently reported that conditional homozygous deletion of either of two different eIF2 $\alpha$  kinases (Perk, Gcn2) in forebrain neurons improved spatial memory impairments in the APP<sup>swe</sup>/PSEN1<sup>dE9</sup> mouse model of Alzheimer's disease (Ma et al., 2013). Deletion of either Perk or Gcn2 led to reduced p-eIF2 $\alpha$  levels in this model (Ma et al., 2013), suggesting that these genetic manipulations were more effective in suppressing eIF2 $\alpha$  phosphorylation than the heterozygous eIF2 $\alpha^{S51A}$  mutation used in the present study. Accordingly, limited effects on neurological impairments observed in our study could be related to a less effective suppression of p-eIF2 $\alpha$  levels by the heterozygous eIF2 $\alpha^{S51A}$  mutation. Homozygous eIF2 $\alpha^{S51A}$  mutants could not be examined because of early postnatal lethality associated with this genotype (Scheuner et al., 2001). Moreover, amyloid pathology progresses at a faster pace in 5XFAD animals (used in the present study) than in the model examined by Ma *et al.* (APP<sup>swe</sup>/PSEN1<sup>dE9</sup> mice) and, hence, neurological impairments in the 5XFAD model may generally be less accessible to amelioration than those in APP<sup>swe</sup>/PSEN1<sup>dE9</sup> mice. One exception to the notion that the eIF2 $\alpha^{+/S51A}$  genotype did not influence 5XFAD phenotypes was the observation of restored motor hyperactivity in 5XFAD;eIF2 $\alpha^{+/S51A}$  mice. Elevated motor activity levels are a consistent feature of AD

rodent models (Dodart et al., 1999; Filali et al., 2011; Holcomb et al., 1998; Holcomb et al., 1999) and may also be observed in human individuals affected by the disorder (White et al., 2004). Alzheimer's disease is associated with a profound degeneration of cholinergic neurons in the basal forebrain (Cullen and Halliday, 1998; Jope et al., 1997; Vogels et al., 1990; Whitehouse et al., 1982). Given the role of basal forebrain cholinergic neurons in the regulation of motor activity levels (ablation of basal forebrain cholinergic nuclei, as well as anti-cholinergic pharmacological interventions increase motor activity in rats (Whishaw et al., 1985), we asked whether the eIF2 $\alpha$ <sup>S51A</sup> allele might restore hyperactivity by rescuing basal forebrain cholinergic neuron loss in 5XFAD mice. Our stereological analyses showed, however, no significant reduction of ChAT-immunoreactive neurons in the MS and VDB of 5XFAD mice, indicating that frank loss of cholinergic neurons was limited in the model at the age assessed. Nevertheless, immunoblot analyses were sensitive enough to pick up clear 5XFAD-related reductions in ChAT expression in one of the target areas of basal forebrain cholinergic nuclei, namely the hippocampus, which is consistent with prior studies in transgenic AD mouse models (Bellucci et al., 2006; Boncristiano et al., 2002; Christensen et al., 2010; Devi and Ohno, 2010; Perez et al., 2007). 5XFAD and 5XFAD;eIF2 $\alpha$ <sup>+S51A</sup> mice did not differ significantly in their hippocampal ChAT levels, indicating that the eIF2 $\alpha$ <sup>S51A</sup> allele did not rescue the aberrant cholinergic system of 5XFAD mice. Future studies should further assess the possible mechanistic underpinnings of the eIF2 $\alpha$ <sup>S51A</sup> effect on 5XFAD-related motor hyperactivity. In conclusion, our study revealed few effects of the eIF2 $\alpha$ <sup>+S51A</sup> genotype on disease progression in the 5XFAD mouse model of Alzheimer's disease (with the exception of a possible amelioration of 5XFAD-related motor hyperactivity). Future studies need to further elaborate on the specific conditions, under which a 5XFAD genotype may be associated with eIF2 $\alpha$  hyperphosphorylation, as well as elevated BACE1 levels.

### **Acknowledgements**

This work has been funded by the German Center for Neurodegenerative Diseases (DZNE) and by the Federal Institute for Drugs and Medical Devices (BfArM). We would like to thank the DZNE animal caretaker team for excellent technical support.



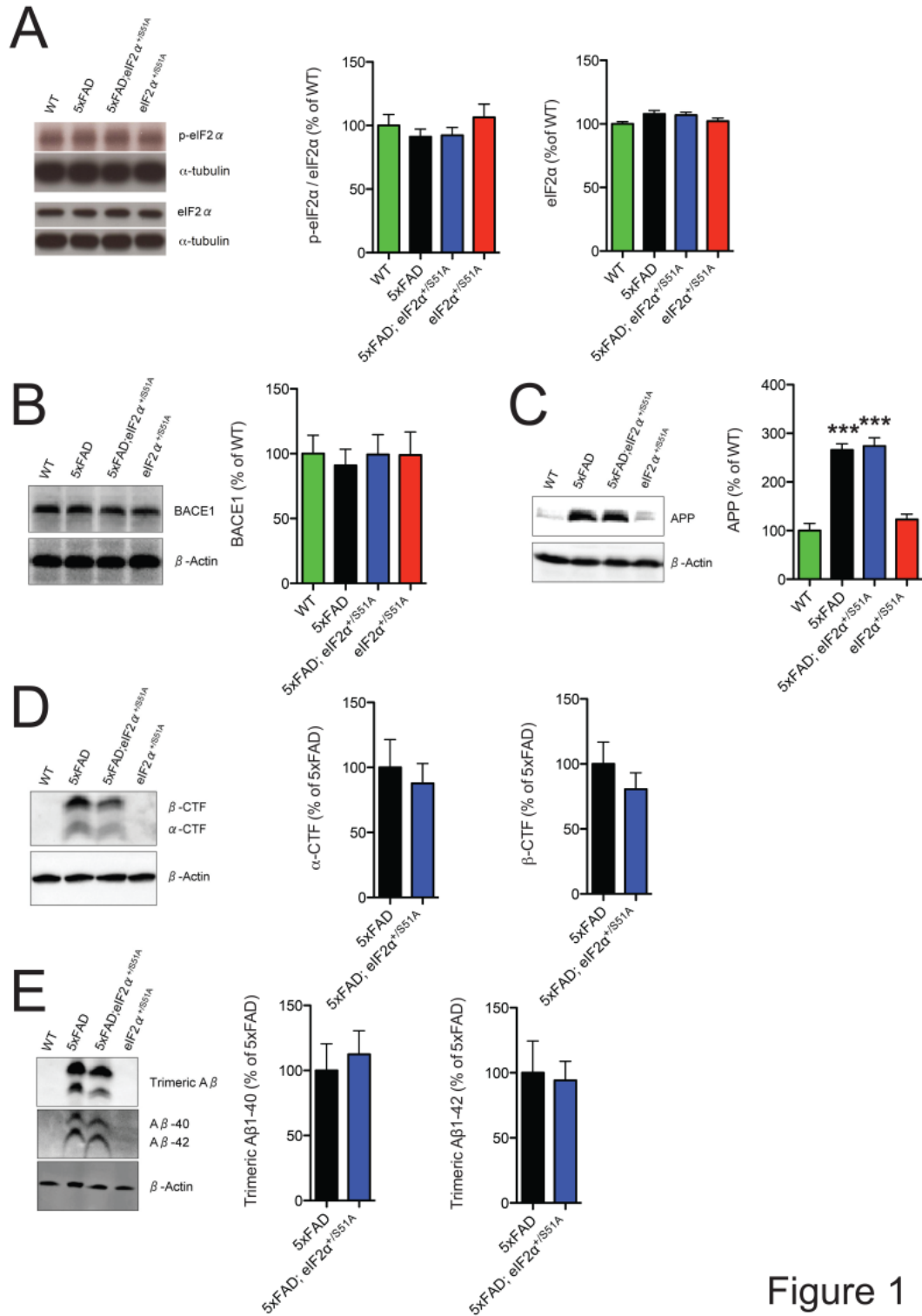


Figure 1

**Figure 1. The eIF2α<sup>S51A</sup> mutation had no measurable effects on eIF2α phosphorylation and APP processing.** Shown are representative immunoblots of p-eIF2α and total eIF2α (A), human APP and total APP (B), α-CTF and β-CTF (C), BACE1 (E), all prepared from hippocampal homogenates, along with the respective quantitative data from densitometric analyses ( $n = 5-7$  mice per group). (D) Concentrations of abundant Aβ-species, Aβ40 and Aβ42, in 5XFAD hippocampal

homogenates were determined using enzyme-linked immunosorbent assays. All data are presented as mean  $\pm$  SEM. Data were analyzed using 2-way ANOVAs with the between-subjects factors 5XFAD genotype / eIF2 $\alpha$  genotype (effect of 5XFAD transgenes; effect of eIF2 $\alpha$  genotype; 5XFAD x eIF2 $\alpha$  interaction) and t-tests (5XFAD vs. 5XFAD;eIF2 $\alpha^{S51A}$ ) as appropriate. Statistically significant differences ( $P < 0.05$ ) are denoted by bold font.

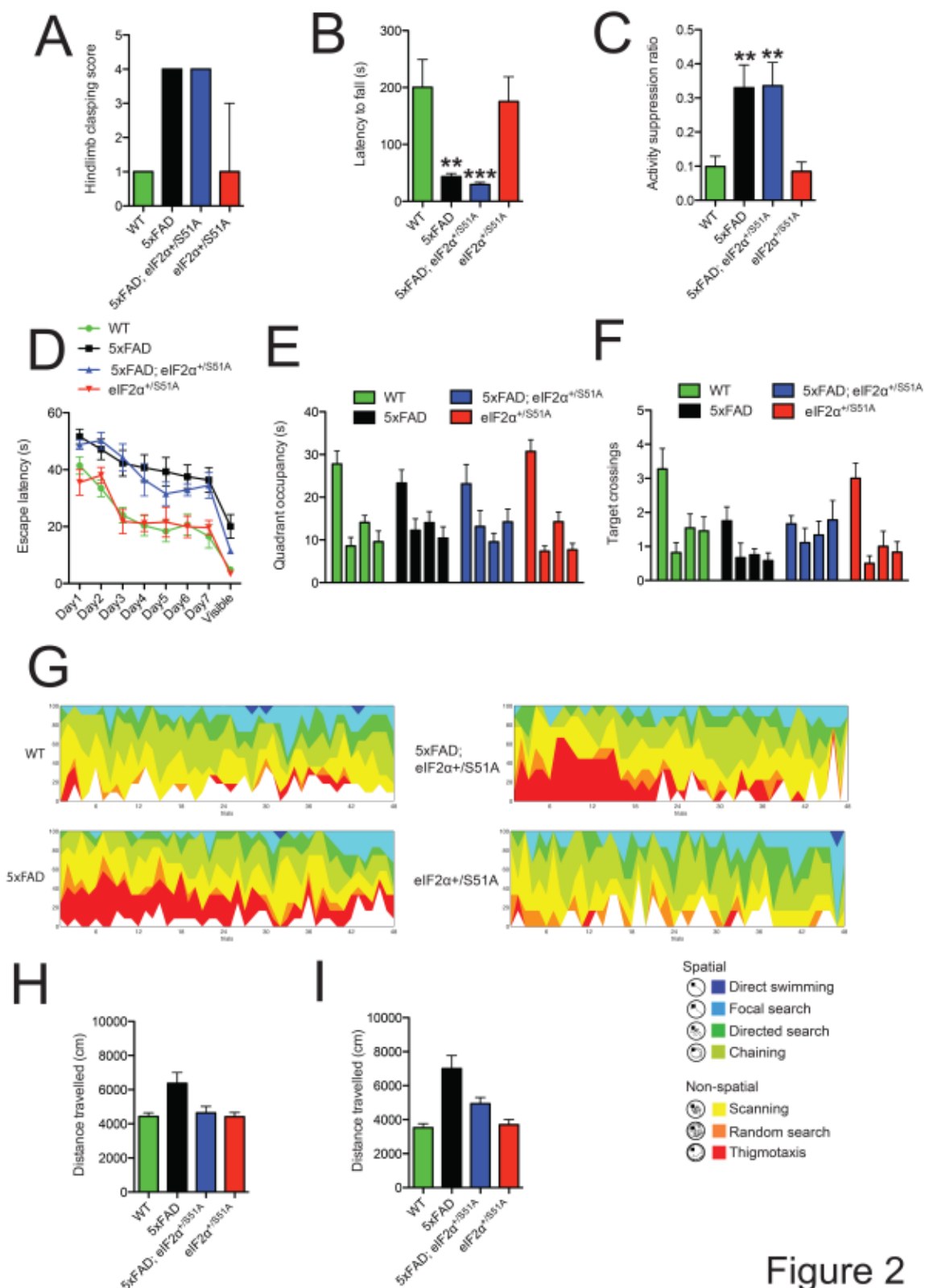


Figure 2

**Figure 2. The eIF2α<sup>S51A</sup> had limited effects on most neurological phenotypes, but restored hyperactivity in 5XFAD mice. (A):** Hindlimb clasping scores, as assessed in the tail suspension test ( $n = 6-12$  mice per group). **(B):** Latencies to fall in the context of

a wire hang test ( $n = 8-13$  mice per group). **(C)**: Activity suppression ratios in a context fear conditioning paradigm ( $n = 6-12$  mice per group). **(D–G)**: Results of an assessment of spatial learning and memory in the Morris water maze ( $n = 6-12$  mice per group). **(D)**: Escape latencies during training trials. **(E,F)**: Quadrant occupancy **(E)** and target crossings **(F)** measures obtained during a probe trial given after the completion of training day 7. For each genotype, bars represent (from left to right): target quadrant, opposite quadrant, adjacent right quadrant, adjacent left quadrant. **(G)**: Results of an extended swim path analysis: For each group, the proportion of animals in the respective search categories is plotted against training trial. **(H,I)**: Distance travelled in two independent open field experiments performed at 8 months (**H**;  $n = 8-13$  mice per group) and 11 months of age (**I**;  $n = 6-11$  mice per group), respectively. Data were analyzed using 2-way ANOVAs with the between-subjects factors 5XFAD genotype and eIF2 $\alpha$  genotype (**A–C,H,I**) or using 3-way ANOVAs with the between-subjects factors 5XFAD genotype and eIF2 $\alpha$  genotype and the within-subjects factor trial (**D**) or quadrant (**E,F**). Statistically significant differences ( $P < 0.05$ ) are denoted by bold font. For additional information regarding the results of statistical analyses, see main text. Bar and line graphs show means  $\pm$  SEM.

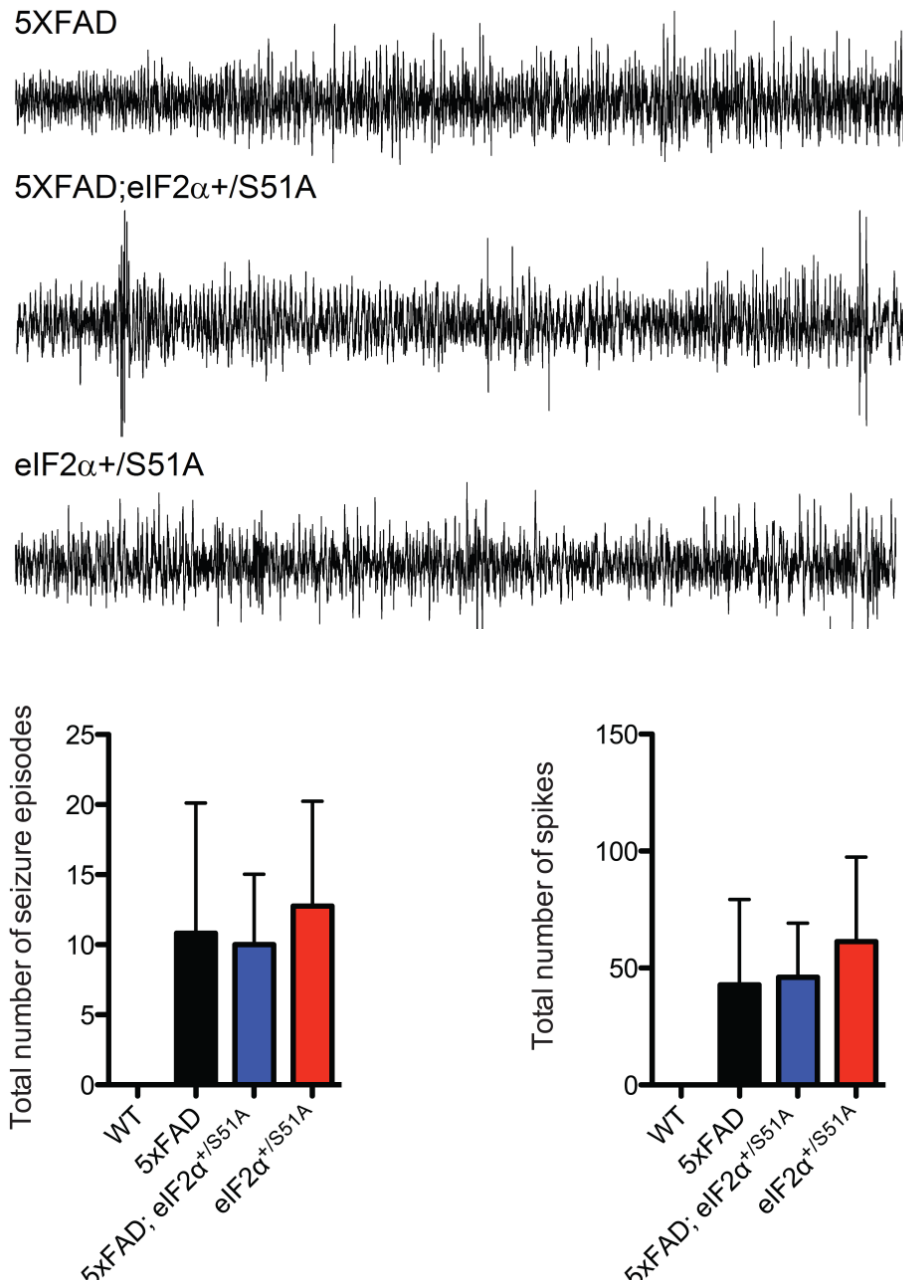
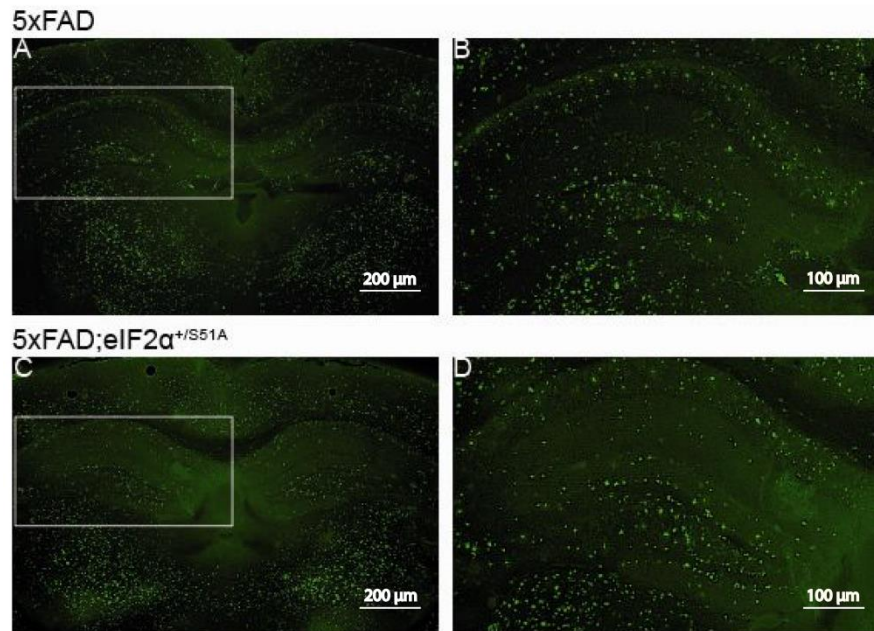


Figure 3

**Figure 3. EEG recordings revealed non-convulsive seizure activity in the motor cortex of animals carrying the 5XFAD transgenes and/or the eIF2 $\alpha$ <sup>+/S51A</sup> allele.** Radiotelemetric recordings from the primary motor cortex (M1) of wild-type, 5XFAD, 5XFAD;eIF2 $\alpha$ <sup>+/S51A</sup> and eIF2 $\alpha$ <sup>+/S51A</sup> mice ( $n = 3-6$  mice per group). Wild-type mice did not exhibit seizure activity, whereas all other genotypes showed episodes of spike, poly-spike and spike-wave activity. Shown are example traces, as well as a quantification of the number of seizure episodes and the number of spikes, respectively. Bar graphs show mean  $\pm$  SEM.

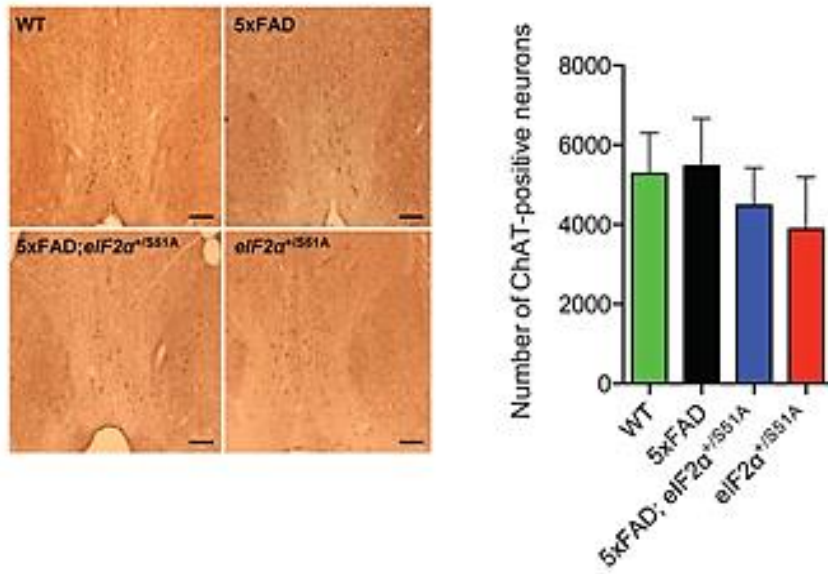
## Supplement



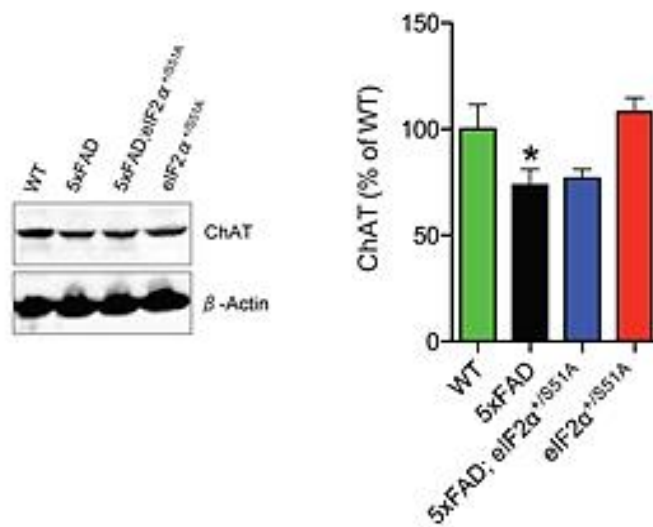
Supplementary Figure 1

**Supplementary Figure 1. The cholinergic system was not involved in the eIF2α<sup>+/S51A</sup>-related restoration of hyperactivity in 5XFAD mice.** (A) Shown are micrographs of ChAT-immunoreactive neurons in the basal forebrain of wild-type, 5XFAD, 5XFAD;eIF2α<sup>+/S51A</sup> and eIF2α<sup>+/S51A</sup> mice. Scale bar = 150 μm. Stereological quantification of ChAT-immunoreactive neurons in the MS and VDB of the basal forebrain demonstrated no significant differences between the four groups of mice ( $n = 3$  mice per group). (B) Shown are immunoblots of ChAT from hippocampal homogenates of wild-type, 5XFAD, 5XFAD;eIF2α<sup>+/S51A</sup> and eIF2α<sup>+/S51A</sup> mice ( $n = 5-7$  mice per group). Data were analyzed using 2-way ANOVAs with the between-subjects factors 5XFAD genotype and eIF2α genotype. Statistically significant differences ( $P < 0.05$ ) are denoted by bold font. Bar graphs show mean  $\pm$  SEM.

A



B



Supplementary Figure 2

**Supplementary Figure 2. The eIF2α<sup>S51A</sup> allele had limited effects on transcriptional dysregulation in 5XFAD mice.** Differentially regulated transcripts (unadjusted  $p < 0.05$ ) with a fold change higher than 1.6 were subjected to hierarchical clustering to visualize gene expression changes between groups ( $n = 3$  mice per group).

## Supplementary Table Legends

**Supplementary Table 1.** A gene ontology analysis revealed a significant enrichment of immune-related transcripts in gene set differentially expressed in 5XFAD hippocampus.

Enrichment Score: 19.126206534555482			
Term	Count	PValue	Fold Enrichment
glycoprotein	80	2,24E-23	2,961042774
disulfide bond	63	2,64E-20	3,434502443
glycosylation site:N-linked (GlcNAc...)	76	6,78E-20	2,730986068
signal	68	1,00E-19	3,081638523
signal peptide	68	2,85E-18	2,870982381
disulfide bond	60	1,53E-17	3,15814549
Enrichment Score: 7.52946739972749			
Term	Count	PValue	Fold Enrichment
GO:0005764~lysosome	16	9,90E-11	9,515476363
GO:0000323~lytic vacuole	16	1,07E-10	9,462018631
GO:0005773~vacuole	16	6,84E-10	8,2967454
lysosome	12	1,08E-08	11,05764411
mmu04142:Lysosome	12	1,61E-07	8,086894587
hydrolase	18	0,05278226	1,601912225
Enrichment Score: 5.619809905239803			
Term	Count	PValue	Fold Enrichment
topological domain:Extracellular	51	6,36E-13	2,901109156
topological domain:Cytoplasmic	52	1,59E-09	2,315137268
transmembrane region	63	2,63E-08	1,896390439
membrane	72	4,73E-08	1,741488245
GO:0005886~plasma membrane	50	4,46E-06	1,832607195
transmembrane	64	6,67E-06	1,635015533
receptor	29	0,0107878	1,598031624
GO:0016021~integral to membrane	63	0,05797149	1,176457745
GO:0031224~intrinsic to membrane	63	0,11288155	1,135369339
Enrichment Score: 4.99067817222587			
Term	Count	PValue	Fold Enrichment
GO:0006955~immune response	30	8,57E-18	7,601765853
GO:0006952~defense response	29	1,69E-17	7,825762201
GO:0002684~positive regulation of immune system process	20	5,55E-15	11,57283757
GO:0048002~antigen processing and presentation of peptide antigen	11	2,85E-13	35,53825536
GO:0050778~positive regulation of immune response	16	2,95E-13	14,20543726
GO:0002252~immune effector process	15	2,61E-12	13,95684211
GO:0002443~leukocyte mediated immunity	13	9,67E-12	17,1817185
GO:0002478~antigen processing and presentation of exogenous peptide antigen	9	1,42E-11	43,61513158
GO:0002449~lymphocyte mediated immunity	12	3,26E-11	18,60912281



GO:0048584~positive regulation of response to stimulus	16	3,36E-11	10,28128332
GO:0019884~antigen processing and presentation of exogenous antigen	9	8,01E-11	36,09528131
GO:0016064~immunoglobulin mediated immune response	11	1,00E-10	20,63511602
GO:0002250~adaptive immune response	12	1,01E-10	16,81547242
GO:0002460~adaptive immune response based on somatic recombination of immune receptors built from immunoglobulin superfamily domains	12	1,01E-10	16,81547242
GO:0019724~B cell mediated immunity	11	1,39E-10	19,99026864
GO:0019882~antigen processing and presentation	11	1,35E-09	15,99221491
GO:0002699~positive regulation of immune effector process	8	4,79E-08	22,6940522
GO:0002821~positive regulation of adaptive immune response	7	2,07E-07	26,26287493
GO:0002824~positive regulation of adaptive immune response based on somatic recombination of immune receptors built from immunoglobulin superfamily domains	7	2,07E-07	26,26287493
GO:0002474~antigen processing and presentation of peptide antigen via MHC class I	6	2,35E-07	41,0495356
GO:0009897~external side of plasma membrane	13	2,44E-07	7,127314815
GO:0002822~regulation of adaptive immune response based on somatic recombination of immune receptors built from immunoglobulin superfamily domains	8	3,02E-07	17,55577623
GO:0002819~regulation of adaptive immune response	8	3,02E-07	17,55577623
GO:0002708~positive regulation of lymphocyte mediated immunity	7	4,45E-07	23,26140351
GO:0002705~positive regulation of leukocyte mediated immunity	7	4,45E-07	23,26140351
GO:0002697~regulation of immune effector process	9	5,03E-07	12,61160431
GO:0009986~cell surface	15	5,77E-07	5,426028725
GO:0002706~regulation of lymphocyte mediated immunity	8	7,21E-07	15,50760234
GO:0050766~positive regulation of phagocytosis	6	9,65E-07	31,72009569
GO:0002703~regulation of leukocyte mediated immunity	8	1,25E-06	14,31470985
GO:0050764~regulation of phagocytosis	6	1,54E-06	29,07675439
GO:0006909~phagocytosis	7	3,07E-06	16,96144006
transmembrane protein	14	3,70E-06	5,075639919
GO:0019864~IgG binding	4	4,24E-06	103,96
GO:0006911~phagocytosis, engulfment	5	4,69E-06	41,53822055
GO:0045576~mast cell activation	5	4,69E-06	41,53822055
GO:0042590~antigen processing and presentation of exogenous peptide antigen via MHC class I	4	5,95E-06	93,04561404
GO:0045807~positive regulation of endocytosis	6	8,07E-06	21,14673046
GO:0002495~antigen processing and presentation of peptide antigen via MHC class II	5	1,09E-05	34,20794634
GO:0019886~antigen processing and presentation of exogenous peptide antigen via MHC class II	5	1,09E-05	34,20794634
GO:0002504~antigen processing and presentation of peptide or polysaccharide antigen via MHC class II	5	1,76E-05	30,60710988

GO:0032403~protein complex binding	7	2,57E-05	11,81363636
GO:0019865~immunoglobulin binding	4	6,77E-05	47,25454545
GO:0051130~positive regulation of cellular component organization	8	6,92E-05	7,818959163
GO:0030100~regulation of endocytosis	6	7,07E-05	13,68317853
GO:0031349~positive regulation of defense response	6	7,77E-05	13,42004049
GO:0002712~regulation of B cell mediated immunity	5	8,75E-05	20,76911028
GO:0002889~regulation of immunoglobulin mediated immune response	5	8,75E-05	20,76911028
GO:0002864~regulation of acute inflammatory response to antigenic stimulus	4	9,46E-05	42,29346093
GO:0002883~regulation of hypersensitivity	4	9,46E-05	42,29346093
GO:0002714~positive regulation of B cell mediated immunity	4	1,25E-04	38,76900585
GO:0002891~positive regulation of immunoglobulin mediated immune response	4	1,25E-04	38,76900585
GO:0001817~regulation of cytokine production	8	1,60E-04	6,841589267
mmu05322: Systemic lupus erythematosus	8	1,99E-04	6,436507937
GO:0001803~regulation of type III hypersensitivity	3	2,15E-04	116,3070175
GO:0001805~positive regulation of type III hypersensitivity	3	2,15E-04	116,3070175
GO:0002861~regulation of inflammatory response to antigenic stimulus	4	2,55E-04	31,01520468
GO:0042742~defense response to bacterium	7	2,58E-04	7,82835695
GO:0002673~regulation of acute inflammatory response	4	3,11E-04	29,07675439
GO:0009617~response to bacterium	8	3,17E-04	6,121421976
igg-binding protein	3	3,30E-04	99,51879699
GO:0019763~immunoglobulin receptor activity	3	3,41E-04	97,4625
GO:0060627~regulation of vesicle-mediated transport	6	6,30E-04	8,615334633
GO:0001912~positive regulation of leukocyte mediated cytotoxicity	4	7,17E-04	22,15371763
GO:0031343~positive regulation of cell killing	4	7,17E-04	22,15371763
GO:0006897~endocytosis	8	0,00105586	5,002452367
GO:0010324~membrane invagination	8	0,00105586	5,002452367
immunoglobulin receptor	3	0,00113768	56,867884
GO:0001796~regulation of type IIa hypersensitivity	3	0,00147024	49,84586466
GO:0001798~positive regulation of type IIa hypersensitivity	3	0,00147024	49,84586466
GO:0001810~regulation of type I hypersensitivity	3	0,00147024	49,84586466
GO:0002888~positive regulation of myeloid leukocyte mediated immunity	3	0,00147024	49,84586466
GO:0002892~regulation of type II hypersensitivity	3	0,00147024	49,84586466
GO:0002894~positive regulation of type II hypersensitivity	3	0,00147024	49,84586466
GO:0032101~regulation of response to external stimulus	6	0,00162814	6,978421053
GO:0001910~regulation of leukocyte mediated cytotoxicity	4	0,00169061	16,61528822
GO:0031341~regulation of cell killing	4	0,00169061	16,61528822
GO:0002885~positive regulation of hypersensitivity	3	0,00194941	43,61513158

GO:0002866~positive regulation of acute inflammatory response to antigenic stimulus	3	0,00194941	43,61513158
GO:0016044~membrane organization	9	0,00211085	3,891312855
GO:0001916~positive regulation of T cell mediated cytotoxicity	3	0,00249245	38,76900585
GO:0002675~positive regulation of acute inflammatory response	3	0,00249245	38,76900585
GO:0002863~positive regulation of inflammatory response to antigenic stimulus	3	0,00309825	34,89210526
GO:0001914~regulation of T cell mediated cytotoxicity	3	0,00376572	31,72009569
domain:Ig-like C2-type 1	6	0,00387581	5,736073553
domain:Ig-like C2-type 2	6	0,00400537	5,691949911
GO:0002711~positive regulation of T cell mediated immunity	3	0,00449379	29,07675439
GO:0006910~phagocytosis, recognition	3	0,00449379	29,07675439
GO:0051050~positive regulation of transport	6	0,00490073	5,409628723
GO:0002886~regulation of myeloid leukocyte mediated immunity	3	0,00528139	26,84008097
GO:0002709~regulation of T cell mediated immunity	3	0,00900633	20,5247678
GO:0050727~regulation of inflammatory response	4	0,01090708	8,615334633
GO:0050729~positive regulation of inflammatory response	3	0,0136022	16,61528822
GO:0001819~positive regulation of cytokine production	4	0,01386451	7,885221528
GO:0016192~vesicle-mediated transport	10	0,01714017	2,517467912
GO:0032680~regulation of tumor necrosis factor production	3	0,02047792	13,42004049
GO:0032103~positive regulation of response to external stimulus	3	0,03757426	9,692251462
IPR013151:Immunoglobulin	5	0,04086841	3,838750881
GO:0051240~positive regulation of multicellular organismal process	5	0,04433638	3,727789024
GO:0008037~cell recognition	3	0,05845242	7,585240275
domain:Ig-like C2-type 3	3	0,15227306	4,302055165
GO:0005783~endoplasmic reticulum	6	0,90268751	0,754587507



### 3.3 Altered muscarinic signalling in 5XFAD mice – Bridging the gap between seizure activity, theta oscillations and Alzheimer's disease

Magdalena Elisabeth Siwek<sup>1,§</sup>, Ralf Müller<sup>2,§</sup>, Astrid Becker<sup>3</sup>, Andreas Lundt<sup>1</sup>, Carola Wormuth<sup>1</sup>, Christina Henseler<sup>1</sup>, Karl Broich<sup>1</sup>, Dan Ehninger<sup>4</sup>, Marco Weiergräber<sup>1</sup> and Anna Papazoglou<sup>1</sup>

<sup>1</sup>Federal Institute for Drugs and Medical Devices (Bundesinstitut für Arzneimittel und Medizinprodukte, BfArM), Kurt-Georg-Kiesinger-Allee 3, 53175 Bonn, Germany; <sup>2</sup>Department of Psychiatry and Psychotherapy, University of Cologne, Kerpener Str. 62, 50937 Cologne, Germany; <sup>3</sup>Institute of Molecular Psychiatry, University of Bonn, Sigmund-Freud-Str. 25, 53125 Bonn, Germany; <sup>4</sup>German Center for Neurodegenerative Diseases (Deutsches Zentrum für Neurodegenerative Erkrankungen, DZNE), Ludwig-Erhard-Allee 2, 53175 Bonn, Germany; <sup>§</sup> Both authors contributed equally to this work

**Submitted: April, 2014; In Revision**

#### **Abstract**

Alzheimer's disease (AD) is an age-related neurodegenerative disorder characterized by impairment of memory function. Eurhythmic activity in the brain is mandatory for cognitive function and recent evidence suggests that accumulation of soluble amyloid-beta (A $\beta$ ) in AD patients induces reorganisation in hippocampal and other neuronal networks resulting in an imbalance of inhibition and excitation. 5XFAD mouse model was analysed and compared with wild type controls for functional interdependence between seizure activity and hippocampal theta oscillations by using simultaneous video-electroencephalogram (EEG) monitoring, seizure scoring and time-frequency analysis. Seizure staging revealed that 5XFAD mice exhibited non-convulsive seizure activity of different severity whereas controls did not. 5XFAD mice displayed a significant increase in theta activity from the light to dark phase during non-motor activity. In addition, we observed a reduction in mean theta frequency in 5XFAD mice compared to controls that was again most prominent during non-motor activity. Transcriptome analysis of hippocampal probes and subsequent qPCR validation revealed an upregulation of PLC $\delta$ 4 that might be indicative of enhanced muscarinic signalling. The latter was shown to be involved in both ictogenesis and theta genesis. Our study suggests that dysfunction of the muscarinic signaling contributes to hippocampal dysrhythmicity and seizure activity in 5XFAD mice thus providing a potent target cascade in AD treatment.

**Key words:** 5XFAD, hippocampus, microarray, neurodegeneration, seizure, theta

## Introduction

Alzheimer's disease is an irreversible, progressive brain disorder slowly destroying learning and memory skills. The histopathology of Alzheimer's disease (AD) is characterized by two hallmark lesions, extracellular amyloid- $\beta$  plaques made of the A $\beta$  peptide, and intra cellular neurofibrillary tangles (NFT) composed of hyperphosphorylated tau protein. In addition to the presence of plaques and tangles in the brain, considerable neuron loss is also a cardinal feature of AD, but the mechanisms of neural cell death still remain unclear. Importantly, familial AD (FAD) mutations in the genes for amyloid precursor protein (APP), presenilin 1 (PSEN1), and presenilin 2 (PSEN2) implicate A $\beta$  as an initiating factor in AD pathogenesis. These FAD mutations increase the production of A $\beta$ 42 from APP, which is sequentially cleaved by the  $\beta$ - and  $\gamma$ -secretase enzymes to release the peptide. The A $\beta$ 42 fragment plays a central early role in the pathophysiology of AD that ultimately leads to neuronal cell loss, e.g. in the septum, entorhinal cortex and hippocampus (Scott et al., 2012; Yamaguchi et al., 1989) and dementia (Selkoe, 2002; Selkoe and Schenk, 2003).

Transgenic mouse models of AD exhibiting homology, isomorphism and predictivity have proven to be valuable tools in investigating the etiopathogenesis of the disease (Ashe, 2001; Duff and Suleman, 2004; Eriksen and Janus, 2007; Glenner et al., 1984; Glenner and Wong, 1984; Ohno et al., 2007; Torres-Aleman, 2010). Studies on various AD mouse models exhibited dysregulation of the  $\beta$ -site APP cleaving enzyme 1 (BACE1) that is ultimately responsible for the generation of A $\beta$  plaques (Devi and Ohno, 2013; Sinha and Lieberburg, 1999; Vassar et al., 1999). Therefore, increased translation of BACE1 leads to an increased number of plaques and finally to a disruption of neuronal functioning within the hippocampus (Oakley et al., 2006; Ohno et al., 2004). Among different AD models, the 5XFAD model is a most progressive, growth retarded AD model expressing multiple FAD mutations that additively increase A $\beta$ 42 production: three human APP mutations (Swedish mutations: K670N, M671L; Florida mutation: I716V; London mutation: V717I) and two mutant PSEN1 (M146L, L286V). Individually, each FAD mutation enhances A $\beta$ 42 generation, but together they act synergistically in the transgenic mouse to predominantly accumulate A $\beta$ 42. 5XFAD mice exhibit intraneuronal A $\beta$ 42 accumulation at 1.5 months, amyloid deposition at 2 months, and memory deficits by 4 months of age (Crouzin et al., 2013; Games et al., 1995; Goutagny and Krantic, 2013; Oakley et al., 2006; Rockenstein et al., 1995).

Furthermore, the 5XFAD model is one of a few known mouse models that exhibits significant neuronal loss in the hippocampus that correlates with accumulation of A $\beta$  plaques (Casas et al., 2004; Jawhar et al., 2012; Oakley et al., 2006). In the cortex the neuronal loss was reported to be predominately related to layer 5 (Eimer and Vassar, 2013; Oakley et al., 2006). Quantification of layer 5 neurons in 12 months old 5XFAD mice confirmed neuronal loss in this brain region (Eimer and Vassar, 2013; Oakley et al., 2006). However, the overall number of neurons in the frontal cortex and hippocampal CA1 region remained unchanged compared with age-matched wild type (WT) mice (Jawhar et al., 2012). Whereas cortical layer 5 neurons accumulate considerable amounts of A $\beta$ , CA1 neurons did not show high levels of transgenic APP expression compared to WT animals. It's noteworthy that there is only a weak correlation between plaque density and hippocampus-related memory deficits in e.g. 8 months old 5XFAD mice (Kaczorowski and Disterhoft, 2009). Thus, cortical plasticity is impaired prior to hippocampal-dependent learning and memory deficits in 6 month-old 5XFAD mice (Casas et al., 2004; Games et al., 1995; Ohno et al., 2004). The motor phenotype in 5XFAD mice correlates with abundant spinal cord pathology resulting in impaired performance in sensory-motor tasks as a consequence of axonopathy. Interestingly, 12 months old 5XFAD were reported to exhibit less anxiety, but normal locomotor behaviour (Jawhar et al., 2012). In addition, efforts were carried out to characterize the transcription and expression profile in 5XFAD mice compared to WT. Using quantitative mass spectrometry to investigate proteome-wide changes in 4 months old 5XFAD mice (Kaczorowski and Disterhoft, 2009), alterations were predominantly identified in ApoE, ApoJ (clusterin), and nicastrin expression. NRF2 and p53 transcriptional pathways were activated, as well as IGF-1 signaling. Furthermore, various neurological glial marker proteins and factors implicated in neurological disorders such as AD, Parkinson's disease, Huntington's disease, and amyotrophic lateral sclerosis were affected (Hong et al., 2013). Transcriptome analysis has also been carried out for the frontal cortex and cerebellum of 7 week old 5XFAD mice (Kim et al., 2012).

Although different neuropathological changes have been well described previously, direct effects on systemic electrophysiological alterations in AD have received less attention in the past. Currently, the impact of brain oscillation analysis as a novel tool in early diagnosis and prediction of disease progression is strongly discussed as functional impairments in AD can occur even without any significant neuronal loss and therefore

could be independent of plaque formation (Blanchet, 2003; Martino and Giovannoni, 2004; Palop et al., 2006; Palop et al., 2007; Palop and Mucke, 2009). Recent studies showed that altered hippocampal oscillatory activity correlates with an increase of A $\beta$  level and the appearance of plaques (Buzsaki, 2002; Colom, 2006; Scott et al., 2012) but slight changes in hippocampal and cortical network activity can also occur much earlier prior to clinical onset of AD (Chin and Scharfman, 2013; Minkeviciene et al., 2009; Palop et al., 2006; Palop et al., 2007; Palop and Mucke, 2009). Alterations in network activities are reorganised in AD by an early imbalance of excitation and inhibition that elicits overall changes in theta activity as a hallmark of hippocampal functioning (Goutagny and Krantic, 2013; Scott et al., 2012; Verret et al., 2012). These alterations due to A $\beta$ -induced neuronal hyperexcitability (Minkeviciene et al., 2009) are accompanied by decreased GABAergic transmission within the hippocampus and can trigger seizure activity (Hauser et al., 1986; Lerner, 2010; Mendez and Lim, 2003; Morrison and Hof, 1997; Price et al., 2001; Romanelli et al., 1990; Scarneas et al., 2009; Terry et al., 1991). Neurons that are early affected in AD pathogenesis are those of the septohippocampal circuitry, including cholinergic, GABAergic and glutamatergic cells (Auld et al., 2002; Cullen and Halliday, 1998; Gutierrez-Lerma et al., 2013; Ikarashi et al., 2004; Klingner et al., 2003; Kordower et al., 2001; Luth et al., 2003; Palhalmi et al., 2004; Reich et al., 2005). Interestingly, various mouse models of AD can exhibit opposing alterations in theta rhythmicity, i.e. a number of them were reported to present cognitive decline associated with increased theta activity (Babiloni et al., 2007; Blanchet, 2003; Cummins et al., 2008; Pena-Ortega and Bernal-Pedraza, 2012) whereas others displayed reduced theta rhythm (Cummins et al., 2008). The reason for either enhanced or decreased theta activity - remains largely unknown. Though, recent studies have gained substantial insight into the etiopathogenesis of AD, we are still missing detailed information about how septohippocampal networks functionally disintegrate theta rhythm and epilepsy in AD. In this study we combined seizure analysis, time-frequency based theta analysis and transcriptome data from 5XFAD mice to detect a missing link in AD phenomenology. Our study suggests that alterations in muscarinic signalling can account for complex changes in hippocampal theta and exacerbation of seizure activity in the 5XFAD model of AD.



## Material and Methods

### *Study Animals*

This study was performed in Tg (APP<sup>S<sub>w</sub>FIL<sub>on</sub></sup>,PSEN1\*<sup>M146L</sup>\*<sup>L286V</sup>)<sup>6799V</sup>as (5XFAD) transgenic mice with a B6/SJL background overexpressing mutant forms of human APP (the Swedish mutations: K670N, M671L; the Florida mutation: I716V; the London mutation: V717I) and mutant *PSEN1* (M146L, L286V). Five WT controls (mean body weight: 35.32 ± 2.40 g, mean age: 74.00 ± 5.76 weeks, 4 ♂, 1 ♀) and five 5XFAD mice (mean body weight: 24.89 ± 1.40 g, mean age: 72.20 ± 2.85 weeks, all ♂) were used in this study. All mice were housed in groups of 3-4 in clear Macrolon cages type II with ad libitum access to drinking water and standard food pellets. Using ventilated cabinets (Model 9AV125P, Techniplast, Germany), mice were maintained at a temperature of 21 ± 2 °C, 50 – 60% relative humidity, and on a conventional 12 h light/dark cycle with the light cycle beginning at 5:00 AM for spontaneous epidural and deep, intracerebral EEG recordings. All animal procedures were performed according to guidelines of the German Council on Animal Care and all protocols were approved by the local institutional and national committee on animal care (Landesamt für Natur, Umwelt und Verbraucherschutz, LANUV, Germany). The authors further certify that all animal experimentation was carried out in accordance with the European Communities Council Directive of 24 November 1986 (86/609/EEC). Specific effort was made to minimize the number of animals used and their suffering.

### *Stereotaxic EEG electrode implantation and radiotelemetric EEG recordings*

Mice were anesthetized using ketamine / xylazine (100/10 mg/kg ip.) and the radiotelemetry transmitter (TL11M2-F20-EET 2-channel transmitter, Data Science International (DSI), specifications: weight 3.9 g, volume 1.9 cc, input voltage range ± 1.25 mV, channel bandwidth 1 - 50 Hz) was implanted into a subcutaneous pouch on the back of the animals. The EEG electrodes of both transmitter channels were stereotaxically positioned using a computerized 3D stereotaxic StereoDrive<sup>®</sup> (Neurostar, Germany). The differential epidural electrode of channel 1 targeting the primary motor cortex (M1) was positioned at the following coordinates referring to bregma craniometric landmark: (+)-lead cranial +1 mm, lateral of bregma 1.5 mm (left hemisphere). For deep, intracerebral brain recordings targeting the hippocampal CA1 region the differential electrode of channel 2 was positioned as follows: (-)-lead, caudal

-2 mm, lateral of bregma 1.5 mm (right hemisphere), dorsoventral (depth) 1.5 mm. For both channels, epidural reference electrodes were placed on the cerebellar cortex at: bregma -6 mm, lateral of bregma 1 mm (left hemisphere) and bregma -6 mm, lateral of bregma 1 mm (right hemisphere), respectively (**Fig. 1**) Electrodes were fixed using glas ionomer cement (Kent Express, UK) and the scalp was closed using over and over sutures (Ethilon, 6-0). To avoid hypothermia, supplemental warmth is given to the animal during the whole surgery procedure. A detailed description of the implantation procedure is given in (Weiergraber et al., 2005). For postoperative pain management animals were administered carprofen (5 mg/kg sc., Rimadyl, Parke-Davis/Pfizer, Germany). Animals were allowed to recover for 10 days prior to subsequent recordings. This recovery period is based on the observation that 10 days post-surgery no difference in physiological parameters between transmitter implanted, non-implanted and sham-operated animals could be detected (Kramer and Kinter, 2003).

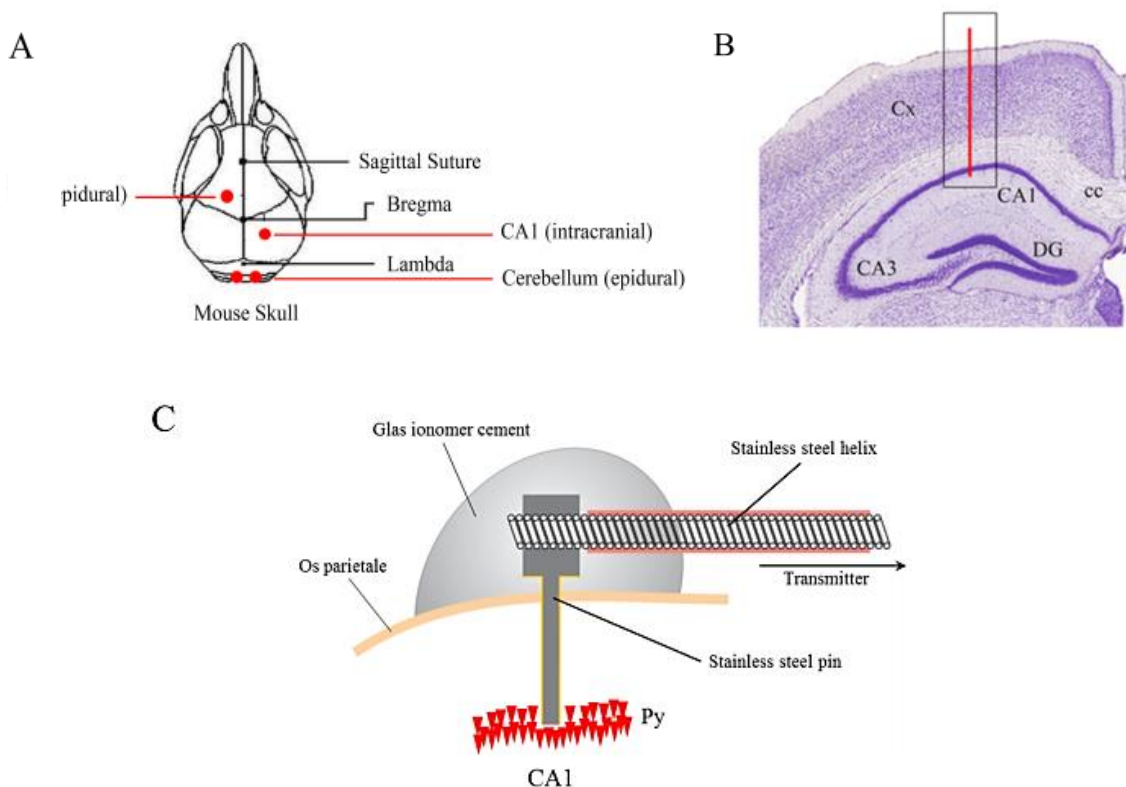


**Figure 1: Stereotaxic EEG electrode placement.** **A)** One epidural, differential electrode is placed on the motor (M1) cortex, an additional intrahaippocampal (CA1) differential electrode is placed in the CA1 region of the hippocampus. Both pseudoreference electrodes are localized on the cerebellum. **B)** Coronal section (scheme) illustrating the localisation of the deep, intracranial electrode for recording the electrohippocamogram. **C)** Close-up of the deep EEG electrode, the sensing lead of the radiofrequency transmitter and their arrangement on top of the murine skull.

### ***Validation of EEG electrode placement***

To verify the correct electrode placement targeting the CA1 region, brains were extirpated post mortem and fixed in 4% paraformaldehyde. Afterward, brains were cut to 60  $\mu\text{m}$  slices using a Vibroslice Tissue Cutter EMS 5000-MZ (Campden Instruments Limited) and hematoxylin-stained for visualization of the branch canal. Animals with false EEG electrode placement were removed from the study.

### ***EEG data acquisitions***

Ten days after radiotracer implantation, simultaneous video-EEG recordings from the motor cortex (M1) and the hippocampal CA1 region were performed for 48 h using Dataquest ART 4.2 software (DSI) at a sampling rate of 500 Hz with no a priori filter cut-off.

### ***Electroencephalographic and behavioural seizure analysis***

For further analysis data were exported to Neuroscore 2.1 (DSI). Qualitative and quantitative seizure analysis was performed using the Neuroscore seizure detection module. Spike parameters including dynamic and absolute threshold, spike duration and spike intervals were adapted for different seizure protocols. Dynamic thresholds were based on multiplication of RMS values of the EEG signals one minute prior to EEG segments being analyzed. The threshold ratio (minimum threshold) was defined by 2 while the maximum ratio was defined as 15. The minimum amplitude value of spikes was 100  $\mu\text{V}$  for the dynamic range. In case of the absolute threshold the maximum amplitude was fixed at 1000  $\mu\text{V}$  with a threshold value of 200  $\mu\text{V}$ . In both seizure protocols the minimum spike duration was determined at 1 ms and the maximum spike / short/slow-wave duration at 100 ms. Spike trains were detected with a minimum train duration of 0.5 s including at least 4 individual spikes. Spike intervals within a train were ranging between 0.05 and 0.3 s. The interval between individual spike trains was determined at 1 s. Seizure protocols contained total number of seizure episodes and spikes, spike frequency, total spike train duration, shortest and longest spike train duration. Data were calculated and plotted throughout the figures as mean  $\pm$  standard error of the mean (SEM). Significance was calculated using Student's t-test which included pretesting for normal distributions via the Kolmogorov-Smirnov test.

### ***Urethane induced theta oscillations***

Urethane (Sigma, Germany) was freshly dissolved in 0.9% NaCl and systemically (ip.) administered at 800 mg/kg to induce atropine-sensitive type II theta oscillations. Four control mice (mean body weight:  $32.98 \pm 0.65$  g, mean age:  $77.00 \pm 2.31$  weeks, 3 ♂, 1 ♀) and four 5XFAD animals (mean body weight:  $25.52 \pm 1.61$  g, mean age:  $73.75 \pm 3.09$  weeks, all ♂) were used for this approach. CA1 recordings under baseline conditions (30 min duration) and under urethane (30 min duration 15 to 45 min post injection) were used for analysis of hippocampal theta oscillations.

### ***EEG data analysis***

Complex EEG analysis was performed for spontaneous 48 h recordings at a sampling rate of 500 Hz. Data segments with a length of 60 min each were extracted from the 48 h recording time. Data segments were analyzed using complex Morlet wavelets to calculate both frequency and amplitude of oscillations. The complex Morlet wavelet is defined by  $\Psi(x) = (\pi b)^{(-1/2)} \exp(2\pi i c x) \exp(-x^2/b)$  where  $b$  is the bandwidth parameter,  $c$  the center frequency, and  $i$  the imaginary unit (Kronland-Martinet et al., 1987). This wavelet or similar ones have often been applied in literature to study EEG data, as they guarantee optimal resolution in both frequency and time (Kronland-Martinet et al., 1987; Montgomery and Buzsaki, 2007). In our case, the bandwidth parameter and centre frequency were both set to 3 in order to particularly weight the frequency resolution to distinguish frequency differences on the 0.1 Hz level, but not to neglect a sufficient time resolution. EEG data were analyzed in the frequency range of 0.2–12 Hz with a step size of 0.1 Hz, thus including the typical delta, theta, and alpha frequency ranges (**Fig.2**). In order to apply the wavelet technique for extraction of theta-oscillatory segments, we developed a task-adjusted detection criterion. This theta detection method imitates the standard visual inspection of theta oscillations and is substantially based on a complex elaboration of the frequency architecture of theta activity. For details see Müller et al. 2012 (Muller et al., 2012). Theta oscillations are defined, where the ratio of the maximum amplitude in the theta-alpha range (4-12 Hz) is at least two times the maximum amplitude in the upper delta frequency range (2–3.9 Hz) for a time window of 2.5 s. This time length is suited to precisely analyze theta activity (Goutagny and Krantic, 2013). Some extracted theta segments do not correspond to the normal theta activity, but show times where mice are eating or scratching which was controlled via

video analysis of the mice. To eliminate those segments, an algorithm was developed and tested for a valid application. Theta segments with mean frequency lower than 5 Hz or higher than 10 Hz, where the mean frequency changes only slightly over time, are excluded. Finally, cleaned EEG segments identified as theta oscillation epochs were statistically analyzed and all data displayed as mean  $\pm$  SEM. For further analysis, additional information about the activity of mice during 48 hours is used to link theta activity of the CA1 region to times with and without motor activity. Additionally, we divided the 48 hours EEG recordings into a conventional 12 h dark/light cycle with the dark cycle beginning at 5:00 PM. All EEG calculations were done using custom-made programs in Matlab<sup>®</sup> (The MathWorks Inc., Version R2012b).

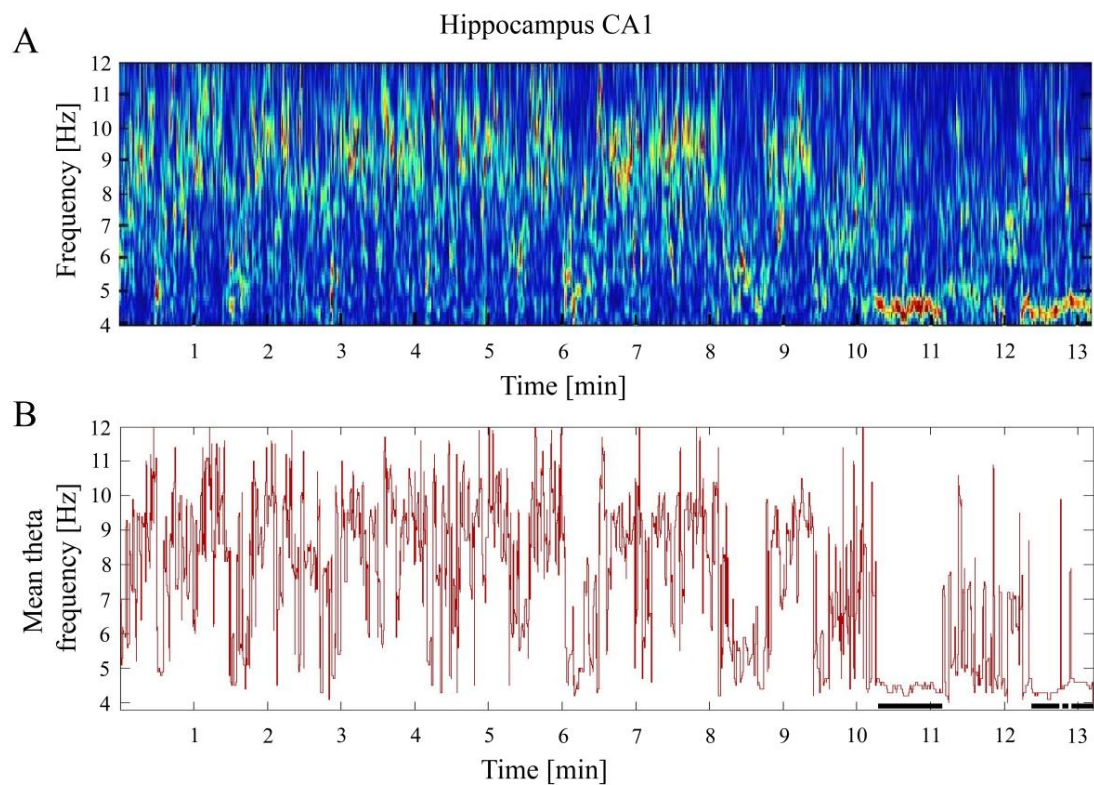


**Figure 2: Time-frequency analysis of theta activity in control and 5XFAD mice. A)** Colour-coded time-frequency plot of extracted theta segments from EEG data. These segments were clued together (13 minutes in total) for a better demonstration of the oscillatory activity. The y-axis represents the frequency range of 4-12 Hz. **B)** Mean theta frequency (Hz) calculated for the hippocampal theta-alpha band (4-12 Hz). Note, that **A)** and **B)** display specific episodes of consistent, high amplitude, low frequency EEG activity that was proven to be related to behavioural aspects such as grooming, scratching or eating based on video analysis. A specific algorithm was defined to automatically detect and eliminate these episodes from further evaluation (black bars, **B)**).

### ***Gene expression profiling using microarray procedure***

Total RNA (250 ng) was prepared from the hippocampi of three control mice (age:  $68.10 \pm 0.05$  weeks, 2 ♂, 1 ♀) and three 5XFAD animals (age:  $68.24 \pm 0.75$  weeks, 2 ♂, 1 ♀) using RNeasy Lipid Tissue Mini Kit (Qiagen). Microarray experiments were carried out using Mouse Exon ST arrays (Affymetrix). Arrays were washed and stained according to the manufacturer's recommendations. Labeled and purified cDNA was fragmented (5.5  $\mu$ g) and subsequently hybridized to the arrays before scanning in a GeneChip 3000 7G scanner (Affymetrix). Normalization to the median of all samples, background correction as well as statistical analysis was performed with GeneSpringGX software (Agilent technologies). An implemented GC-RMA algorithm was applied on all chips to summarize probe level information. Microarray data were analyzed using unpaired t-tests. An uncorrected significance level  $p < 0.05$  was adopted in all instances. Differentially regulated transcripts with a fold change (FC) greater than 1.6 were then subjected to hierarchical clustering analysis in order to visualize gene expression changes across groups. Array data are available in the GEO database under GSE50521. DAVID (Huang et al., 2009) used to carry out gene ontology enrichment analyses in the gene set differentially expressed between 5XFAD and WT controls.

### ***RNA extraction and quantitative Real-time PCR (qPCR)***

Quantitative Real-time PCR was used to validate potential gene candidates that exhibited transcriptional alterations in microarray analysis. The cDNA synthesis from hippocampal RNA (see above) was carried out using anchored-oligo(dt)18 and hexamer primer in a two-step RT-PCR approach (Transcriptor First Strand cDNA Synthesis Kit, Qiagen) and qPCR reaction protocol was based on LightCycler 480 SYBR Green I Master (Roche). The qPCR was performed in a Light Cycler 480 System (Roche) thermocycler. The following cycler protocol was used for all primer pairs (**Tab. 1**): 95°C (10 min, pre-incubation step); 95°C (10 s, melting step); 60°C (20 s, annealing step); 72°C (30 s, extension step), 35 cycles. The specificity of the amplification was checked by melting curve analysis and the products were identified by electrophoresis. Deionized, nuclease-free water (no cDNA) and total RNA samples (without RT) were used as controls and HPRT was used as an internal reference gene. The Ct-values (cycle threshold) were calculated using the LightCycler 480 System software. Fold changes (FC) of *Cacna2d1*, *Kcnma1*, *Cacna1e*, *Prkcb*, *Plc $\delta$ 4*, *Scn8a*, *Plc $\beta$ 1* and *Casp8* gene

expression in 5XFAD transgenic mice related to WT controls were calculated according to Schmittgen and Livak (2008) (Schmittgen and Livak, 2008).

### *Statistical analysis*

Further statistical analyses concerning duration, frequency, amplitude of theta segments, and comparisons between groups and experimental conditions were done with IBM® SPSS® Statistics, Version 22 (IBM Corporation, 2013). The Kolmogorov-Smirnov test was used to test for normal distributions. A Student's t-test was used to detect differences between the two groups of the above mentioned parameters. For data that does not show a normal distribution, the Mann-Whitney U-test was used instead was applied, where we made use of the exact solution. This is necessary, since the asymptotic solution overestimates the p-value for small numbers of animals per group. For analysis of urethane induced theta oscillations the repeated measures ANOVA with within-subjects factor "experimental condition" (baseline vs. post urethane) and between-subjects factor "genotype" (control mice vs. 5XFAD mice) was used. The Simes-Hochberg "step up" procedure was applied to correct for multiple testing, if necessary (Hochberg, 1988). This procedure was utilized at a p-level of 0.05.

## Results

### *Phenotypical characterization*

As reported previously, 5XFAD mice exhibited a reduced body weight in comparison to their WT littermates ( $24.89 \pm 1.40$  g v.  $35.32 \pm 2.40$  g,  $p=0.006$ ,  $n=5$ ;  $p=0.006$ ). The same is true for a characteristic clasping phenotype involving a simultaneous retraction of both fore- and hind-paws (Jawhar et al., 2012).

### *Electrocorticographic characteristics of control and 5XFAD mice*

In this study epidural surface (M1) and deep intrahippocampal CA1 long-term (48 h) EEG recordings were obtained in 5XFAD and WT mice (**Fig. 3**).

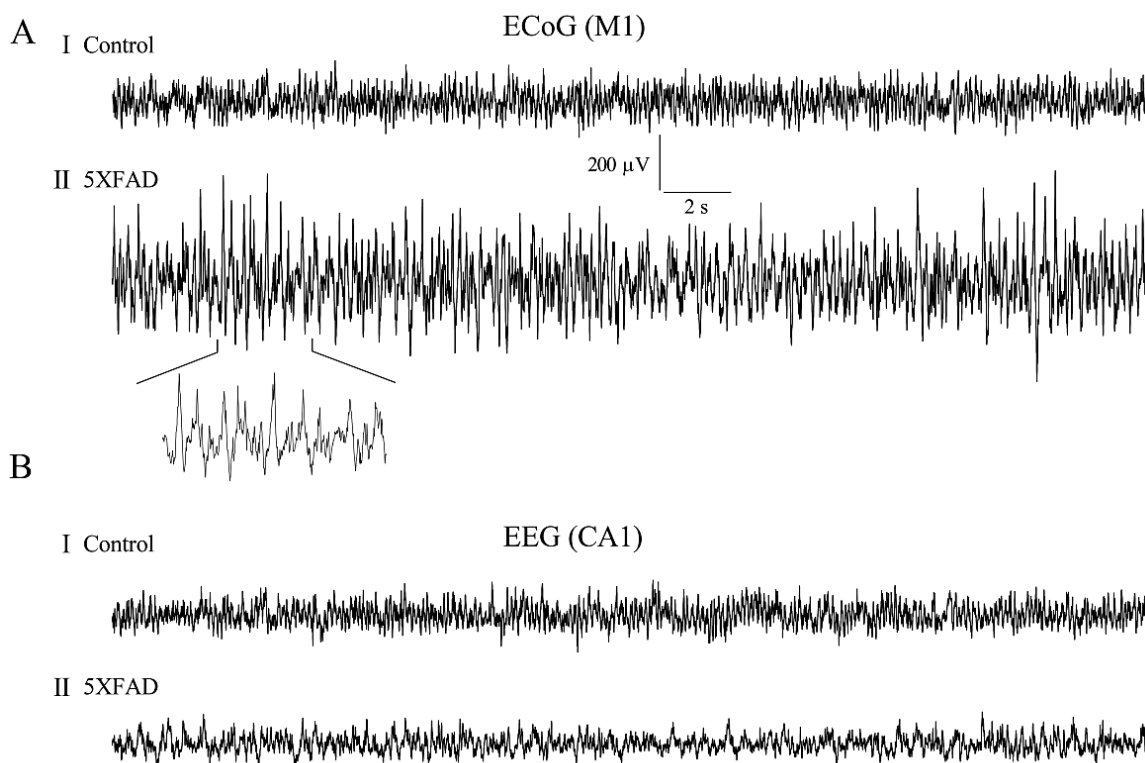


**Figure 3: Electroencephalographic (EEG) characteristics of controls and 5XFAD mice.** EEGs recorded from the primary motor cortex (M1) as Electrocorticogram (ECoG) (**A**) and hippocampal CA1 region as electrohippocampogram (**B**) from both WT and 5XFAD mice. In the CA1 electrohippocampogram neither controls (**B<sub>I</sub>**) nor 5XFAD mice (**B<sub>II</sub>**) exhibited typical ictal discharges / epileptiform graphoelements in 48 h long-term recordings. Electrocorticographic M1 recording however, exhibited subclinical, i.e. electroencephalographic seizure activity in 5XFAD mice of different severity (**A<sub>II</sub>**) that was not detectable in control mice (**A<sub>I</sub>**).



EEG recordings were combined with simultaneous video-recordings to detect potential movement artefacts and to differentiate convulsive from non-convulsive seizure activity.

Despite the WT mice (**Fig. 3A<sub>I</sub>,B<sub>I</sub>**), 5XFAD mice exhibited seizure activity in the M1 recording depicting episodes or trains of spike, poly-spike and spike-wave activity (**Fig. 3A<sub>II</sub>**). Video analysis revealed that none of the motor cortex seizures were associated with motoric exacerbation thus remaining subclinical or non-convulsive.

#### *Seizure analysis in control and 5XFAD mice*

The seizure phenotype of 5XFAD mice was analysed using simultaneous video-EEG recordings for a total duration of 48 h (**Fig. 4**). None of the WT littermates exhibited epileptiform graphoelements according to the automated seizure scoring system (Neuroscore 2.1<sup>®</sup>, DSI). In contrast, 5XFAD mice displayed apparent ictal discharges, such as spikes, polyspikes and spike-waves. In summary, the total number of seizure episodes was  $13.00 \pm 11.05$ , the total number of spikes:  $51.40 \pm 43.37$ , the spike frequency  $5.26 \pm 1.32$  Hz and the total spike train duration:  $8.84 \pm 7.55$  sec (**Fig. 4A-D**). Further seizure parameters in 5XFAD mice included the average spike train duration  $0.51 \pm 0.13$  sec, the average number of spikes per train  $3.22 \pm 0.81$ , the maximum spike train duration  $0.64 \pm 0.19$  and the minimum spike train duration  $0.46 \pm 0.12$  sec (**Fig. 4E-H**). These seizures turned out to be subclinic or non-convulsive and turned to be most prominent in the M1 deflection. No forelimb clonus, no rearing and falling and no generalized tonic-clonic seizures were observed. However, a single 5XFAD mouse exhibited convulsive tonic-clonic seizures of status-like character with prominent interictal spike activity (not shown) and died during the first recovery period. It was excluded from further analysis. Interestingly, 5XFAD mice did not show predominate ictal discharges in the deep, intra-hippocampal CA1 recording (**Fig. 3B<sub>II</sub>**). Disinhibitory tendencies as become apparent in our seizure analysis were speculated to be relevant also for reduced anxiety in 5XFAD mice (Jawhar et al., 2012).

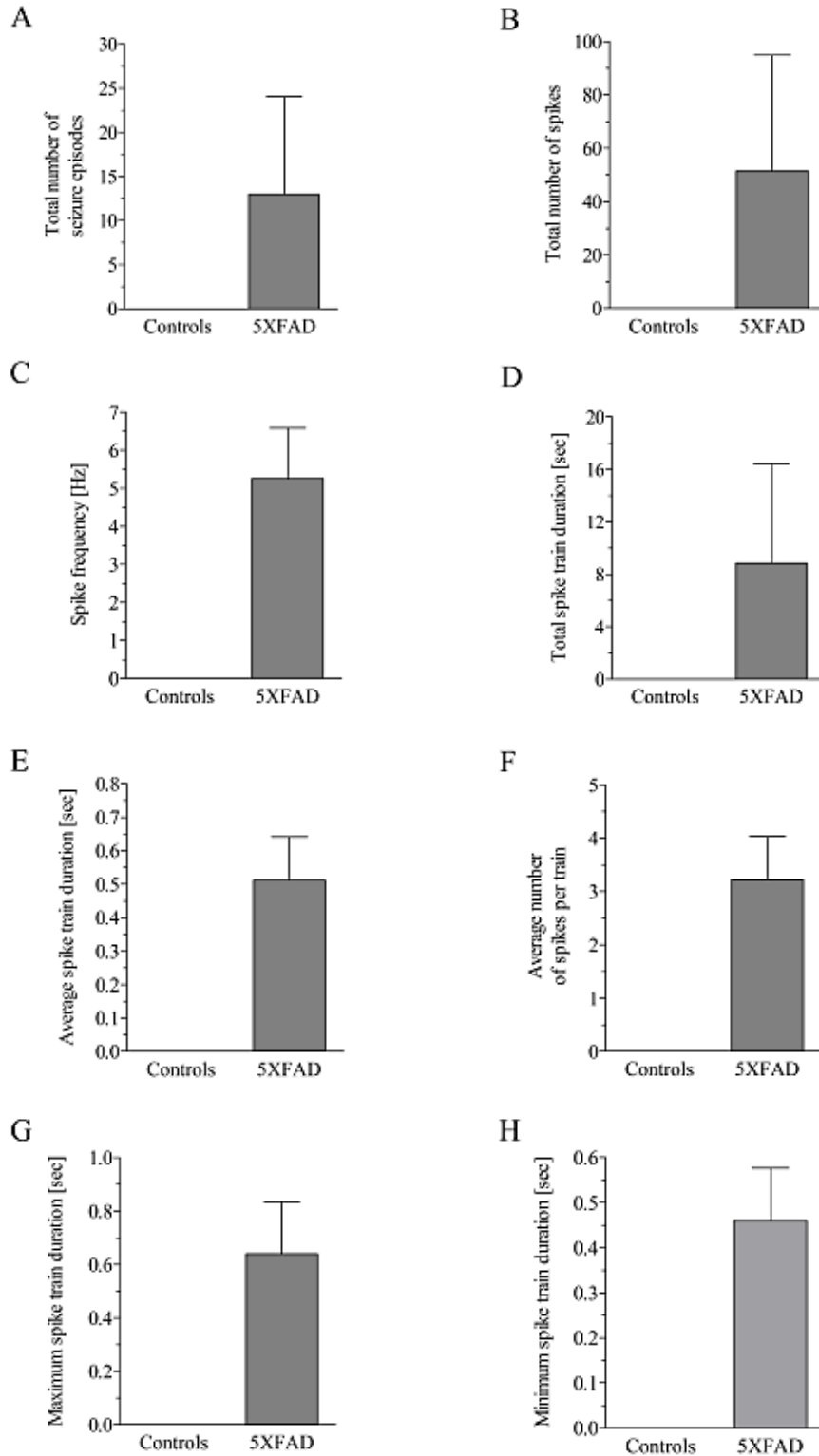


**Figure 4: Seizure characteristics in control and 5XFAD mice.** Total number of seizure episodes (A) and spikes (B), spike frequency (C), total (D) and average (E) spike train duration, average number of spikes per train (F) as well as maximum (G) and minimum spike train duration (H) are depicted. Parameters were analysed using the Neuroscore® Automated Seizure Module (DSI). Whereas 5XFAD mice exhibited ictal discharges of highly variable degree, none of the controls displayed epileptiform graphoelements.

### ***Differential gene expression detected by microarray***

Alzheimer's disease is associated with considerable transcriptional alterations in key brain areas. Gene expression analysis employing Mouse Exon ST arrays (Affymetrix) on hippocampal tissue revealed 1421 transcripts differentially regulated between 5XFAD mice and WT controls. The statistical analysis applied an uncorrected significance level of  $p < 0.05$ . Array data and further detailed information are available in the GEO database under GSE50521. Candidates that are likely to be of interest for seizure and theta activity are depicted in **Supplementary Tab. 1**. Those with FC > 2 are listed in **Supplementary Tab. 2**. Gene ontology analysis revealed that the strongest transcriptional alterations belong to immune-response and inflammation related genes observed in the context of late-stage cerebral amyloidosis.

### ***Changes in gene expression levels in 5XFAD mice compared WT controls***

We performed qRT-PCR on hippocampus from three WT controls and three 5XFAD mice to determine gene expression changes. Among the differentially expressed genes in the microarray assay, we chose eight genes for qRT-PCR analysis based on their involvement in the theta-genesis pathway. The selected genes and their qPCR primers are listed in **Tab. 1**. Among the eight genes tested, qPCR revealed upregulation of Casp8 (FC: 2.0979, **Tab. 2**) which is likely to be responsible for neuronal cell loss in 5XFAD mice based on altered regulating of microglia activation through a PKC- $\delta$  dependent pathway (Burguillos et al., 2011).

	Forward Sequence	Reverse Sequence	Accession No	Size (bp)
HPRT <sup>1</sup>	GCTGGTGAAGGACCTCT	CACAGGACTAGAACACCTGC	J00423	249
Kcnma1 <sup>2</sup>	CCTGAAGGACTTCTGCACAAGG	ACTCCACCTGAGTGAAATGCCG	NM_010610	122
Cacna2d1 <sup>2</sup>	GTGGAAGTGTGAGCGGATTGAC	TCGCTTGAACCAGGTGCTGGAA	NM_001110843	150
Prkcb <sup>2</sup>	CCAAGATGACGATGTGGAGTGC	CTCCATCACAAGTACAGGCGG	NM_008855	127
Ca <sub>v</sub> 2.3 <sup>II-III loop</sup> <sup>1</sup>	GGAGTCTAGCCCGATGTC	GGGCTCCTCTGGTTGTC	L29346	420, 399, 363
Plcd4 <sup>2</sup>	TCTCGCGCAATATGCCTTCCAG	ATCTCGGTCAGATGGTGTGCCA	NM_148937	108
Scn8a	CCCGCAGGAGCCGA	CACTGTTGGCTTGGGCTTG	NM_001077499.2	235
Plcb1	AGCCAGATGGAAGAGGAGAAG	TCATGGCAACCTTCCGACAA	NM_019677.2	200
Casp8 <sup>2</sup>	ATGGCTACGGTGAAGAAGTGGC	TAGTTCACGCCAGTCAGGATGC	NM_009812	138

<sup>1</sup>Weiergräber et al 2005 Basic Res Cardiol

<sup>2</sup>commercially available at OriGene.com

**Table 1: Sequence of primer pairs used for qRT-PCR.** Based on micro-array analysis comparing controls and 5XFAD mice eight candidates were chosen that were thought to be related to theta or seizure activity.

The Scn8a Na<sup>+</sup> channels as well as Kcnma1 K<sup>+</sup> channels were not changed in transcription. Interestingly, microarray analysis suggested alterations in the muscarinic signal transduction pathway including Plcb1, Plcd4, Prkcb, Cacna1e and Cacna2d1 that might be relevant for theta oscillations (Muller et al., 2012).

Validation of these components finally supported an increase in PLCd4 transcript levels (FC: 1.6105) whereas no substantial fold change could be detected for the other factors (Fig. 5, Tab. 2).

<b>Gene</b>	<b>Fold change</b>
Kcnma1	-1,0643
Cacna2d1	-1,0331
Prkcb	-1,0546
Cacna1e	1,0437
Plcd4	1,6105
Scn8a	-1,0344
Plcb1	-1,1765
Casp8	2,0979

**Table 2: Fold changes in gene expression of 5XFAD transgenic mice compared to controls.** Calculations were performed according to Schmittgen and Livak (2008).

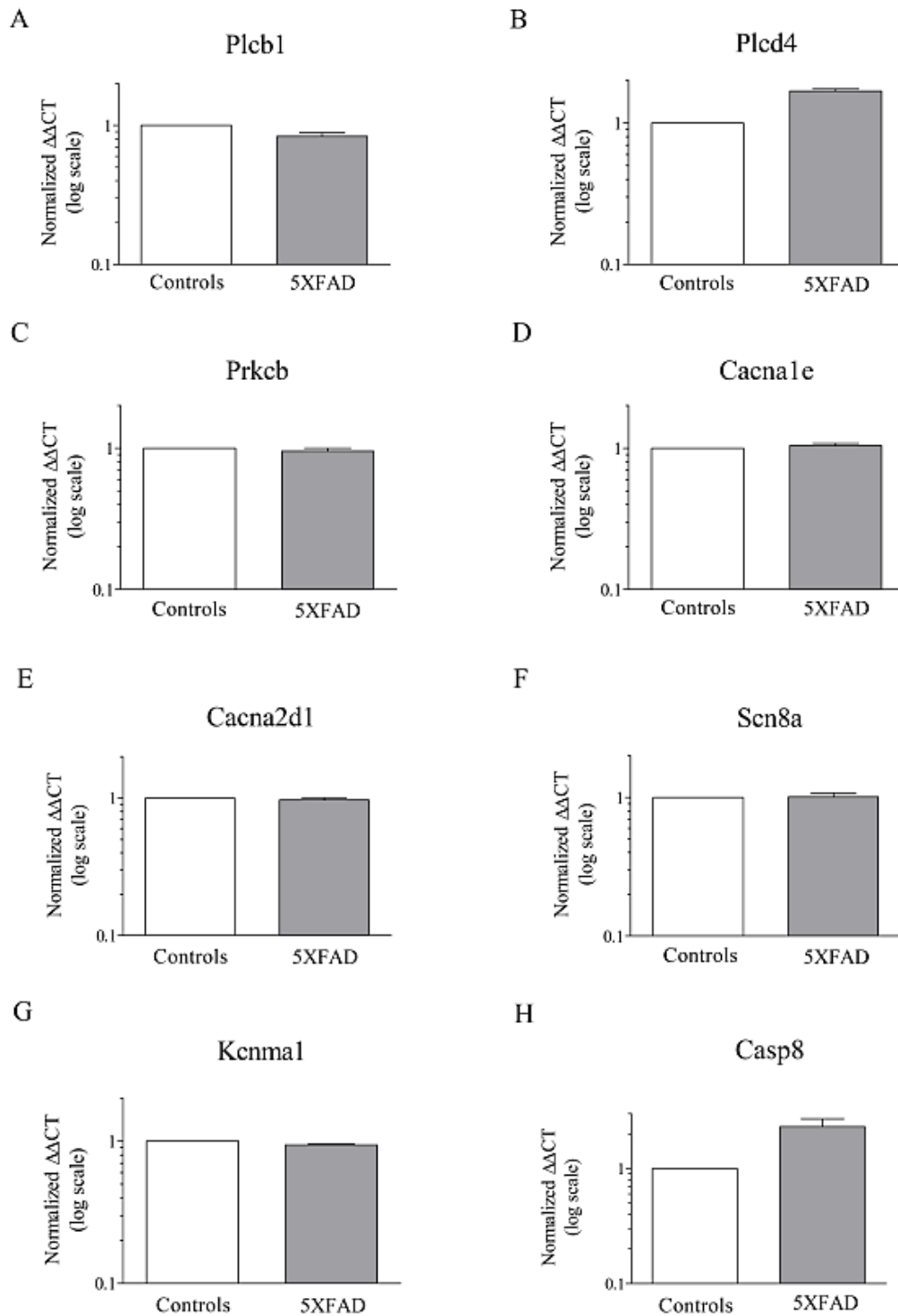


**Figure 5: Gene transcription profiles in 5XFAD mice.** RNA extracted from the hippocampus of control and 5XFAD mice was used for microarray analysis. A selected number of candidates which exhibited altered expression profile in microarray analysis were further validated using quantitative Real-time PCR (qPCR). Normalized  $\Delta\Delta CT$  (log scale) for *Cacna2d1*, *Kcnma1*, *Ca<sub>v</sub>2.3<sub>II-III-loop</sub>*, *Prkcb*, *Plcd4*, *Scn8a*, *Plcb1* and *Casp8* are depicted. Note that there turned out to be a minor decrease in *PLCb1* transcript levels but a clear increase in *Plcd4* in 5XFAD mice.

### *Intrinsic hippocampal oscillatory activity in WT control and 5XFAD mice*

Prior to analysis of the hippocampal oscillatory behaviour, we analyzed motor activity in control and 5XFAD mice as active exploratory behaviour is associated with a different type of theta entity as compared to e.g. alert immobility (**Fig. 2A,B**). Movement in the horizontal plane was automatically determined by the recording system. The total time of motor activity did not change between controls and 5XFAD mice ( $9.1021 \pm 0.7242$  min/h v.  $9.5924 \pm 1.7658$  min/h, **Fig. 6A**). The same hold true for motor activity during the light phase ( $8.1097 \pm 1.2257$  min/h v.  $8.7222 \pm 1.3571$  min/h, **Fig. 6B**) and dark phase ( $10.0944 \pm 1.0526$  min/h v.  $10.4625 \pm 2.5194$  min/h, **Fig. 6C**). These results correlate with finding from Jawhar et al., 2012 for exploratory and spontaneous locomotor activity in 5XFAD mice aged 9 to 12 months. As expected however, there was an increase in motor activity from light to dark phase in both genotypes (**Fig. 6B,C**).

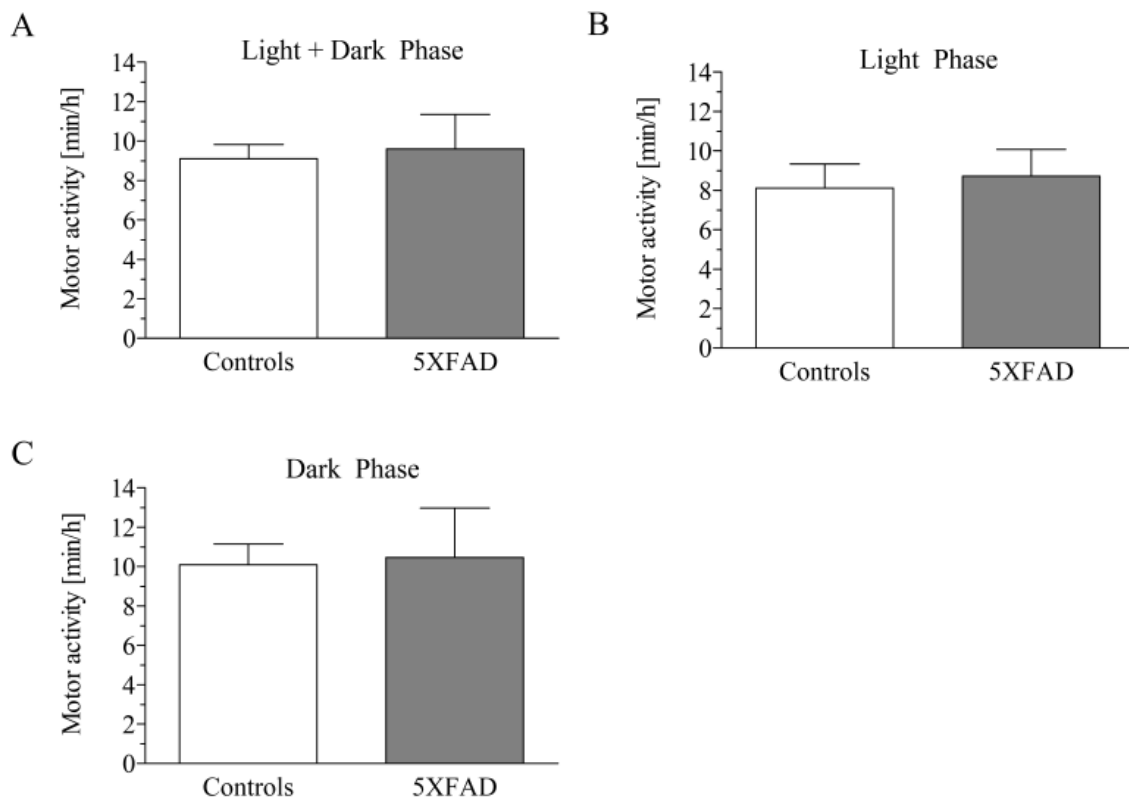


**Figure 6: Motor activity in controls and 5XFAD mice.** The radiotelemetry system is capable of measuring movement in the horizontal plane as rel. units. 10s epochs were categorized in a binary fashion as motor segments or non-motor segments. Motor activity was then calculated as [min/h] for the whole observation period (light + dark phase, **A**) and the light (**B**) and dark phase (**C**) separately. No difference was observed between both genotypes.

Based on these findings, alterations in 5XFAD theta architecture cannot be attributed to changes in activity pattern. To determine whether hippocampal theta oscillations were indeed altered in 5XFAD mice, we performed spontaneous 48 h video-EEG recordings from the CA1 region of the hippocampus from both controls and 5XFAD mice. Using a time-frequency approach, theta duration, theta frequency and theta amplitude were calculated. First, theta duration was calculated for both motor and non-motor activity. No significant changes were observed for controls compared to 5XFAD mice during the total observation period ( $5.4418 \pm 2.2384$  min/h v.  $7.3587 \pm 0.8902$  min/h, **Fig. 7A**), the light phase ( $5.2910 \pm 2.2141$  min/h v.  $6.0306 \pm 1.0558$  min/h, **Fig. 7B**) or the dark phase ( $5.5927 \pm 2.2731$  min/h v.  $8.6868 \pm 1.1632$  min/h, **Fig. 7C**). However, data suggested that there might be an increase in theta during the dark phase (**Fig. 7C**). During non-motor activity again no significant differences were detected for the total duration ( $3.8852 \pm 1.5287$  min/h v.  $4.8691 \pm 0.5677$  min/h, **Fig. 7D**), the light phase ( $3.9122 \pm 1.4981$  min/h v.  $4.0313 \pm 0.5944$  min/h, **Fig. 7E**) or the dark phase ( $3.8583 \pm 1.5605$  min/h v.  $5.7069 \pm 0.6974$  min/h, **Fig. 7F**).

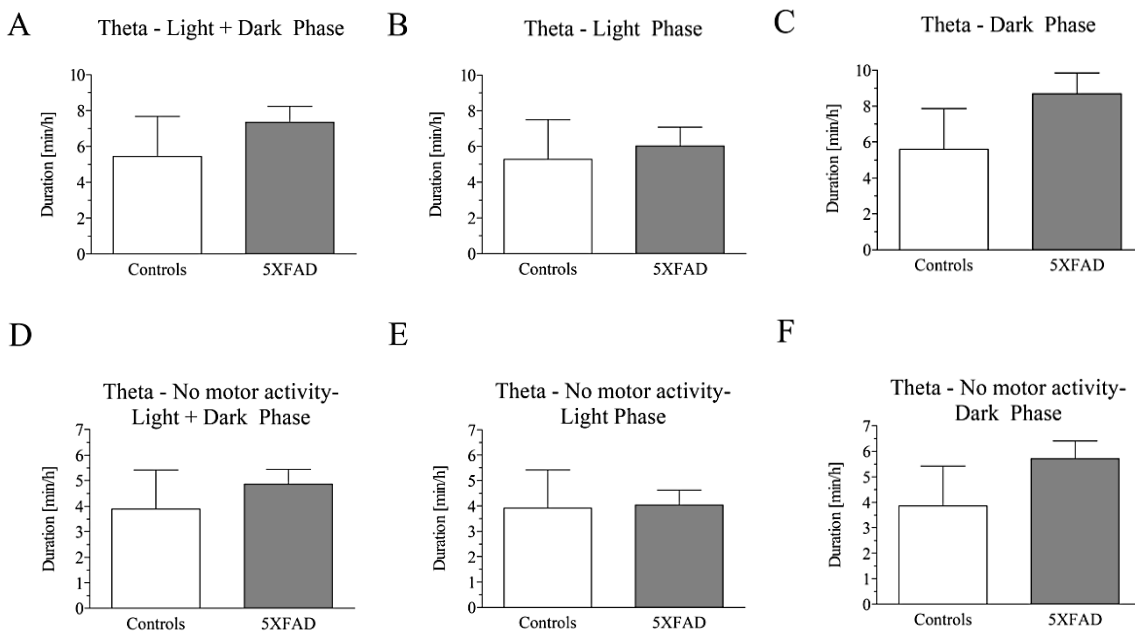


**Figure 7: Characteristics of Theta duration in control and 5XFAD mice.** The theta-alpha band was analysed using a time-frequency approach. Behavioural artefacts were removed using an algorithm as described above. Theta-segments (10s) were summed to determine theta duration [min/h]. Theta duration was calculated for both genotypes for the total observation period (**A**) and the light (**B**) and dark (**C**) phase, respectively. Total and phase-specific analysis was also done for non-motor activity (**D-F**) and motor activity (not shown). Mean values suggest an increase in theta duration in 5XFAD mice, particularly during the dark phase (**C,F**).

During the dark phase of no motor activity a tendency of increased theta duration was observed again, particularly in relation to the light phase. Based on this observation we analysed the percentage change of theta from light phase (LP) to dark phase (DP) via  $(LP/DP-1)*100$ . For the total 48h observation period, a significant trend was observed between controls and 5XFAD mice ( $-5.5515 \pm 5.7781$  v.  $-28.7790 \pm 10.5690$ ,  $p = 0.090$ , **Fig. 8A**), for non-motor activity this change turned out to be significant ( $5.1135 \pm 4.8816$  v.  $-27.5153 \pm 8.9914$ ,  $p = 0.013$ , **Fig. 8B**).

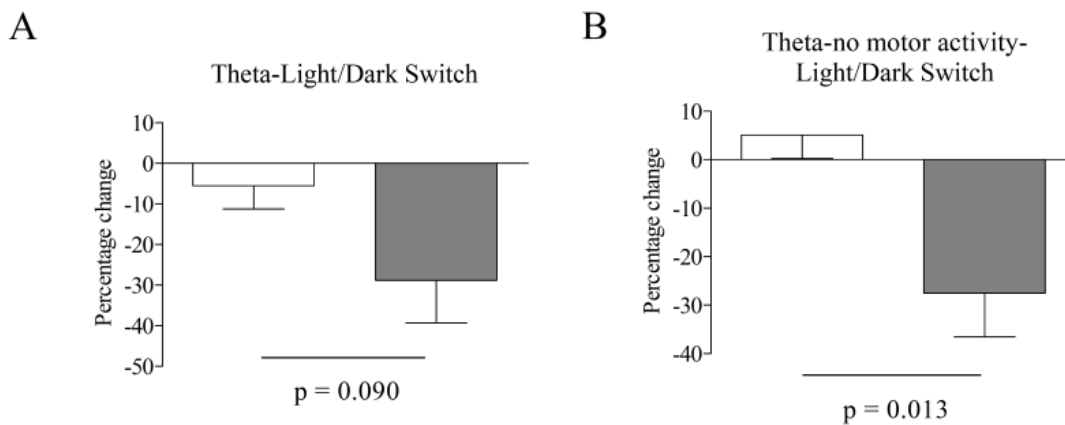


**Figure 8: Percentage change in theta duration during light/dark switch.** Data from **Figure 7 (B,C,E,F)** were used to calculate the percentage change in theta duration for every individual mouse during the total observation period (48 h, **A**), during non-motor activity (**B**) and motor activity (not shown). During switch from light to dark cycle there turned out to be a statistic trend for theta duration increase in 5XFAD mice (**A**). Again, this effect was most prominent and significant during no motor activity (**C**) and absent during motor activity.

Theta analysis during motor activity did not reveal any statistical differences (light and dark:  $1.5566 \pm 0.7158$  min/h v.  $2.4896 \pm 0.4803$  min/h; light:  $1.3788 \pm 0.7246$  min/h v.  $1.9993 \pm 0.4987$  min/h; dark:  $1.7344 \pm 0.7550$  min/h v.  $2.9799 \pm 0.7444$  min/h). An important parameter to be affected during the pathogenesis of Alzheimer's disease in humans is theta frequency. For the total recording period (light and dark phase) and the dark phase there was a tendency of reduced theta frequency in 5XFAD mice ( $7.0439 \pm 0.2821$  Hz v.  $6.5019 \pm 0.1957$  Hz, **Fig. 9A**;  $6.7709 \pm 0.2537$  Hz v.  $6.2876 \pm 0.2294$  Hz, **Fig. 9C**) with a statistical trend during the light phase ( $7.0923 \pm 0.2624$  Hz v.  $6.4782 \pm 0.1899$  Hz,  $p = 0.095$ , **Fig. 9B**). For the non-motor activity, the same phenomenon was observed with no significant change during the dark phase ( $6.7709 \pm 0.2537$  Hz v.  $6.2876 \pm 0.2294$  Hz, **Fig. 9F**), a significant trend for the total observation period



( $6.9171 \pm 0.2161$  Hz v.  $6.3187 \pm 0.2092$  Hz,  $p = 0.082$ , **Fig. 9D**) and a significant reduction during the light phase ( $7.0632 \pm 0.2170$  Hz v.  $6.3498 \pm 0.2077$  Hz,  $p = 0.045$ , **Fig. 9E**). No significant differences were observed for motor activities (light and dark:  $7.1707 \pm 0.3754$  Hz v.  $6.6851 \pm 0.1848$  Hz; light:  $7.1214 \pm 0.3250$  Hz v.  $6.6066 \pm 0.1752$  Hz; dark:  $7.2327 \pm 0.4162$  Hz v.  $6.7580 \pm 0.2253$  Hz). Finally, the mean theta amplitudes were calculated. For the total recording period, no changes in theta amplitude could be detected (light and dark:  $0.0192 \pm 0.0039$  mV v.  $0.0183 \pm 0.0031$  mV, light:  $0.0194 \pm 0.0040$  mV v.  $0.0184 \pm 0.0033$  mV; dark:  $0.0189 \pm 0.0039$  mV v.  $0.0183 \pm 0.0029$  mV). The same hold true for the non-motor activity (light and dark:  $0.0199 \pm 0.0039$  mV v.  $0.0183 \pm 0.0030$  mV; light:  $0.0204 \pm 0.0040$  mV v.  $0.0184 \pm 0.0032$  mV, dark:  $0.0193 \pm 0.0038$  mV v.  $0.0181 \pm 0.0028$  mV) and non-motoric phase. This finding correlates with previous observations in 5XFAD but also TgCRND8 mice (Goutagny and Krantic, 2013).

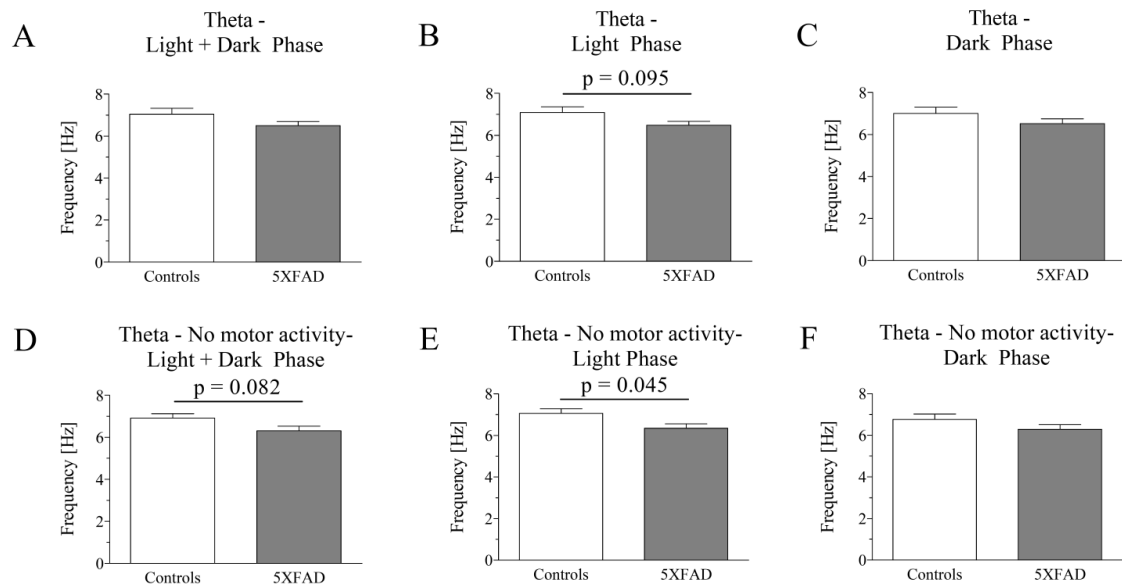


**Figure 9: Theta-frequency in controls and 5XFAD mice.** The mean theta frequency was calculated for the total observation period (48 h, **A-C**), no motor activity (**D-F**) and motor activity (not shown). In all cases, theta frequency is reduced. Again, this reduction turned out to be significant during no motor activity (**E**).

#### *Urethane induced hippocampal theta oscillations in controls and 5XFAD mice*

Besides analysis of spontaneous theta activity, we also investigated urethane induced theta oscillations. Pharmacodynamically, urethane has a multi-target character capable

of inducing atropine-sensitive type II theta. Theta oscillations were analyzed for 30 min baseline and 30 min post injection episodes (**Fig. 10**). The duration of hippocampal theta oscillations for the total analytical period, i.e. including theta oscillations during episodes with either motor or non-motor activity, was increased in control mice ( $1.59 \pm 0.47$  min/h to  $4.20 \pm 1.40$  min/h,  $n = 4$ ) as in 5XFAD mice ( $5.09 \pm 2.06$  min/h to  $18.08 \pm 6.25$  min/h,  $n = 4$ ) and where the factor “experimental condition/urethane effect” shows a significance ( $p = 0.036$ ). The factor “genotype” exhibited a statistical trend ( $p = 0.062$ ) (**Fig. 10A**).

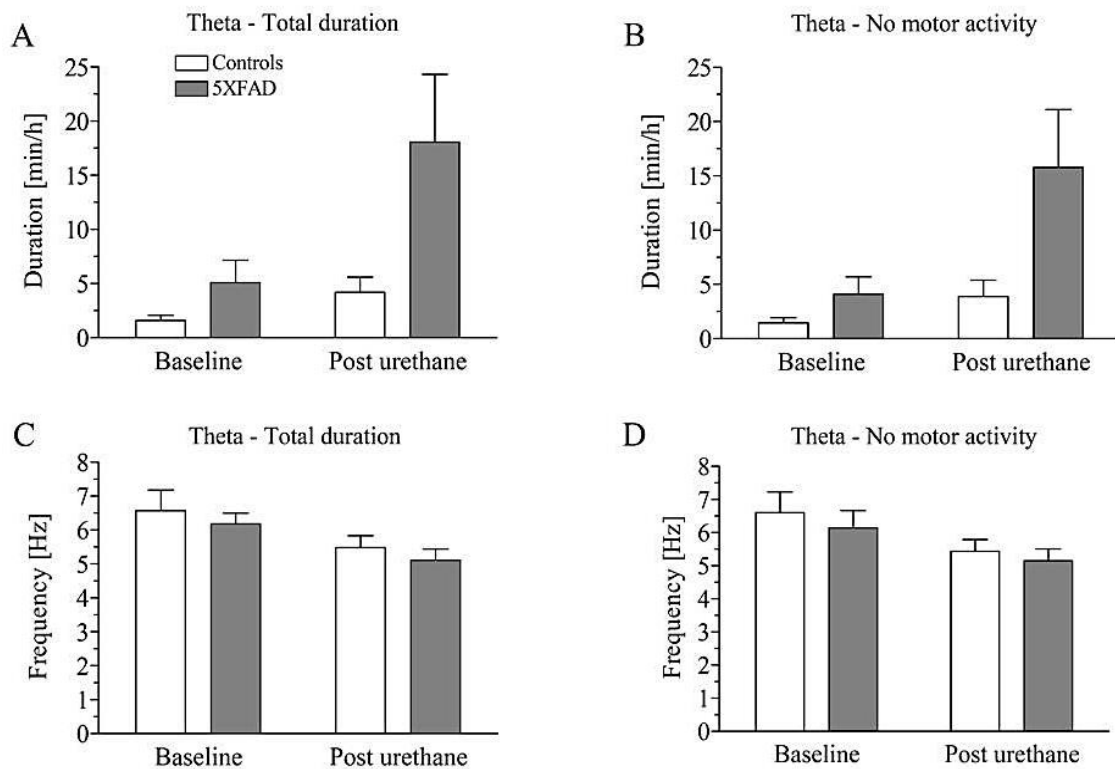


**Figure 10: Urethane induced hippocampal theta oscillations in control and 5XFAD mice.** CA1 hippocampal theta recordings from both genotypes were analyzed for duration of atropine-sensitive type II theta oscillations regarding total observation period (**A**) and non-motor episodes (**B**). In addition, theta frequency was calculated for total duration (**C**) and non-motor episodes (**D**).

As type II theta is characteristic of alert immobility data were also analyzed for non-motor activity EEG segments. As expected, the results matched those for the total analytical period, i.e. a significant effect for the factor “experimental condition/urethane effect” ( $p = 0.032$ ) with increase in controls ( $1.45 \pm 0.48$  min/h to  $3.88 \pm 1.52$  min/h,  $n = 4$ ) and 5XFAD mice ( $4.11 \pm 1.59$  min/h to  $15.78 \pm 5.34$  min/h,  $n = 4$ ). The factor

“genotype” exhibited a statistical trend ( $p = 0.064$ ) (**Fig. 10B**). These findings demonstrate that 5XFAD mice even of higher age are capable of displaying increased theta oscillations upon urethane provocation. However, it remains to be determined whether such theta activity is physiologically integrated or the result of hyperactive, functionally dislinked neuronal clusters within the hippocampus. Interestingly, besides an effect for theta-duration, there was a significant effect for the factor “experimental condition/urethane effect” ( $p = 0.010$ ) on theta oscillation frequency for the total analytical period ( $6.57 \pm 0.61$  Hz to  $5.48 \pm 0.36$  Hz, ( $n = 4$ ) in controls versus  $6.18 \pm 0.31$  Hz to  $5.11 \pm 0.33$  Hz ( $n = 4$ ) in 5XFAD mice) (**Fig. 10C**). This significant effect ( $p = 0.030$ ) also hold true for the non-motor episodes ( $6.60 \pm 0.63$  Hz to  $5.44 \pm 0.35$  Hz ( $n = 4$ ) in controls versus  $6.14 \pm 0.53$  Hz to  $5.15 \pm 0.36$  ( $n = 4$ ) in 5XFAD mice (**Fig. 10D**).

## Discussion

Alzheimer's disease is a complex neurodegenerative disorder accompanied by cognitive impairment that ultimately leads to dementia. In the present study, we investigated transcriptional alterations and the EEG phenotype of 5XFAD mice. This mouse model harbors five early-onset familial FAD mutations and displays substantial A $\beta$  plaques and neurodegeneration (Crouzin et al., 2013; Eimer and Vassar, 2013). Our study demonstrates that 5XFAD mice exhibit non-convulsive seizure activity of different severity, predominantly in the M1 deflection, whereas there was hardly any seizure activity in the CA1 recordings. It's noteworthy that A $\beta$  formation in certain mouse models can differentially alter cholinergically induced rhythmicity according to the structure of A $\beta$  plaques (Crouzin et al., 2013) and therefore leading to different phenotypes of seizure activity. In addition, stereological quantification of pyramidal neurons of the CA1 layer showed no significant difference between the number of neurons of WT and 5XFAD mice, however a significant loss was detected in cortical layer 5 (Crouzin et al., 2013). A single 5XFAD mouse exhibited status like generalized tonic-clonic seizures and early death and thus was not included into the study analysis. Experimental studies in genetically engineered mice support these findings, highlighting the presence of subclinical seizures and overlapping pathophysiological cascades (Noebels, 2011). Lowered convulsant thresholds and spontaneous convulsive seizure phenotypes have been observed in AD mouse models (Kumar et al., 2000; LaFerla et al., 1995; Lalonde et al., 2005; Moechars et al., 1996). Interestingly, deletion of APP (Steinbach et al., 1998) and BACE1, the secretase that participates in A $\beta$  release (Hu et al., 2010) also causes an epileptic phenotype, indicating that normal APP signaling is important for the development of hippocampal excitability (Minkeviciene et al., 2009). In some models, lower thresholds for induced or spontaneous seizures are found even in the absence of amyloid deposits, further stressing the role of soluble forms of A $\beta$  as a pathogen (Kumar et al., 2000; Steinbach et al., 1998). Chronic EEG monitoring in J20 mice overexpressing hAPP (Palop et al., 2007) revealed that most frequent seizures were purely electroencephalographic, i.e. non-convulsive without complete motoric arrest as observed in our study using 5XFAD mice (Palop et al., 2007; Palop and Mucke, 2009). Similarly, in rare cases motor seizures were observed. This observation raises the question whether abnormal hippocampal neuronal synchronization remains undetected in human AD patients, and whether this network level abnormality might

accelerate a more rapid cognitive decline in patients suffering from FAD (Palop et al., 2006; Palop et al., 2007; Pandis and Scarmeas, 2012). Histological evaluation of the J20 mouse hippocampus revealed striking evidence for hippocampal network remodeling that is similar, but not identical, to the changes identified in both patients with temporal lobe epilepsy and experimental models of hippocampal seizures. The cellular changes included ectopic sprouting of dentate granule cell mossy fibres and sprouting of fibers containing the inhibitory neurotransmitter NPY (de Lanerolle et al., 1989; Sutula et al., 1989). Convulsive seizures with associated hippocampal network plasticity have been confirmed in other AD mouse models (Minkeviciene et al., 2008; Minkeviciene et al., 2009; Sutula et al., 1989). Interestingly, impairments of GABA transmission in the J20 brain provide an interesting basis for epileptogenesis in these models. Increased adult neurogenesis is found in both human AD and temporal lobe epilepsy (TLE) cases (Jin et al., 2004; Sutula et al., 1989). The multiple lines of evidence discussed above show that soluble forms of A $\beta$  are cytotoxic inducing the appearance of aberrant excitatory neuronal network activity *in vivo*, and triggering complex molecular and cellular patterns of compensatory inhibitory and excitatory mechanisms in hippocampal circuitry (Amatniek et al., 2006; Goutagny and Krantic, 2013; Hauser et al., 1986; Pandis and Scarmeas, 2012; Westmark et al., 2008). The toxic accumulation of A $\beta$  peptides underlying Alzheimer's disease (AD) triggers synaptic degeneration, circuit remodeling, and abnormal synchronization within the same networks. Because neuronal hyperexcitability amplifies the synaptic release of A $\beta$ , seizures create a vicious spiral that accelerates cell death and cognitive decline in the AD brain (Chin and Scharfman, 2013). While degenerative processes in the nervous system ultimately result in loss of neural signaling, when active inhibitory mechanisms fail early, the resulting disinhibition may destabilize network oscillatory activity at formative stages of the disease.

How can seizure activity correlate with altered theta oscillations in the hippocampus? Complex cognitive operations are depended on a sophisticated coordination of activity across a plethora of neuronal groups. One of the most intriguing mechanisms for neuronal coordination and communication is through neuronal synchronization by brain oscillations (Womelsdorf et al., 2007). Theta oscillations represent one of these oscillations and are modulated by specific behavioural and cognitive states and are related to memory deficits, e.g. in AD (Buzsaki, 2002; Chin and Scharfman, 2013; Gutierrez-Lerma et al., 2013; Moretti et al., 2010; Palop et al., 2007; Pena-Ortega and

Bernal-Pedraza, 2012). Disruption of theta activity results in spatial memory deficits, whereas the restoration of theta-like rhythmicity restores learning capabilities in rats (McNaughton et al., 2006). Theta duration analysis in our study suggests an increase of theta oscillations in 5XFAD mice during the dark phase. This phenomenon was most prominent during the switch from light to dark phase and non-motor activity. As analysis of motor/non-motor activity did not reveal any difference between controls and 5XFAD mice, the difference in theta duration is likely to be based on theta-subtype composition. We speculate that mice in the non-active dark phase predominately exhibit alert-immobility which is characterized by atropine-sensitive type II theta (Bland et al., 1996; Shin et al., 2005). As in our study, a statistical trend for an increase in theta duration has been described in the TgCRND8 mouse model (Goutagny and Krantic, 2013). These changes in theta duration in 5XFAD mice are an important variable because they are known to be associated with memory effectiveness. Animals displaying a higher amount of theta activity are faster in novel task learning than animals that exhibit less pronounced theta oscillations (Berry et al., 1978; Moretti et al., 2010). Unlike the common assumption of decreased theta activity in dementia, an increase in theta activity is observed in various mouse models of AD. Administration of urethane to induce hippocampal type II theta clearly proved that 5XFAD mice can exhibit increased atropine sensitive theta oscillations upon provocation (**Fig. 7A,B**). One might speculate that hyperexcitable neuronal clusters surrounded by degenerated neurons might account for this increase in theta which disrupts the ability of neuronal networks to dynamically adjust the amplitude of these oscillations during memory processes. Interestingly, the mean theta frequency was reduced in 5XFAD mice, i.e. theta oscillations turned out to be significantly slower than in control animals. This phenomenon is commonly observed in Alzheimer patients (Czigler et al., 2008; Jelic et al., 2000; Jelic and Nordberg, 2000; Moretti et al., 2010). It has been suggested that theta frequency could change as a function of novelty and familiarity (Jeewajee et al., 2008). Thus, the significant decrease in theta frequency could dramatically skew the delicate balance of theta frequency dynamics between novelty and familiarity. Previous studies have shown that the muscarinic signaling transduction cascade (Felder, 1995) is severely affected in AD, e.g. carbachol-induced PKC activation is disrupted by A $\beta$  (Huang et al., 2009) that might correlate with a very slight down-regulation of PLC1 as observed in our study (**Fig. 11**). Ca $_v$ 2.3 voltage-gated Ca $^{2+}$  channels are involved in both the generation of cellular correlates of ictal discharges, i.e. afterdepolarisation and

plateau potentials (Kuzmiski et al., 2005; Tai et al., 2006) and the generation of atropine-sensitive type II theta (Jansen et al., 2011; Muller et al., 2012; Shin et al., 2005; Shin et al., 2009). Transcriptome analysis of 5XFAD hippocampal probes performed in this study suggests an upregulation of PLCd4 which could results in type II theta acceleration via the PKC, Ca<sub>v</sub>2.3 cascade (Muller et al., 2012) however, other muscarinic signaling targets could also be involved (**Fig. 11**).

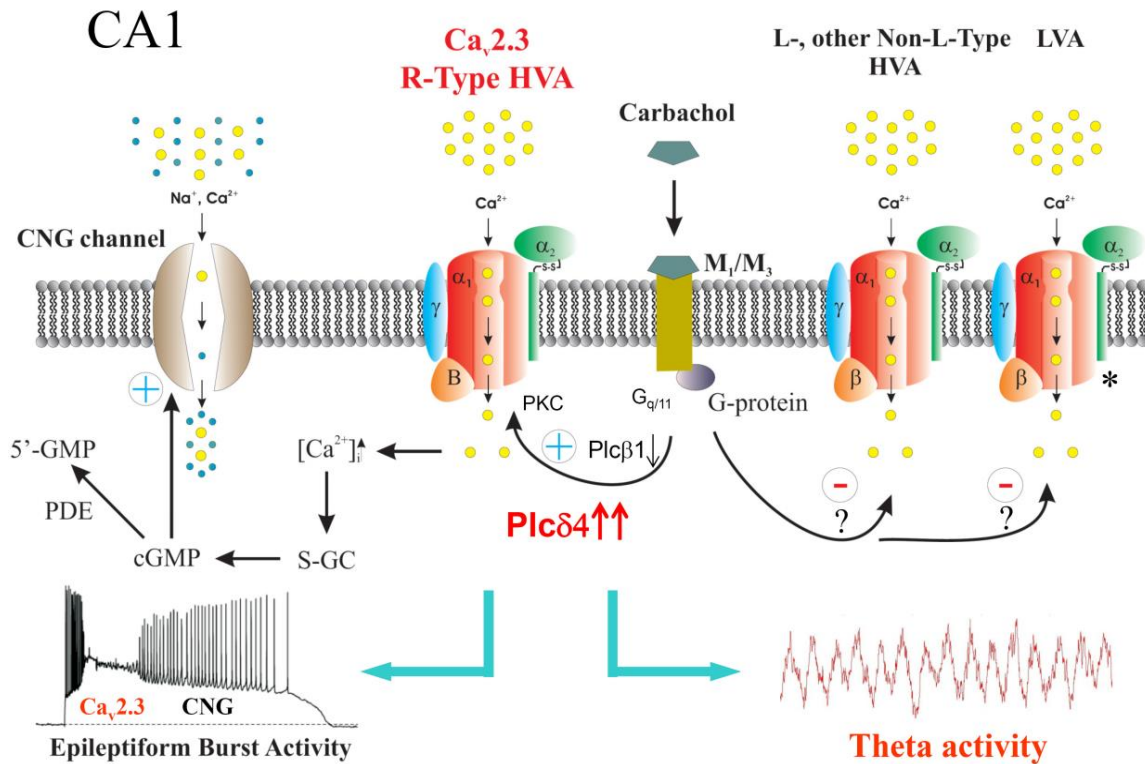


**Figure 11: Functional integration of seizure activity and theta oscillations in the 5XFAD model of Alzheimer’s disease.** Time-frequency analysis in 5XFAD mice revealed changes in theta duration and theta frequency which are related to no motor activity, particularly during the dark phase. Under these conditions, the animals either sleep or rest. Hippocampal activity during the state of alert immobility is characterized by atropine-sensitive type II theta, which is related to the muscarinic signal transduction pathway. Activation of PLC was shown to enhance Ca<sup>2+</sup> influx via Ca<sub>v</sub>2.3 R-type Ca<sup>2+</sup> channels which can lead to the generation of epileptiform burst activity via CNG mediated plateau potentials. However, Ca<sub>v</sub>2.3 R-type channels were also shown to be involved in the generation of hippocampal theta oscillations. Enhanced transcription of PLCd4 might thus trigger both enhanced theta duration and theta frequency alteration in 5XFAD mice but also seizure activity in this severe model of AD.

Summing up, we conclude that Aβ accumulation in 5XFAD mice results in altered muscarinic signaling that accounts for both seizure activity and altered theta architecture. Although some caution is warranted in interpreting results from the

aggressive amyloid mouse model 5XFAD that over expresses multiple FAD mutations as, our results stress that pharmacological interference with muscarinic signaling is a valuable target in AD treatment. Finally, our study suggests that alterations in theta characteristics might serve as a diagnostic and prognostic biomarker in AD in the future.



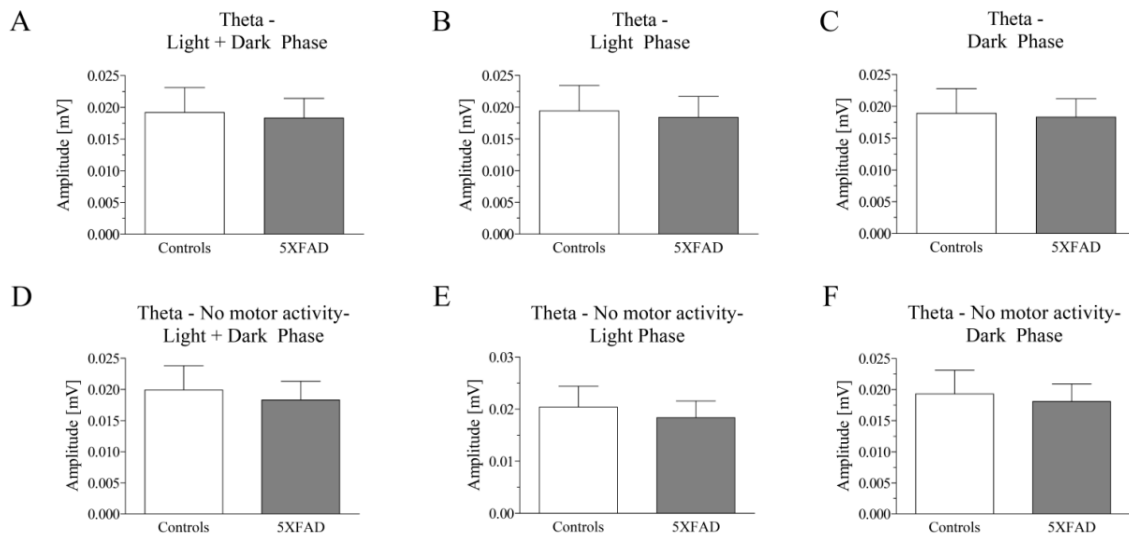
**Acknowledgments**

The authors would like to thank Dr. Ylva Mende (German Center for Neurodegenerative Diseases, DZNE) and Dr. Michaela Moehring (DZNE) for assistance in animal breeding and animal health care. This work was financially supported by the Federal Institute for Drugs and Medical Devices (Bundesinstitut für Arzneimittel und Medizinprodukte, BfArM, Bonn, Germany).

**Conflict of interest**

The authors confirm that there are no conflicts of interests.

## Supplement



**Supplementary Figure 1: Characteristics of theta amplitude in control and 5XFAD mice.** The theta-alpha band was analysed using a time-frequency approach. Behavioural artefacts were removed using an algorithm as described above. Amplitude was calculated for both genotypes for the total observation period (A) and the light (B) and dark (C) phase, respectively. Total and phase-specific analysis was also done for non-motor activity (D-F) and motor activity (not shown). No difference was observed between both genotypes.

<b>AFC TG vs WT</b>	<b>Regulation</b>	<b>Candidate Genes</b>
1.1079566	down	Cacna2d1, Calcium Channel, L Type, Alpha
1.1112925	down	Cacna1e, Cav2.3 calcium channel
1.1162357	up	Cacng5, calcium channel, voltage-dependent, gamma subunit 5
1.2483352	down	Cacng2, calcium channel, voltage-dependent, gamma subunit 2
1.2776582	down	Kcna4, potassium voltage-gated channel
1.1231822	down	Kcnab1, potassium voltage-gated channel
1.0865682	down	Kcne4, potassium voltage-gated channel, Isk-related family, member 4
1.3661991	down	Kcnh5, potassium voltage-gated channel, subfamily H (eag-related), member 5
1.4835429	down	Kcnh7, potassium voltage channel, subfamily H, member 7
1.1978878	down	Kcnip4, potassium channel interacting protein
1.1670644	down	Kcnj11, potassium inwardly-rectifying channel, subfamily J, member 11
1.0783806	down	Kcnma1, potassium large conductance calcium-activated channel, subfamily M, $\alpha$ 1
1.2284602	down	Kcnn2, potassium intermediate/small conductance calcium-activated channel, subfamily N, member 2
1.2311752	down	Kcnq3, potassium voltage-gated channel, KQT-like subfamily, member 3
1.1255795	down	Scn8a, sodium channel, voltage-gated, type VIII, alpha
1.0604281	up	Ank, progressive ankylosis protein
1.1039068	down	Ankra2, ankyrin repeat, family A (RFXANK-like), 2
1.2761725	up	Ankrd13a, ankyrin repeat domain 13A
1.7455606	down	Ankrd34c, ankyrin repeat domain 34C
1.1975257	down	Ankrd43, ankyrin repeat domain-containing protein 43
1.1477777	down	Ankzf1, ankyrin repeat and zinc finger domain containing 1
1.1017654	up	Aplp2, amyloid beta (A4) precursor-like protein 2
1.0611709	down	Calm2, calmodulin 2
1.4713943	up	Chrm5, cholinergic receptor, muscarinic 5
1.158719	up	Eef1b2, eukaryotic translation elongation factor 1 beta 2
1.1446922	down	Gabra4, gamma-aminobutyric acid (GABA) A receptor, subunit alpha 4
1.2972732	down	Gabrb2, gamma-aminobutyric acid (GABA) A receptor, subunit beta 2
1.0849586	down	Gabrb3, gamma-aminobutyric acid (GABA) A receptor, subunit beta 3
1.0767342	down	Gria3, AMPA-selective glutamate receptor 3
1.185587	down	Gria4, AMPA-selective glutamate receptor 4
1.1791353	down	Grid1 Mir346, gluR delta-1 subunit
1.1244333	down	Grin2a, N-methyl D-aspartate receptor subtype 2A
1.1251612	down	Grin2b, N-methyl D-aspartate receptor 2B
1.0896682	down	Kank3, KN motif and ankyrin repeat domains 3
1.1632725	down	Negr1, neuronal growth regulator 1
1.1632118	down	Pde1b, phosphodiesterase 1B, Ca <sup>2+</sup> -calmodulin dependent
1.149241	down	Plcb1, phospholipase C, beta 1
1.1644183	up	Plcb3, phospholipase C, beta 3
1.2514523	up	Plcd4 Zfp142, phospholipase C, delta 4, PLC-delta-4
1.9414148	up	Plce1, phospholipase C, epsilon
1.2460053	up	Plcg2, phospholipase C, gamma 2

1.1797961	down	Prkar2b, protein kinase, cAMP dependent regulatory, type II beta
1.1495365	down	Prkcb, protein kinase C, beta
1.1005048	up	Prkx, protein kinase PKX1
1.1885214	up	Rapgef3, Rap1 guanine-nucleotide-exchange factor directly activated by cAMP
1.2769251	down	Scg2, secretogranin II
1.1976677	down	Stx1b, syntaxin-1B
1.5812538	up	Syng2, synaptogyrin 2
1.2852507	down	Trank1, tetratricopeptide repeat and ankyrin repeat containing 1
1.5507693	up	Vamp8, vesicle-associated membrane protein 8
1.5849916	up	Casp8, Caspase 8
1.4427319	up	Cflar, Casp8 and FADD-like apoptosis regulator

**Supplementary Table 1: Representation of interesting candidate genes revealed from microarray analysis.** The absolute fold change (AFC) between transgenic Alzheimer's 5XFAD mice and WT control littermates.

<b>AFC TG vs WT</b>	<b>Regulation</b>	<b>Candidate Genes</b>
30,691187	up	Cst7, cystatin F (leukocystatin); 2310001A20Rik, RIKEN cDNA 2310001A20 gene
25,800545	up	Cst7, cystatin F (leukocystatin); 2310001A20Rik, RIKEN cDNA 2310001A20 gene
11,236571	up	Ccl3, chemokine (C-C motif) ligand 3
6,5900187	up	Gpnmb, glycoprotein (transmembrane) nmb
6,0320563	up	Olfrl11, olfactory receptor 111; Olfrl10, olfactory receptor 110
4,5509095	up	Lyz2, lysozyme 2; Lyz1, lysozyme 1
4,509695	up	Tyrobp, TYRO protein tyrosine kinase binding protein
4,4565377	up	CD68 antigen
4,2304597	up	Serpina3nm, serine (or cysteine) peptidase inhibitor, clade A, member 3N
4,0053725	up	Osmr, oncostatin M receptor
3,980827	up	Trem2, triggering receptor expressed on myeloid cells 2
3,9256482	up	Gfap, glial fibrillary acidic protein
3,8248506	up	C3ar1, complement component 3a receptor 1
3,6593776	up	Ly86, lymphocyte antigen 86; Igsf21, immunoglobulin superfamily, member 21
3,6451392	up	Clec7a, C-type lectin domain family 7, member a
3,6262984	up	C4b, complement component 4B (Childo blood group); C4a, complement component 4A (Rodgers blood group)
3,5611908	up	Itgax, integrin alpha X; Mcart1, mitochondrial carrier triple repeat 1; Itgad, integrin, alpha D
3,4145424	up	Lilrb4, leukocyte immunoglobulin-like receptor, subfamily B, member 4; Gp49a, glycoprotein 49 A
3,4005163	up	CD180 antigen
3,2523582	up	CD84 antigen
3,074628	up	Ctss, cathepsin S
3,0741098	up	Fcer1g, Fc receptor, IgE, high affinity I, gamma polypeptide
3,0641675	up	Fcgr3, Fc receptor, IgG, low affinity III
3,0616438	up	Lgals3bp, lectin, galactoside-binding, soluble, 3 binding protein
3,0302508	up	C1qc, complement component 1, q subcomponent, C chain
2,9237657	up	C1qb, complement component 1, q subcomponent, beta polypeptide
2,905447	up	Laptm5, lysosomal-associated protein transmembrane 5
2,8482487	up	C1qa, complement component 1, q subcomponent, alpha polypeptide
2,8451812	up	Fcgr2b, Fc receptor, IgG, low affinity IIb
2,8256595	up	Ctsd, cathepsin D
2,8111982	up	Plek, pleckstrin
2,8064747	up	Ctsz, cathepsin Z
2,7769005	up	Hexb, hexosaminidase B
2,7556384	up	Tlr7, toll-like receptor 7
2,615431	up	Bcl2a1d, B-cell leukemia/lymphoma 2 related protein A1d; Bcl2a1b, B-cell leukemia/lymphoma 2 related protein A1b; Bcl2a1a, B-cell leukemia/lymphoma 2 related protein A1a
2,543658	up	Slc11a1, solute carrier family 11 (proton-coupled divalent metal ion transporters), member 1
2,4172409	up	CD52 antigen
2,4062214	up	CD9 antigen
2,3877494	up	Slc14a1, solute carrier family 14 (urea transporter), member 1
2,385867	up	CD53 antigen
2,3474405	up	Cybb, cytochrome b-245, beta polypeptide
2,3225377	up	Lcn2, lipocalin 2
2,3032408	up	Hvcn1, hydrogen voltage-gated channel 1; Tctn1, tectonic family member 1

2,2871568	up	Gp49a, glycoprotein 49 A; AB056442, cDNA sequence AB056442; Lilrb4, leukocyte immunoglobulin-like receptor, subfamily B, member 4; D630002G06Rik, RIKEN cDNA D630002G06 gene
2,2849452	up	Csf3r, colony stimulating factor 3 receptor (granulocyte)
2,2655497	up	Gm11428, predicted gene 11428
2,2569838	up	Irf8, interferon regulatory factor 8
2,231863	up	H2-K1, histocompatibility 2, K1K region; Gm7035, predicted gene 7035; H2-Q2, histocompatibility 2, Q region locus 2; LOC100044874, similar to H-2K(d) antigen
2,2273088	up	Cybrd1, cytochrome b reductase 1
2,1967485	up	Tlr13, toll-like receptor 13
2,1918335	up	4632428N05Rik, RIKEN cDNA 4632428N05 gene
2,191425	up	Cx3cr1, chemokine (C-X3-C) receptor 1
2,182198	up	H2-D1, histocompatibility 2, D region locus 1; H2-Q2, histocompatibility 2, Q region locus 2; H2-L, histocompatibility 2, L region; H2-K1, histocompatibility 2, K1, K region
2,1029935	up	Hpgds, hematopoietic prostaglandin D synthase
2,0661345	up	Nckap1l, NCK associated protein 1 like
2,040309	up	Csf1r, colony stimulating factor 1 receptor
2,0336578	up	Havcr2, hepatitis A virus cellular receptor 2
2,0043225	up	Man2b1, mannosidase 2, alpha B1
2,001403	up	Trf, transferrin

**Supplementary Table 2: Presentation of candidate genes revealed from microarray analysis with absolute fold change (AFC) > 2 between transgenic Alzheimer's 5XFAD (TG) mice and WT control littermates (WT).** Gene ontology analysis revealed that the strongest transcriptional alterations belong to immune-response and inflammation related genes observed in the context of late-stage cerebral amyloidosis.

### 3. Discussion

Previous studies address the crucial role of VGCCs in etiology and pathogenesis of theta rhythms and seizure activity. Herby, the  $\text{Ca}_v2.3$  R-type  $\text{Ca}^{2+}$  channel is likely to be important in hippocampal (Metz et al., 2005) and thalamocortical circuits (Zaman et al., 2011) providing its overall extraordinary function in certain central rhythmicity. Based on these recent findings, it is a question of debate how electrophysiological alterations in theta activity can share at least in some aspects similar underlying mechanisms that are potentially existing for sleep disorders, AD and seizure susceptibility.

Here, we demonstrate that sleep architecture is fundamentally modulated by  $\text{Ca}_v2.3$  R-type  $\text{Ca}^{2+}$  channels in a light-dark dependent manner.  $\text{Ca}_v2.3^{-/-}$  mice show significantly decreased wake duration and increased SWS1 compared to their WT littermates indicating an abbreviation of sleep stage transitions. Therefore, we conclude that the functional role of  $\text{Ca}_v2.3$  R-type  $\text{Ca}^{2+}$  channels in sleep regulation might be related to the synchronization of oscillatory activity in the TC network. Changes in sleep stage transitions shown in our study are furthermore supported by sleep scoring results from pharmacologically induced SWS after urethane administration. Following urethane injection  $\text{Ca}_v2.3^{-/-}$  mice exhibit increased SWS1 and decreased wake duration in comparison to  $\text{Ca}_v2.3^{+/+}$  animals. However, it has to be pointed out that urethane is a multi-targeting drug not exclusively effecting one specific signaling pathway. Urethane at a dosage of 800mg/kg i.p used in our study elicits light SWS but not deep anesthesia. Previous studies demonstrated that TC rhythmicity can be differentially modulated according the pharmacodynamic profiles of several anesthetics (Takei et al., 2003). For instance, isoflurane is capable of inhibiting presynaptic  $\text{Ca}_v2.3$  R-type  $\text{Ca}^{2+}$  channels which are necessary for inhibitory  $\text{GABA}_A$  transmission in RTN cells but leads to an inhibition of T-type currents as well (Joksovic et al., 2005; Joksovic et al., 2009; Todorovic et al., 2000). Thus, it still remains striking to predict the final consequences of anesthetics on the TC system. Analysis of sleep deprivation in  $\text{Ca}_v2.3^{-/-}$  mice revealed a non-significant trend of higher delta amplitude in  $\text{Ca}_v2.3^{-/-}$  mice in comparison to WT mice suggesting a less impact of sleep deprivation provoked by TC hyperoscillations. In line with this, Zaman et al. recently illustrated that  $\text{Ca}_v2.3$  R-type  $\text{Ca}^{2+}$  channels promote rebound burst firing in RTN neurons through the activation of SK2 channels. Taken this finding into consideration, it seems astonishing that ablation of  $\text{Ca}_v2.3$  R-type  $\text{Ca}^{2+}$

channels did not result in decreased SWS as illustrated in our study. To explain this initially controversial observation one has to keep in mind that initiation and regulation of sleep is not uniquely restricted to the RTN physiology but also includes the functional involvement of LVA  $Ca_v3.1-3.3$  T-type  $Ca^{2+}$  channels, HCN and non-specific cation channels as well as extrathalamocortical sleep modulators. Within the TC system relay cells and RTN neurons represent a functional unit. For instance, region specific deletion of 3.1 T-type  $Ca^{2+}$  channels results in lack of  $Ca_v3.1$  triggered  $Ca^{2+}$  influx in relay cells finally leading to altered burst activity that is in line with massive sleep disruption as recently demonstrated by Lee et al., 2004. Unlike the deletion of  $Ca_v3.1$  T-type  $Ca^{2+}$  channels, blockade of  $Ca_v3.2$  T-type  $Ca^{2+}$  channels is related to enhanced sleep duration, whereas sleep architecture remains to be altered (Lee and Shin, 2007). These findings clearly illustrate the complex nature of TC rhythmicity and the contribution of VGCC as its functional modulators. To test possible compensatory mechanisms on TC rhythmicity by T-type  $Ca^{2+}$  channels, we performed qPCR experiments. Our results depict no significant changes in T-type  $Ca^{2+}$  channel expression indicating that no thalamic disruption in these  $Ca^{2+}$  channels can account for changed oscillatory pattern in  $Ca_v2.3^{-/-}$  mice. However, we are not able to assume this for the extrathalamocortical regions as well. Extrathalamocortical structures like the hippocampus, the basal ganglia, mesopontine REM-NREM neuronal entities in the ACE and hypothalamic nuclei can act as sleep onset controllers and modulators. Therefore, they are able to influence oscillatory activity in the TC system substantially (Deransart et al., 1998; Khosravani and Zamponi, 2006; Manning et al., 2003; Pace-Schott and Hobson, 2002) by regulating excitability in Wake-ON, REM-ON and NREM-ON cell entities of the ACE via  $Ca_v2.3$  R-type based  $Ca^{2+}$  current (Lee et al., 2002). Our results might be indeed considerable for the isolated TC system in vivo. However, they are not sufficient enough to explain all molecular mechanisms in detail. For elucidating the functional role of  $Ca_v2.3$  R-type  $Ca^{2+}$  channels in the TC system more precisely and drawing our understanding on TC rhythmicity one step closer, future studies on sleep architecture have to consider investigations of extrathalamocortical structures as well. In terms of a global neuronal network it is furthermore necessary to look at altered properties of VGCC and neuronal ensembles under pathophysiological conditions like occurring in AD. AD is an age-related neurodegenerative disorder characterized by impairment of memory function and massive synaptic loss. Because highly



synchronized neuronal activity is mandatory for proper cognitive functions, imbalance of inhibitory and excitatory processes can finally contribute to disruption in oscillatory rhythmicity (Kordower et al., 2001; Morrison and Hof, 1997; Price et al., 2001; Terry et al., 1991). In this regard, recent investigations suggest that accumulation of soluble A $\beta$  in AD is capable of eliciting reorganisation in neuronal networks resulting in seizure activity. Previously, it was believed that seizure activity marks a secondary process which is closely related to age-dependent neurodegeneration within the hippocampus and the entorhinal cortex (Deipolyi et al., 2007; Deipolyi et al., 2008). Nowadays this notion might be seen more in context of animal models indicating that altered excitatory neuronal activity represents rather a primary upstream mechanism than being related to secondary processes of neurodegeneration. Observations in patients with AD also stress this assumption. It could be shown that increased incidence of unprovoked seizures appears independently of disease stages in sporadic form of AD (Amatniek et al., 2006). However, it has to be pointed out that a whole causal interdependence between high levels of A $\beta$  peptide and cognitive decline in humans still remains to be not fully understood. Animal models of AD so far provide important and indispensable tools for investigations on pathophysiological neuronal interactions but they are always limited to the experimental issue they are referring to. In accordance to the complex nature of AD, it is still striking to determine whether given changes in signaling cascades drive disease pathology or simply illustrate diffused responses of neuronal activity or increased seizure susceptibility. To set light on this issue, we investigated the electrophysiological and behavioural phenotype of the 5XFAD mouse model of familial AD to dissect the causal relationship between A $\beta$ -induced aberrant neuronal activity and cognitive decline and furthermore to provide evidence for possible protective effects on seizure susceptibility. Pathophysiological cell signaling is strongly related to the presence of subclinical seizure activity (Noebels, 2011). Deletion of APP causes epileptic phenotypes indicating the importance of APP signaling in proper hippocampal excitability (Steinbach et al., 1998). In addition, recent studies suggested that elevated phosphorylated levels of eIF2 $\alpha$  lead to increased expression of ATF4 and BACE1 promoting inhibition of synaptic plasticity and enhanced accumulation of A $\beta$  plaques in the brain (Hu et al., 2010). A $\beta$  peptides trigger synaptic loss and neuronal degeneration, finally complementing the vicious circle of neuronal remodeling, hyperexcitability and cell death. In conjunction with previous findings, genetic deletion of eIF2 $\alpha$  results in

restored neuronal plasticity in APP/PS1 mice (Ma et al., 2013). Hence, we hypothesize a possible rescue effect of non-phosphorylatable eIF2 $\alpha$  allele (eIF2 $\alpha^{S51A}$ ) on learning and memory impairments and epileptiform seizure activity in 5XFAD mice. Our study demonstrates that seizure activity in 5XFAD mice is characterized by electroencephalographic ictal graphoelements predominantly in the motor cortex (M1). 5XFAD mice exhibit a subclinical or non-convulsive phenotype depicting episodes or spike trains, poly-spike and spike-wave activity in the M1 recording which was hardly found in the hippocampal CA1 deflection. In agreement, recent data revealed that in mouse models overexpressing hAPP (Palop et al., 2007) most seizures remained to be non-conclusive without any motoric exacerbation. Seizure detection scoring including number and duration of episodes and spikes showed that seizure activity did not significantly differ between the individual transgenic mouse genotypes. Hence, 5XFAD mice expressing the non-phosphorylatable eIF2 $\alpha$  variant are not retarded concerning amyloidogenesis progression. Enhanced motor activity levels as well as seizure activity can be a result of differentially affected cholinergic neuronal loss according to structure and length of A $\beta$  peptides (Crouzin et al., 2013; Gutierrez-Lerma et al., 2013). Concerning this, A $\beta$  formation leads to a more profoundly impaired LTP in the somatosensory cortex of 5XFAD mice, especially in the cortical layer 5, compared to the hippocampal CA1 region as illustrated in previous studies (Crouzin et al., 2013). Although hippocampal ChAT expression was reduced in our study, we could not depict any differences between 5XFAD WTs and 5XFAD;eIF2 $\alpha^{+/S51A}$  mice. Consequently, we could show that the non-phosphorylated eIF2 $\alpha$  allele has no preventive effect on the aberrant cholinergic system from exhibiting seizure-like activity in 5XFAD mice. This might be due to the fact that heterozygous eIF2 $\alpha$  mutants are less effective in suppressing kinase phosphorylation in comparison to homozygous deletion of eIF2 $\alpha$  that results in reduced p-eIF2 $\alpha$  level in the APP/PSEN1 mouse model (Ma et al., 2013). The limited effects on behavioural performance in our study furthermore support our assumption. 5XFAD mice show higher active suppression scores in fear conditioning paradigm and less use of hippocampal dependent strategies indicating cognitive impairment. However, all effects were not significantly improved by the heterozygous eIF2 $\alpha$  mutation. To verify a possible correlation between hippocampal theta oscillations and seizure activity, we performed time-frequency analysis on theta duration. Theta activity is related to memory impairment in AD (Buzsaki, 2002; Chin and Scharfman,

2013; Gutierrez-Lerma et al., 2013; Palop et al., 2007) and can be modified by different behavioural states (Buzsaki, 2002). Restoration of theta rhythmicity is capable of improving learning and memory functions as well as inhibiting seizure production which correlates with neuronal desynchronization (Colom, 2006). Our results display a significant increase in theta activity from the light to dark phase during non-motor activity in 5XFAD mice. Due to the theta-subtype composition, we consider 5XFAD mice to mainly exhibit alert-immobility during the non-active dark phase. Alert immobility is characterized by atropine-sensitive type II theta (Bland et al., 1996; Shin et al., 2005) indicating the muscarinic pathway to be crucial involved in immobility onset. Unlike the assumption that cognitive decline would be necessarily related to a decrease of theta activity, an increase of theta power can be also found in the TgCRND8 mouse model (Goutagny et al., 2013). Because theta activity is required for successful recall and memory formation (Rutishauser et al., 2010), it is fair to expect that higher amount of theta activity result from hyperexcitability of healthy neurons contributing to the adjustment of dynamical changes and cellular disruption in neuronal networks. Furthermore, we observed a reduction in mean theta frequency in 5XFAD mice compared to controls. This effect was again predominantly detected during non-motor activity. Opposing trends in theta amplitude and frequency can be understood as phenomena occurring in a complex but unbalanced neuronal system (Pena-Ortega and Bernal-Pedraza, 2012). Slower theta oscillations being observed in patients with AD (Jelic et al., 2000; Jelic and Nordberg, 2000) are supposed to represent changes in hippocampal novelty and familiarity detection (Jeewajee et al., 2008). However, it has to be put under consideration if changes in theta rhythms might serve as a possible predictor for disease progression. Despite the evidence obtained from cell biology and genetics, recent studies confirmed that the amyloid hypothesis alone cannot account for the entire AD pathology. Changes in theta activity can even arise before A $\beta$  accumulation (Goutagny et al., 2013; Goutagny and Krantic, 2013) indicating that network over-excitation is not sufficiently linked to overproduction of A $\beta$  plaque deposits. Neuroimaging studies in humans showed that amyloid deposits can be missing in patient with AD, whereas being present in cognitively healthy individuals (Edison 2007, Li Y 2008). These findings raise the question, how mutations in PSEN1 and APP contribute to profound AD pathology independently from elevated A $\beta$  levels. Hence, future studies on AD should address to this topic by distinguishing between different

APP forms and taking non-amyloid factors into consideration (Pimplikar et al., 2010; Pimplikar, 2012). Transcriptome analyses performed from hippocampal RNA tissue revealed an upregulation of PLC $\delta$ 4 shedding light on a potentially enhanced muscarinic signalling resulting in enhanced type II theta acceleration via the Ca<sub>v</sub>2.3 mediated PKC cascade (Muller et al., 2012). Alterations in the muscarinic signal transduction in 5XFAD and other mouse models of AD (Felder, 1995) are involved in theta genesis as well as ictogenesis suggesting to be accountable for hippocampal dysrhythmicity (Tai et al., 2006).

## 4. Conclusion

Summing up, our results provide new insights into how oscillatory activity is attended by physiological and pathophysiological conditions and how oscillations within a neuronal network can be shaped on a molecular level. In this regard, we demonstrated that sleep architecture is substantially modified by the  $\text{Ca}_v2.3$  R-type  $\text{Ca}^{2+}$  channel. Although detailed mechanisms and modulatory effects of especially extrathalamocortical structures on the TC system have still to be determined, the  $\text{Ca}_v2.3$  R-type  $\text{Ca}^{2+}$  channel provides a potential target for treatment of sleep disorders. In special regard to AD, our findings account for a better understanding of the disease pathology by demonstrating the functional and pharmacological interference between A $\beta$  plaques, the muscarinic cascade and theta activity. However, it has to be critically questioned, how disease related mechanisms found in FAD can be transferred to the sporadic, more common form of AD. In the future, it will be necessary to require specific genetically engineered mouse models to assess the molecular and behavioural consequences of AD and to evaluate the muscarinic signaling pathway as potential target cascade in AD treatment.



## 5. Bibliography

Amatniek,J.C., Hauser,W.A., DelCastillo-Castaneda,C., Jacobs,D.M., Marder,K., Bell,K., Albert,M., Brandt,J., and Stern,Y. (2006). Incidence and predictors of seizures in patients with Alzheimer's disease. *Epilepsia* 47, 867-872.

Anderson,M.P., Mochizuki,T., Xie,J., Fischler,W., Manger,J.P., Talley,E.M., Scammell,T.E., and Tonegawa,S. (2005). Thalamic Cav3.1 T-type Ca<sup>2+</sup> channel plays a crucial role in stabilizing sleep. *Proc. Natl Acad Sci. U. S. A* 102, 1743-1748.

Ashe,K.H. (2001). Learning and memory in transgenic mice modeling Alzheimer's disease. *Learn. Mem.* 8, 301-308.

Astori,S., Wimmer,R.D., Prosser,H.M., Corti,C., Corsi,M., Liaudet,N., Volterra,A., Franken,P., Adelman,J.P., and Luthi,A. (2011). The Ca(V)3.3 calcium channel is the major sleep spindle pacemaker in thalamus. *Proc. Natl Acad Sci. U. S. A* 108, 13823-13828.

Auld,D.S., Kornecook,T.J., Bastianetto,S., and Quirion,R. (2002). Alzheimer's disease and the basal forebrain cholinergic system: relations to beta-amyloid peptides, cognition, and treatment strategies. *Prog. Neurobiol.* 68, 209-245.

Babiloni,C., Cassetta,E., Binetti,G., Tombini,M., Del,P.C., Ferreri,F., Ferri,R., Frisoni,G., Lanuzza,B., Nobili,F., Parisi,L., Rodriguez,G., Frigerio,L., Gurzi,M., Prestia,A., Vernieri,F., Eusebi,F., and Rossini,P.M. (2007). Resting EEG sources correlate with attentional span in mild cognitive impairment and Alzheimer's disease. *Eur J Neurosci.* 25, 3742-3757.

Balschun,D., Wolfer,D.P., Gass,P., Mantamadiotis,T., Welzl,H., Schutz,G., Frey,J.U., and Lipp,H.P. (2003). Does cAMP response element-binding protein have a pivotal role in hippocampal synaptic plasticity and hippocampus-dependent memory? *J Neurosci.* 23, 6304-6314.

Beenhakker,M.P. and Huguenard,J.R. (2009). Neurons that fire together also conspire together: is normal sleep circuitry hijacked to generate epilepsy? *Neuron* 62, 612-632.

Bellucci,A., Luccarini,I., Scali,C., Prospero,C., Giovannini,M.G., Pepeu,G., and Casamenti,F. (2006). Cholinergic dysfunction, neuronal damage and axonal loss in TgCRND8 mice. *Neurobiol. Dis* 23, 260-272.

Berry,S.D., Rinaldi,P.C., Thompson,R.F., and Verzeano,M. (1978). Analysis of temporal relations among units and slow waves in rabbit hippocampus. *Brain Res. Bull.* 3, 509-518.

Bers,D.M. and Weber,C.R. (2002). Na/Ca exchange function in intact ventricular myocytes. *Ann N Y. Acad Sci.* 976, 500-512.

Bird,C.M. and Burgess,N. (2008). The hippocampus and memory: insights from spatial processing. *Nat. Rev Neurosci.* 9, 182-194.

Blais,J.D., Filipenko,V., Bi,M., Harding,H.P., Ron,D., Koumenis,C., Wouters,B.G., and Bell,J.C. (2004). Activating transcription factor 4 is translationally regulated by hypoxic stress. *Mol. Cell Biol.* 24, 7469-7482.

Blalock,E.M., Geddes,J.W., Chen,K.C., Porter,N.M., Markesbery,W.R., and Landfield,P.W. (2004). Incipient Alzheimer's disease: microarray correlation analyses reveal major transcriptional and tumor suppressor responses. *Proc. Natl Acad Sci. U. S. A* 101, 2173-2178.

Blanchet,P.J. (2003). Antipsychotic drug-induced movement disorders. *Can J Neurol Sci.* 30 *Suppl 1*, S101-S107.

Bland,B.H., Trepel,C., Oddie,S.D., and Kirk,I.J. (1996). Intraseptal microinfusion of muscimol: effects on hippocampal formation theta field activity and phasic theta-ON cell discharges. *Exp. Neurol.* 138, 286-297.



Bloodgood,B.L. and Sabatini,B.L. (2007). Nonlinear regulation of unitary synaptic signals by CaV(2.3) voltage-sensitive calcium channels located in dendritic spines. *Neuron* 53, 249-260.

Boncrisiano,S., Calhoun,M.E., Kelly,P.H., Pfeifer,M., Bondolfi,L., Stalder,M., Phinney,A.L., Abramowski,D., Sturchler-Pierrat,C., Enz,A., Sommer,B., Staufenbiel,M., and Jucker,M. (2002). Cholinergic changes in the APP23 transgenic mouse model of cerebral amyloidosis. *J Neurosci.* 22, 3234-3243.

Burguillos,M.A., Deierborg,T., Kavanagh,E., Persson,A., Hajji,N., Garcia-Quintanilla,A., Cano,J., Brundin,P., Englund,E., Venero,J.L., and Joseph,B. (2011). Caspase signalling controls microglia activation and neurotoxicity. *Nature* 472, 319-324.

Buttini,M., Yu,G.Q., Shockley,K., Huang,Y., Jones,B., Masliah,E., Mallory,M., Yeo,T., Longo,F.M., and Mucke,L. (2002). Modulation of Alzheimer-like synaptic and cholinergic deficits in transgenic mice by human apolipoprotein E depends on isoform, aging, and overexpression of amyloid beta peptides but not on plaque formation. *J Neurosci.* 22, 10539-10548.

Buzsaki,G. (2002). Theta oscillations in the hippocampus. *Neuron* 33, 325-340.

Casas,C., Sergeant,N., Itier,J.M., Blanchard,V., Wirths,O., van der Kolk,N., Vingtdoux,V., van de Steeg,E., Ret,G., Canton,T., Drobecq,H., Clark,A., Bonici,B., Delacourte,A., Benavides,J., Schmitz,C., Tremp,G., Bayer,T.A., Benoit,P., and Pradier,L. (2004). Massive CA1/2 neuronal loss with intraneuronal and N-terminal truncated Abeta42 accumulation in a novel Alzheimer transgenic model. *Am J Pathol.* 165, 1289-1300.

Catterall,W.A. (2011). Voltage-gated calcium channels. *Cold Spring Harb. Perspect. Biol.* 3, a003947.

Catterall,W.A., Perez-Reyes,E., Snutch,T.P., and Striessnig,J. (2005). International Union of Pharmacology. XLVIII. Nomenclature and structure-function relationships of voltage-gated calcium channels. *Pharmacol Rev* 57, 411-425.

Catterall,W.A., Striessnig,J., Snutch,T.P., and Perez-Reyes,E. (2003). International Union of Pharmacology. XL. Compendium of voltage-gated ion channels: calcium channels. *Pharmacol Rev* 55, 579-581.

Chang,R.C., Wong,A.K., Ng,H.K., and Hugon,J. (2002). Phosphorylation of eukaryotic initiation factor-2alpha (eIF2alpha) is associated with neuronal degeneration in Alzheimer's disease. *Neuroreport* 13, 2429-2432.

Cheong,E. and Shin,H.S. (2013). T-type Ca channels in absence epilepsy. *Biochim. Biophys. Acta*.

Chin,J. and Scharfman,H.E. (2013). Shared cognitive and behavioral impairments in epilepsy and Alzheimer's disease and potential underlying mechanisms. *Epilepsy Behav* 26, 343-351.

Choi,Y., Kim,H.S., Shin,K.Y., Kim,E.M., Kim,M., Kim,H.S., Park,C.H., Jeong,Y.H., Yoo,J., Lee,J.P., Chang,K.A., Kim,S., and Suh,Y.H. (2007). Minocycline attenuates neuronal cell death and improves cognitive impairment in Alzheimer's disease models. *Neuropsychopharmacology* 32, 2393-2404.

Christensen,D.Z., Bayer,T.A., and Wirths,O. (2010). Intracellular A $\beta$  triggers neuron loss in the cholinergic system of the APP/PS1KI mouse model of Alzheimer's disease. *Neurobiol. Aging* 31, 1153-1163.

Cloues,R.K. and Sather,W.A. (2003). Afterhyperpolarization regulates firing rate in neurons of the suprachiasmatic nucleus. *J Neurosci.* 23, 1593-1604.

Colangelo,V., Schurr,J., Ball,M.J., Pelaez,R.P., Bazan,N.G., and Lukiw,W.J. (2002). Gene expression profiling of 12633 genes in Alzheimer hippocampal CA1: transcription

and neurotrophic factor down-regulation and up-regulation of apoptotic and pro-inflammatory signaling. *J Neurosci. Res* 70, 462-473.

Colgin,L.L. (2013). Mechanisms and functions of theta rhythms. *Annu. Rev Neurosci.* 36, 295-312.

Colom,L.V. (2006). Septal networks: relevance to theta rhythm, epilepsy and Alzheimer's disease. *J Neurochem.* 96, 609-623.

Colom,L.V., Castaneda,M.T., Reyna,T., Hernandez,S., and Garrido-Sanabria,E. (2005). Characterization of medial septal glutamatergic neurons and their projection to the hippocampus. *Synapse* 58, 151-164.

Contreras,D. (2006). The role of T-channels in the generation of thalamocortical rhythms. *CNS Neurol Disord. Drug Targets.* 5, 571-585.

Costa-Mattioli,M., Gobert,D., Harding,H., Herdy,B., Azzi,M., Bruno,M., Bidinosti,M., Ben,M.C., Marcinkiewicz,E., Yoshida,M., Imataka,H., Cuello,A.C., Seidah,N., Sossin,W., Lacaille,J.C., Ron,D., Nader,K., and Sonenberg,N. (2005). Translational control of hippocampal synaptic plasticity and memory by the eIF2alpha kinase GCN2. *Nature* 436, 1166-1173.

Costa-Mattioli,M., Sossin,W.S., Klann,E., and Sonenberg,N. (2009). Translational control of long-lasting synaptic plasticity and memory. *Neuron* 61, 10-26.

Crouzin,N., Baranger,K., Cavalier,M., Marchalant,Y., Cohen-Solal,C., Roman,F.S., Khrestchatisky,M., Rivera,S., Feron,F., and Vignes,M. (2013). Area-specific alterations of synaptic plasticity in the 5XFAD mouse model of Alzheimer's disease: dissociation between somatosensory cortex and hippocampus. *PLoS One* 8, e74667.

Cullen,K.M. and Halliday,G.M. (1998). Neurofibrillary degeneration and cell loss in the nucleus basalis in comparison to cortical Alzheimer pathology. *Neurobiol. Aging* 19, 297-306.

Cummins,T.D., Broughton,M., and Finnigan,S. (2008). Theta oscillations are affected by amnesic mild cognitive impairment and cognitive load. *Int J Psychophysiol.* 70, 75-81.

Czigler,B., Csikos,D., Hidasi,Z., Anna,G.Z., Csibri,E., Kiss,E., Salacz,P., and Molnar,M. (2008). Quantitative EEG in early Alzheimer's disease patients - power spectrum and complexity features. *Int. J. Psychophysiol.* 68, 75-80.

Dalo,N.L. and Hackman,J.C. (2013). The anesthetic urethane blocks excitatory amino acid responses but not GABA responses in isolated frog spinal cords. *J Anesth.* 27, 98-103.

Day,N.C., Shaw,P.J., McCormack,A.L., Craig,P.J., Smith,W., Beattie,R., Williams,T.L., Ellis,S.B., Ince,P.G., Harpold,M.M., Lodge,D., and Volsen,S.G. (1996). Distribution of alpha 1A, alpha 1B and alpha 1E voltage-dependent calcium channel subunits in the human hippocampus and parahippocampal gyrus. *Neuroscience* 71, 1013-1024.

de Lanerolle,N.C., Kim,J.H., Robbins,R.J., and Spencer,D.D. (1989). Hippocampal interneuron loss and plasticity in human temporal lobe epilepsy. *Brain Res.* 495, 387-395.

Deipolyi,A.R., Fang,S., Palop,J.J., Yu,G.Q., Wang,X., and Mucke,L. (2008). Altered navigational strategy use and visuospatial deficits in hAPP transgenic mice. *Neurobiol. Aging* 29, 253-266.

Deipolyi,A.R., Rankin,K.P., Mucke,L., Miller,B.L., and Gorno-Tempini,M.L. (2007). Spatial cognition and the human navigation network in AD and MCI. *Neurology* 69, 986-997.

Deransart,C., Vercueil,L., Marescaux,C., and Depaulis,A. (1998). The role of basal ganglia in the control of generalized absence seizures. *Epilepsy Res* 32, 213-223.

Devi,L. and Ohno,M. (2010). Phospho-eIF2alpha level is important for determining abilities of BACE1 reduction to rescue cholinergic neurodegeneration and memory defects in 5XFAD mice. *PLoS One* 5, e12974.

Devi,L. and Ohno,M. (2013). Deletion of the eIF2alpha Kinase GCN2 fails to rescue the memory decline associated with Alzheimer's disease. *PLoS One* 8, e77335.

Ding,Q., Markesbery,W.R., Chen,Q., Li,F., and Keller,J.N. (2005). Ribosome dysfunction is an early event in Alzheimer's disease. *J Neurosci.* 25, 9171-9175.

Dodart,J.C., Meziane,H., Mathis,C., Bales,K.R., Paul,S.M., and Ungerer,A. (1999). Behavioral disturbances in transgenic mice overexpressing the V717F beta-amyloid precursor protein. *Behav Neurosci.* 113, 982-990.

Duff,K. and Suleman,F. (2004). Transgenic mouse models of Alzheimer's disease: how useful have they been for therapeutic development? *Brief. Funct. Genomic. Proteomic.* 3, 47-59.

Eimer,W.A. and Vassar,R. (2013). Neuron loss in the 5XFAD mouse model of Alzheimer's disease correlates with intraneuronal Abeta42 accumulation and Caspase-3 activation. *Mol. Neurodegener.* 8, 2.

Eriksen,J.L. and Janus,C.G. (2007). Plaques, tangles, and memory loss in mouse models of neurodegeneration. *Behav Genet.* 37, 79-100.

Ernst,W.L. and Noebels,J.L. (2009). Expanded alternative splice isoform profiling of the mouse Cav3.1/alpha1G T-type calcium channel. *BMC Mol. Biol.* 10, 53.

Felder,C.C. (1995). Muscarinic acetylcholine receptors: signal transduction through multiple effectors. *FASEB J* 9, 619-625.

Filali,M., Lalonde,R., and Rivest,S. (2011). Anomalies in social behaviors and exploratory activities in an APPswe/PS1 mouse model of Alzheimer's disease. *Physiol Behav* 104, 880-885.

Gahwiler,B.H. and Brown,D.A. (1987). Muscarine affects calcium-currents in rat hippocampal pyramidal cells in vitro. *Neurosci. Lett.* 76, 301-306.

Games,D., Adams,D., Alessandrini,R., Barbour,R., Berthelette,P., Blackwell,C., Carr,T., Clemens,J., Donaldson,T., Gillespie,F., and . (1995). Alzheimer-type neuropathology in transgenic mice overexpressing V717F beta-amyloid precursor protein. *Nature* 373, 523-527.

Gamliel,A., Teicher,C., Michaelson,D.M., Pradier,L., Hartmann,T., Beyreuther,K., and Stein,R. (2002). Increased expression of presenilin 2 inhibits protein synthesis. *Mol. Cell Neurosci.* 19, 111-124.

Garthe,A., Behr,J., and Kempermann,G. (2009). Adult-generated hippocampal neurons allow the flexible use of spatially precise learning strategies. *PLoS One* 4, e5464.

Glenner,G.G. and Wong,C.W. (1984). Alzheimer's disease: initial report of the purification and characterization of a novel cerebrovascular amyloid protein. *Biochem. Biophys. Res Commun* 120, 885-890.

Glenner,G.G., Wong,C.W., Quaranta,V., and Eanes,E.D. (1984). The amyloid deposits in Alzheimer's disease: their nature and pathogenesis. *Appl Pathol.* 2, 357-369.

Goutagny,R. and Krantic,S. (2013). Hippocampal oscillatory activity in Alzheimer's disease: toward the identification of early biomarkers? *Aging Dis* 4, 134-140.

Goutagny,R., Loureiro,M., Jackson,J., Chaumont,J., Williams,S., Isope,P., Kelche,C., Cassel,J.C., and Lecourtier,L. (2013). Interactions between the lateral habenula and the hippocampus: implication for spatial memory processes. *Neuropsychopharmacology* 38, 2418-2426.

Goutagny,R., Manseau,F., Jackson,J., Danik,M., and Williams,S. (2008). In vitro activation of the medial septum-diagonal band complex generates atropine-sensitive and atropine-resistant hippocampal theta rhythm: an investigation using a complete septohippocampal preparation. *Hippocampus* 18, 531-535.

Gutierrez-Lerma,A.I., Ordaz,B., and Pena-Ortega,F. (2013). Amyloid Beta peptides differentially affect hippocampal theta rhythms in vitro. *Int J Pept.* 2013, 328140.

Hangya,B., Borhegyi,Z., Szilagyi,N., Freund,T.F., and Varga,V. (2009). GABAergic neurons of the medial septum lead the hippocampal network during theta activity. *J Neurosci.* 29, 8094-8102.

Hara,K. and Harris,R.A. (2002). The anesthetic mechanism of urethane: the effects on neurotransmitter-gated ion channels. *Anesth. Analg.* 94, 313-8, table.

Harding,H.P., Zhang,Y., and Ron,D. (1999). Protein translation and folding are coupled by an endoplasmic-reticulum-resident kinase. *Nature* 397, 271-274.

Hauser,W.A., Morris,M.L., Heston,L.L., and Anderson,V.E. (1986). Seizures and myoclonus in patients with Alzheimer's disease. *Neurology* 36, 1226-1230.

Hofmann,F., Lacinova,L., and Klugbauer,N. (1999). Voltage-dependent calcium channels: from structure to function. *Rev Physiol Biochem. Pharmacol* 139, 33-87.

Holcomb,L., Gordon,M.N., McGowan,E., Yu,X., Benkovic,S., Jantzen,P., Wright,K., Saad,I., Mueller,R., Morgan,D., Sanders,S., Zehr,C., O'Campo,K., Hardy,J., Prada,C.M., Eckman,C., Younkin,S., Hsiao,K., and Duff,K. (1998). Accelerated Alzheimer-type phenotype in transgenic mice carrying both mutant amyloid precursor protein and presenilin 1 transgenes. *Nat. Med* 4, 97-100.

Holcomb,L.A., Gordon,M.N., Jantzen,P., Hsiao,K., Duff,K., and Morgan,D. (1999). Behavioral changes in transgenic mice expressing both amyloid precursor protein and presenilin-1 mutations: lack of association with amyloid deposits. *Behav Genet.* 29, 177-185.

Hong,I., Kang,T., Yoo,Y., Park,R., Lee,J., Lee,S., Kim,J., Song,B., Kim,S.Y., Moon,M., Yun,K.N., Kim,J.Y., Mook-Jung,I., Park,Y.M., and Choi,S. (2013). Quantitative proteomic analysis of the hippocampus in the 5XFAD mouse model at early stages of Alzheimer's disease pathology. *J. Alzheimers. Dis.* 36, 321-334.

Hu,W.T., Chen-Plotkin,A., Arnold,S.E., Grossman,M., Clark,C.M., Shaw,L.M., McCluskey,L., Elman,L., Karlawish,J., Hurtig,H.I., Siderowf,A., Lee,V.M., Soares,H., and Trojanowski,J.Q. (2010). Biomarker discovery for Alzheimer's disease, frontotemporal lobar degeneration, and Parkinson's disease. *Acta Neuropathol.* *120*, 385-399.

Huang,d.W., Sherman,B.T., and Lempicki,R.A. (2009). Systematic and integrative analysis of large gene lists using DAVID bioinformatics resources. *Nat. Protoc.* *4*, 44-57.

Ikarashi,Y., Harigaya,Y., Tomidokoro,Y., Kanai,M., Ikeda,M., Matsubara,E., Kawarabayashi,T., Kuribara,H., Younkin,S.G., Maruyama,Y., and Shoji,M. (2004). Decreased level of brain acetylcholine and memory disturbance in APPsw mice. *Neurobiol. Aging* *25*, 483-490.

Jansen,R., Timmerman,J., Loos,M., Spijker,S., van Ooyen,A., Brussaard,A.B., Mansvelder,H.D., Smit,A.B., de Gunst,M., and Linkenkaer-Hansen,K. (2011). Novel candidate genes associated with hippocampal oscillations. *PLoS. One.* *6*, e26586.

Jawhar,S., Trawicka,A., Jenneckens,C., Bayer,T.A., and Wirths,O. (2012). Motor deficits, neuron loss, and reduced anxiety coinciding with axonal degeneration and intraneuronal Abeta aggregation in the 5XFAD mouse model of Alzheimer's disease. *Neurobiol. Aging* *33*, 196-40.

Jeewajee,A., Lever,C., Burton,S., O'Keefe,J., and Burgess,N. (2008). Environmental novelty is signaled by reduction of the hippocampal theta frequency. *Hippocampus* *18*, 340-348.

Jelic,V., Johansson,S.E., Almkvist,O., Shigeta,M., Julin,P., Nordberg,A., Winblad,B., and Wahlund,L.O. (2000). Quantitative electroencephalography in mild cognitive impairment: longitudinal changes and possible prediction of Alzheimer's disease. *Neurobiol. Aging* *21*, 533-540.



Jelic,V. and Nordberg,A. (2000). Early diagnosis of Alzheimer disease with positron emission tomography. *Alzheimer Dis Assoc Disord. 14 Suppl 1*, S109-S113.

Jha,S.K., Ross,R.J., and Morrison,A.R. (2005). Sleep-related neurons in the central nucleus of the amygdala of rats and their modulation by the dorsal raphe nucleus. *Physiol Behav. 86*, 415-426.

Jin,K., Peel,A.L., Mao,X.O., Xie,L., Cottrell,B.A., Henshall,D.C., and Greenberg,D.A. (2004). Increased hippocampal neurogenesis in Alzheimer's disease. *Proc. Natl. Acad. Sci. U. S. A 101*, 343-347.

Joksovic,P.M., Brimelow,B.C., Murbartian,J., Perez-Reyes,E., and Todorovic,S.M. (2005). Contrasting anesthetic sensitivities of T-type Ca<sup>2+</sup> channels of reticular thalamic neurons and recombinant Ca(v)3.3 channels. *Br J Pharmacol 144*, 59-70.

Joksovic,P.M., Weiergraber,M., Lee,W., Struck,H., Schneider,T., and Todorovic,S.M. (2009). Isoflurane-sensitive presynaptic R-type calcium channels contribute to inhibitory synaptic transmission in the rat thalamus. *J Neurosci. 29*, 1434-1445.

Jones,S.W. (2002). Calcium channels: when is a subunit not a subunit? *J Physiol 545*, 334.

Jopec,R.S., Song,L., and Powers,R.E. (1997). Cholinergic activation of phosphoinositide signaling is impaired in Alzheimer's disease brain. *Neurobiol. Aging 18*, 111-120.

Kaczorowski,C.C. and Disterhoft,J.F. (2009). Memory deficits are associated with impaired ability to modulate neuronal excitability in middle-aged mice. *Learn. Mem. 16*, 362-366.

Kahana,M.J., Caplan,J.B., Sekuler,R., and Madsen,J.R. (1999). Using intracranial recordings to study thetaResponse to J. O'Keefe and N. Burgess (1999). *Trends Cogn Sci. 3*, 406-407.

Kar,S. and Quirion,R. (2004). Amyloid beta peptides and central cholinergic neurons: functional interrelationship and relevance to Alzheimer's disease pathology. *Prog. Brain Res 145*, 261-274.

Kar,S., Slowikowski,S.P., Westaway,D., and Mount,H.T. (2004). Interactions between beta-amyloid and central cholinergic neurons: implications for Alzheimer's disease. *J Psychiatry Neurosci. 29*, 427-441.

Khosravani,H. and Zamponi,G.W. (2006). Voltage-gated calcium channels and idiopathic generalized epilepsies. *Physiol Rev 86*, 941-966.

Kim,D., Song,I., Keum,S., Lee,T., Jeong,M.J., Kim,S.S., McEnery,M.W., and Shin,H.S. (2001). Lack of the burst firing of thalamocortical relay neurons and resistance to absence seizures in mice lacking alpha(1G) T-type Ca(2+) channels. *Neuron 31*, 35-45.

Kim,H.S., Choi,Y., Shin,K.Y., Joo,Y., Lee,Y.K., Jung,S.Y., Suh,Y.H., and Kim,J.H. (2007). Swedish amyloid precursor protein mutation increases phosphorylation of eIF2alpha in vitro and in vivo. *J Neurosci. Res 85*, 1528-1537.

Kim,K.H., Moon,M., Yu,S.B., Mook-Jung,I., and Kim,J.I. (2012). RNA-Seq analysis of frontal cortex and cerebellum from 5XFAD mice at early stage of disease pathology. *J. Alzheimers. Dis. 29*, 793-808.

Kimura,R., Kamino,K., Yamamoto,M., Nuripa,A., Kida,T., Kazui,H., Hashimoto,R., Tanaka,T., Kudo,T., Yamagata,H., Tabara,Y., Miki,T., Akatsu,H., Kosaka,K., Funakoshi,E., Nishitomi,K., Sakaguchi,G., Kato,A., Hattori,H., Uema,T., and Takeda,M. (2007). The DYRK1A gene, encoded in chromosome 21 Down syndrome critical region, bridges between beta-amyloid production and tau phosphorylation in Alzheimer disease. *Hum Mol. Genet. 16*, 15-23.

Klann,E. and Dever,T.E. (2004). Biochemical mechanisms for translational regulation in synaptic plasticity. *Nat. Rev Neurosci. 5*, 931-942.

Klingner,M., Apelt,J., Kumar,A., Sorger,D., Sabri,O., Steinbach,J., Scheunemann,M., and Schliebs,R. (2003). Alterations in cholinergic and non-cholinergic neurotransmitter receptor densities in transgenic Tg2576 mouse brain with beta-amyloid plaque pathology. *Int J Dev. Neurosci.* 21, 357-369.

Kordower,J.H., Chu,Y., Stebbins,G.T., DeKosky,S.T., Cochran,E.J., Bennett,D., and Mufson,E.J. (2001). Loss and atrophy of layer II entorhinal cortex neurons in elderly people with mild cognitive impairment. *Ann Neurol* 49, 202-213.

Kramer,K. and Kinter,L.B. (2003). Evaluation and applications of radiotelemetry in small laboratory animals. *Physiol Genomics* 13, 197-205.

Kronland-Martinet,R., Morlet,J., and Grossmann,A. (1987). Analysis of soundpatterns through wavelet transforms. *Int J Pattern Recognit ArtificialIntelligence* 1, 273-302.

Kumar,V.B., Farr,S.A., Flood,J.F., Kamlesh,V., Franko,M., Banks,W.A., and Morley,J.E. (2000). Site-directed antisense oligonucleotide decreases the expression of amyloid precursor protein and reverses deficits in learning and memory in aged SAMP8 mice. *Peptides* 21, 1769-1775.

Kuzmiski,J.B., Barr,W., Zamponi,G.W., and MacVicar,B.A. (2005). Topiramate inhibits the initiation of plateau potentials in CA1 neurons by depressing R-type calcium channels. *Epilepsia* 46, 481-489.

Kuzmiski,J.B. and MacVicar,B.A. (2001). Cyclic nucleotide-gated channels contribute to the cholinergic plateau potential in hippocampal CA1 pyramidal neurons. *J Neurosci.* 21, 8707-8714.

LaFerla,F.M., Tinkle,B.T., Bieberich,C.J., Haudenschild,C.C., and Jay,G. (1995). The Alzheimer's A beta peptide induces neurodegeneration and apoptotic cell death in transgenic mice. *Nat. Genet.* 9, 21-30.

Lakaye,B., Thomas,E., Minet,A., and Grisar,T. (2002). The genetic absence epilepsy rat from Strasbourg (GAERS), a rat model of absence epilepsy: computer modeling and differential gene expression. *Epilepsia* 43 Suppl 5, 123-129.

Lalonde,R., Dumont,M., Staufenbiel,M., and Strazielle,C. (2005). Neurobehavioral characterization of APP23 transgenic mice with the SHIRPA primary screen. *Behav. Brain Res.* 157, 91-98.

Langstrom,N.S., Anderson,J.P., Lindroos,H.G., Winblad,B., and Wallace,W.C. (1989). Alzheimer's disease-associated reduction of polysomal mRNA translation. *Brain Res Mol. Brain Res* 5, 259-269.

Larner,A.J. (2010). Epileptic seizures in AD patients. *Neuromolecular. Med* 12, 71-77.

Lee,J., Kim,D., and Shin,H.S. (2004). Lack of delta waves and sleep disturbances during non-rapid eye movement sleep in mice lacking alpha1G-subunit of T-type calcium channels. *Proc. Natl Acad Sci. U. S. A* 101, 18195-18199.

Lee,J. and Shin,H.S. (2007). T-type calcium channels and thalamocortical rhythms in sleep: a perspective from studies of T-type calcium channel knockout mice. *CNS Neurol. Disord. Drug Targets.* 6, 63-69.

Lee,S.C., Choi,S., Lee,T., Kim,H.L., Chin,H., and Shin,H.S. (2002). Molecular basis of R-type calcium channels in central amygdala neurons of the mouse. *Proc. Natl Acad Sci. U. S. A* 99, 3276-3281.

Liang,W.S., Dunckley,T., Beach,T.G., Grover,A., Mastroeni,D., Ramsey,K., Caselli,R.J., Kukull,W.A., McKeel,D., Morris,J.C., Hulette,C.M., Schmechel,D., Reiman,E.M., Rogers,J., and Stephan,D.A. (2008). Altered neuronal gene expression in brain regions differentially affected by Alzheimer's disease: a reference data set. *Physiol Genomics* 33, 240-256.

Llinas,R.R. and Steriade,M. (2006). Bursting of thalamic neurons and states of vigilance. *J Neurophysiol.* 95, 3297-3308.

- Lopez-Bendito,G. and Molnar,Z. (2003). Thalamocortical development: how are we going to get there? *Nat. Rev Neurosci.* *4*, 276-289.
- Loring,J.F., Wen,X., Lee,J.M., Seilhamer,J., and Somogyi,R. (2001). A gene expression profile of Alzheimer's disease. *DNA Cell Biol.* *20*, 683-695.
- Luth,H.J., Apelt,J., Ihunwo,A.O., Arendt,T., and Schliebs,R. (2003). Degeneration of beta-amyloid-associated cholinergic structures in transgenic APP SW mice. *Brain Res* *977*, 16-22.
- Ma,T., Trinh,M.A., Wexler,A.J., Bourbon,C., Gatti,E., Pierre,P., Cavener,D.R., and Klann,E. (2013). Suppression of eIF2alpha kinases alleviates Alzheimer's disease-related plasticity and memory deficits. *Nat. Neurosci.* *16*, 1299-1305.
- Manning,J.P., Richards,D.A., and Bowery,N.G. (2003). Pharmacology of absence epilepsy. *Trends Pharmacol Sci.* *24*, 542-549.
- Manseau,F., Goutagny,R., Danik,M., and Williams,S. (2008). The hippocamptoseptal pathway generates rhythmic firing of GABAergic neurons in the medial septum and diagonal bands: an investigation using a complete septohippocampal preparation in vitro. *J Neurosci.* *28*, 4096-4107.
- Martino,D. and Giovannoni,G. (2004). Antibasal ganglia antibodies and their relevance to movement disorders. *Curr Opin Neurol* *17*, 425-432.
- McNaughton,N., Ruan,M., and Woodnorth,M.A. (2006). Restoring theta-like rhythmicity in rats restores initial learning in the Morris water maze. *Hippocampus* *16*, 1102-1110.
- Mendez,M. and Lim,G. (2003). Seizures in elderly patients with dementia: epidemiology and management. *Drugs Aging* *20*, 791-803.

Merica,H. and Fortune,R.D. (2011). The neuronal transition probability (NTP) model for the dynamic progression of non-REM sleep EEG: the role of the suprachiasmatic nucleus. *PLoS One* 6, e23593.

Metz,A.E., Jarsky,T., Martina,M., and Spruston,N. (2005). R-type calcium channels contribute to afterdepolarization and bursting in hippocampal CA1 pyramidal neurons. *J Neurosci.* 25, 5763-5773.

Miller,J.W., Turner,G.M., and Gray,B.C. (1994). Anticonvulsant effects of the experimental induction of hippocampal theta activity. *Epilepsy Res* 18, 195-204.

Minkeviciene,R., Ihalainen,J., Malm,T., Matilainen,O., Keksa-Goldsteine,V., Goldsteins,G., Iivonen,H., Leguit,N., Glennon,J., Koistinaho,J., Banerjee,P., and Tanila,H. (2008). Age-related decrease in stimulated glutamate release and vesicular glutamate transporters in APP/PS1 transgenic and wild-type mice. *J. Neurochem.* 105, 584-594.

Minkeviciene,R., Rheims,S., Dobszay,M.B., Zilberter,M., Hartikainen,J., Fulop,L., Penke,B., Zilberter,Y., Harkany,T., Pitkanen,A., and Tanila,H. (2009). Amyloid beta-induced neuronal hyperexcitability triggers progressive epilepsy. *J Neurosci.* 29, 3453-3462.

Moechars,D., Lorent,K., De Strooper,B., Dewachter,I., and Van Leuven,F. (1996). Expression in brain of amyloid precursor protein mutated in the alpha-secretase site causes disturbed behavior, neuronal degeneration and premature death in transgenic mice. *EMBO J.* 15, 1265-1274.

Montgomery,S.M. and Buzsaki,G. (2007). Gamma oscillations dynamically couple hippocampal CA3 and CA1 regions during memory task performance. *Proc. Natl Acad Sci. U. S. A* 104, 14495-14500.

Moon,M., Hong,H.S., Nam,D.W., Baik,S.H., Song,H., Kook,S.Y., Kim,Y.S., Lee,J., and Mook-Jung,I. (2012). Intracellular amyloid-beta accumulation in calcium-binding

protein-deficient neurons leads to amyloid-beta plaque formation in animal model of Alzheimer's disease. *J Alzheimers. Dis* 29, 615-628.

Moretti,D.V., Pievani,M., Geroldi,C., Binetti,G., Zanetti,O., Rossini,P.M., and Frisoni,G.B. (2010). EEG markers discriminate among different subgroup of patients with mild cognitive impairment. *Am J Alzheimers. Dis Other Demen.* 25, 58-73.

Morrison,J.H. and Hof,P.R. (1997). Life and death of neurons in the aging brain. *Science* 278, 412-419.

Muller,R., Struck,H., Ho,M.S., Brockhaus-Dumke,A., Klosterkötter,J., Broich,K., Hescheler,J., Schneider,T., and Weiergraber,M. (2012). Atropine-sensitive hippocampal theta oscillations are mediated by Cav2.3 R-type Ca(2)(+) channels. *Neuroscience* 205, 125-139.

Noebels,J. (2011). A perfect storm: Converging paths of epilepsy and Alzheimer's dementia intersect in the hippocampal formation. *Epilepsia* 52 *Suppl 1*, 39-46.

O'Connor,T., Sadleir,K.R., Maus,E., Velliquette,R.A., Zhao,J., Cole,S.L., Eimer,W.A., Hitt,B., Bembinster,L.A., Lammich,S., Lichtenthaler,S.F., Hebert,S.S., De,S.B., Haass,C., Bennett,D.A., and Vassar,R. (2008). Phosphorylation of the translation initiation factor eIF2alpha increases BACE1 levels and promotes amyloidogenesis. *Neuron* 60, 988-1009.

Oakley,H., Cole,S.L., Logan,S., Maus,E., Shao,P., Craft,J., Guillozet-Bongaarts,A., Ohno,M., Disterhoft,J., Van,E.L., Berry,R., and Vassar,R. (2006). Intraneuronal beta-amyloid aggregates, neurodegeneration, and neuron loss in transgenic mice with five familial Alzheimer's disease mutations: potential factors in amyloid plaque formation. *J Neurosci.* 26, 10129-10140.

Ohno,M., Chang,L., Tseng,W., Oakley,H., Citron,M., Klein,W.L., Vassar,R., and Disterhoft,J.F. (2006). Temporal memory deficits in Alzheimer's mouse models: rescue by genetic deletion of BACE1. *Eur J Neurosci.* 23, 251-260.

Ohno,M., Cole,S.L., Yasvoina,M., Zhao,J., Citron,M., Berry,R., Disterhoft,J.F., and Vassar,R. (2007). BACE1 gene deletion prevents neuron loss and memory deficits in 5XFAD APP/PS1 transgenic mice. *Neurobiol. Dis.* 26, 134-145.

Ohno,M., Sametsky,E.A., Younkin,L.H., Oakley,H., Younkin,S.G., Citron,M., Vassar,R., and Disterhoft,J.F. (2004). BACE1 deficiency rescues memory deficits and cholinergic dysfunction in a mouse model of Alzheimer's disease. *Neuron* 41, 27-33.

Pace-Schott,E.F. and Hobson,J.A. (2002). The neurobiology of sleep: genetics, cellular physiology and subcortical networks. *Nat. Rev Neurosci.* 3, 591-605.

Palhalmi,J., Paulsen,O., Freund,T.F., and Hajos,N. (2004). Distinct properties of carbachol- and DHPG-induced network oscillations in hippocampal slices. *Neuropharmacology* 47, 381-389.

Palop,J.J., Chin,J., and Mucke,L. (2006). A network dysfunction perspective on neurodegenerative diseases. *Nature* 443, 768-773.

Palop,J.J., Chin,J., Roberson,E.D., Wang,J., Thwin,M.T., Bien-Ly,N., Yoo,J., Ho,K.O., Yu,G.Q., Kreitzer,A., Finkbeiner,S., Noebels,J.L., and Mucke,L. (2007). Aberrant excitatory neuronal activity and compensatory remodeling of inhibitory hippocampal circuits in mouse models of Alzheimer's disease. *Neuron* 55, 697-711.

Palop,J.J. and Mucke,L. (2009). Epilepsy and cognitive impairments in Alzheimer disease. *Arch Neurol* 66, 435-440.

Palop,J.J. and Mucke,L. (2010). Amyloid-beta-induced neuronal dysfunction in Alzheimer's disease: from synapses toward neural networks. *Nat. Neurosci.* 13, 812-818.

Pandis,D. and Scarmeas,N. (2012). Seizures in Alzheimer disease: clinical and epidemiological data. *Epilepsy Curr* 12, 184-187.



Patti,C.L., Zanin,K.A., Sanday,L., Kameda,S.R., Fernandes-Santos,L., Fernandes,H.A., Andersen,M.L., Tufik,S., and Frussa-Filho,R. (2010). Effects of sleep deprivation on memory in mice: role of state-dependent learning. *Sleep* 33, 1669-1679.

Pena-Ortega,F. and Bernal-Pedraza,R. (2012). Amyloid Beta Peptide slows down sensory-induced hippocampal oscillations. *Int J Pept.* 2012, 236289.

Perez,S.E., Dar,S., Ikonovic,M.D., DeKosky,S.T., and Mufson,E.J. (2007). Cholinergic forebrain degeneration in the APP<sup>swe</sup>/PS1<sup>DeltaE9</sup> transgenic mouse. *Neurobiol. Dis* 28, 3-15.

Petrenko,A.B., Tsujita,M., Kohno,T., Sakimura,K., and Baba,H. (2007). Mutation of alpha1G T-type calcium channels in mice does not change anesthetic requirements for loss of the righting reflex and minimum alveolar concentration but delays the onset of anesthetic induction. *Anesthesiology* 106, 1177-1185.

Pierson,P.M., Liu,X., and Raggenbass,M. (2005). Suppression of potassium channels elicits calcium-dependent plateau potentials in suprachiasmatic neurons of the rat. *Brain Res* 1036, 50-59.

Pimplikar,S.W. (2012). Clinical and biomarker changes in Alzheimer's disease. *N Engl J Med* 367, 2050-2051.

Pimplikar,S.W., Nixon,R.A., Robakis,N.K., Shen,J., and Tsai,L.H. (2010). Amyloid-independent mechanisms in Alzheimer's disease pathogenesis. *J Neurosci.* 30, 14946-14954.

Price,J.L., Ko,A.I., Wade,M.J., Tsou,S.K., McKeel,D.W., and Morris,J.C. (2001). Neuron number in the entorhinal cortex and CA1 in preclinical Alzheimer disease. *Arch Neurol* 58, 1395-1402.

Reich,C.G., Karson,M.A., Karnup,S.V., Jones,L.M., and Alger,B.E. (2005). Regulation of IPSP theta rhythm by muscarinic receptors and endocannabinoids in hippocampus. *J Neurophysiol.* 94, 4290-4299.

Roberson,E.D., Searce-Levie,K., Palop,J.J., Yan,F., Cheng,I.H., Wu,T., Gerstein,H., Yu,G.Q., and Mucke,L. (2007). Reducing endogenous tau ameliorates amyloid beta-induced deficits in an Alzheimer's disease mouse model. *Science* 316, 750-754.

Rockenstein,E.M., McConlogue,L., Tan,H., Power,M., Masliah,E., and Mucke,L. (1995). Levels and alternative splicing of amyloid beta protein precursor (APP) transcripts in brains of APP transgenic mice and humans with Alzheimer's disease. *J Biol. Chem.* 270, 28257-28267.

Romanelli,M.F., Morris,J.C., Ashkin,K., and Coben,L.A. (1990). Advanced Alzheimer's disease is a risk factor for late-onset seizures. *Arch Neurol* 47, 847-850.

Rutishauser,U., Ross,I.B., Mamelak,A.N., and Schuman,E.M. (2010). Human memory strength is predicted by theta-frequency phase-locking of single neurons. *Nature* 464, 903-907.

Scarmeas,N., Honig,L.S., Choi,H., Cantero,J., Brandt,J., Blacker,D., Albert,M., Amatniek,J.C., Marder,K., Bell,K., Hauser,W.A., and Stern,Y. (2009). Seizures in Alzheimer disease: who, when, and how common? *Arch Neurol* 66, 992-997.

Scheuner,D., Song,B., McEwen,E., Liu,C., Laybutt,R., Gillespie,P., Saunders,T., Bonner-Weir,S., and Kaufman,R.J. (2001). Translational control is required for the unfolded protein response and in vivo glucose homeostasis. *Mol. Cell* 7, 1165-1176.

Schmittgen,T.D. and Livak,K.J. (2008). Analyzing real-time PCR data by the comparative C(T) method. *Nat. Protoc.* 3, 1101-1108.

Scott,L., Feng,J., Kiss,T., Needle,E., Atchison,K., Kawabe,T.T., Milici,A.J., Hajos-Korcsok,E., Riddell,D., and Hajos,M. (2012). Age-dependent disruption in hippocampal theta oscillation in amyloid-beta overproducing transgenic mice. *Neurobiol. Aging* 33, 1481-23.

Selkoe,D.J. (2002). Alzheimer's disease is a synaptic failure. *Science* 298, 789-791.

- Selkoe,D.J. and Schenk,D. (2003). Alzheimer's disease: molecular understanding predicts amyloid-based therapeutics. *Annu. Rev Pharmacol Toxicol* 43, 545-584.
- Shin,H.S. (2006). T-type Ca<sup>2+</sup> channels and absence epilepsy. *Cell Calcium* 40, 191-196.
- Shin,H.S., Lee,J., and Song,I. (2006). Genetic studies on the role of T-type Ca<sup>2+</sup> channels in sleep and absence epilepsy. *CNS Neurol. Disord. Drug Targets*. 5, 629-638.
- Shin,J., Gireesh,G., Kim,S.W., Kim,D.S., Lee,S., Kim,Y.S., Watanabe,M., and Shin,H.S. (2009). Phospholipase C beta 4 in the medial septum controls cholinergic theta oscillations and anxiety behaviors. *J. Neurosci.* 29, 15375-15385.
- Shin,J., Kim,D., Bianchi,R., Wong,R.K., and Shin,H.S. (2005). Genetic dissection of theta rhythm heterogeneity in mice. *Proc. Natl Acad Sci. U. S. A* 102, 18165-18170.
- Sinha,S. and Lieberburg,I. (1999). Cellular mechanisms of beta-amyloid production and secretion. *Proc. Natl Acad Sci. U. S. A* 96, 11049-11053.
- Siwek,M., Henseler,C., Broich,K., Papazoglou,A., and Weiergraber,M. (2012). Voltage-gated Ca(2+) channel mediated Ca(2+) influx in epileptogenesis. *Adv. Exp. Med Biol.* 740, 1219-1247.
- Song,I., Kim,D., Choi,S., Sun,M., Kim,Y., and Shin,H.S. (2004). Role of the alpha1G T-type calcium channel in spontaneous absence seizures in mutant mice. *J Neurosci.* 24, 5249-5257.
- Steinbach,J.P., Muller,U., Leist,M., Li,Z.W., Nicotera,P., and Aguzzi,A. (1998). Hypersensitivity to seizures in beta-amyloid precursor protein deficient mice. *Cell Death. Differ.* 5, 858-866.
- Steriade,M. (2005). Sleep, epilepsy and thalamic reticular inhibitory neurons. *Trends Neurosci.* 28, 317-324.

- Sutula,T., Cascino,G., Cavazos,J., Parada,I., and Ramirez,L. (1989). Mossy fiber synaptic reorganization in the epileptic human temporal lobe. *Ann. Neurol.* 26, 321-330.
- Tai,C., Kuzmiski,J.B., and MacVicar,B.A. (2006). Muscarinic enhancement of R-type calcium currents in hippocampal CA1 pyramidal neurons. *J Neurosci.* 26, 6249-6258.
- Takei,T., Saegusa,H., Zong,S., Murakoshi,T., Makita,K., and Tanabe,T. (2003). Anesthetic sensitivities to propofol and halothane in mice lacking the R-type (Cav2.3) Ca<sup>2+</sup> channel. *Anesth. Analg.* 97, 96-103, table.
- Talley,E.M., Cribbs,L.L., Lee,J.H., Daud,A., Perez-Reyes,E., and Bayliss,D.A. (1999). Differential distribution of three members of a gene family encoding low voltage-activated (T-type) calcium channels. *J Neurosci.* 19, 1895-1911.
- Talley,E.M., Solorzano,G., Depaulis,A., Perez-Reyes,E., and Bayliss,D.A. (2000). Low-voltage-activated calcium channel subunit expression in a genetic model of absence epilepsy in the rat. *Brain Res Mol. Brain Res* 75, 159-165.
- Tao,J., Hildebrand,M.E., Liao,P., Liang,M.C., Tan,G., Li,S., Snutch,T.P., and Soong,T.W. (2008). Activation of corticotropin-releasing factor receptor 1 selectively inhibits CaV3.2 T-type calcium channels. *Mol. Pharmacol* 73, 1596-1609.
- Terry,R.D., Masliah,E., Salmon,D.P., Butters,N., DeTeresa,R., Hill,R., Hansen,L.A., and Katzman,R. (1991). Physical basis of cognitive alterations in Alzheimer's disease: synapse loss is the major correlate of cognitive impairment. *Ann Neurol* 30, 572-580.
- Todorovic,S.M., Perez-Reyes,E., and Lingle,C.J. (2000). Anticonvulsants but not general anesthetics have differential blocking effects on different T-type current variants. *Mol. Pharmacol* 58, 98-108.
- Torres-Aleman,I. (2010). Toward a comprehensive neurobiology of IGF-I. *Dev. Neurobiol.* 70, 384-396.

Toselli,M., Lang,J., Costa,T., and Lux,H.D. (1989). Direct modulation of voltage-dependent calcium channels by muscarinic activation of a pertussis toxin-sensitive G-protein in hippocampal neurons. *Pflugers Arch* 415, 255-261.

Vanderwolf,C.H. (1969). Hippocampal electrical activity and voluntary movement in the rat. *Electroencephalogr. Clin Neurophysiol.* 26, 407-418.

Vassar,R., Bennett,B.D., Babu-Khan,S., Kahn,S., Mendiaz,E.A., Denis,P., Teplow,D.B., Ross,S., Amarante,P., Loeloff,R., Luo,Y., Fisher,S., Fuller,J., Edenson,S., Lile,J., Jarosinski,M.A., Biere,A.L., Curran,E., Burgess,T., Louis,J.C., Collins,F., Treanor,J., Rogers,G., and Citron,M. (1999). Beta-secretase cleavage of Alzheimer's amyloid precursor protein by the transmembrane aspartic protease BACE. *Science* 286, 735-741.

Verret,L., Mann,E.O., Hang,G.B., Barth,A.M., Cobos,I., Ho,K., Devidze,N., Masliah,E., Kreitzer,A.C., Mody,I., Mucke,L., and Palop,J.J. (2012). Inhibitory interneuron deficit links altered network activity and cognitive dysfunction in Alzheimer model. *Cell* 149, 708-721.

Vogels,O.J., Broere,C.A., ter Laak,H.J., ten Donkelaar,H.J., Nieuwenhuys,R., and Schulte,B.P. (1990). Cell loss and shrinkage in the nucleus basalis Meynert complex in Alzheimer's disease. *Neurobiol. Aging* 11, 3-13.

Weiergraber,M., Henry,M., Hescheler,J., Smyth,N., and Schneider,T. (2005). Electrocorticographic and deep intracerebral EEG recording in mice using a telemetry system. *Brain Res Brain Res Protoc.* 14, 154-164.

Weiergraber,M., Henry,M., Ho,M.S., Struck,H., Hescheler,J., and Schneider,T. (2008). Altered thalamocortical rhythmicity in Ca(v)2.3-deficient mice. *Mol. Cell Neurosci.* 39, 605-618.

Weiergraber,M., Henry,M., Radhakrishnan,K., Hescheler,J., and Schneider,T. (2007). Hippocampal seizure resistance and reduced neuronal excitotoxicity in mice lacking the Cav2.3 E/R-type voltage-gated calcium channel. *J Neurophysiol.* 97, 3660-3669.

Weiergraber,M., Kamp,M.A., Radhakrishnan,K., Hescheler,J., and Schneider,T. (2006). The Ca(v)2.3 voltage-gated calcium channel in epileptogenesis--shedding new light on an enigmatic channel. *Neurosci. Biobehav. Rev* 30, 1122-1144.

Westenbroek,R.E., Sakurai,T., Elliott,E.M., Hell,J.W., Starr,T.V., Snutch,T.P., and Catterall,W.A. (1995). Immunochemical identification and subcellular distribution of the alpha 1A subunits of brain calcium channels. *J Neurosci.* 15, 6403-6418.

Westmark,C.J., Westmark,P.R., Beard,A.M., Hildebrandt,S.M., and Malter,J.S. (2008). Seizure susceptibility and mortality in mice that over-express amyloid precursor protein. *Int J Clin Exp Pathol.* 1, 157-168.

Whishaw,I.Q., O'Connor,W.T., and Dunnett,S.B. (1985). Disruption of central cholinergic systems in the rat by basal forebrain lesions or atropine: effects on feeding, sensorimotor behaviour, locomotor activity and spatial navigation. *Behav Brain Res* 17, 103-115.

White,H.K., McConnell,E.S., Bales,C.W., and Kuchibhatla,M. (2004). A 6-month observational study of the relationship between weight loss and behavioral symptoms in institutionalized Alzheimer's disease subjects. *J Am Med Dir. Assoc* 5, 89-97.

Whitehouse,P.J., Struble,R.G., Clark,A.W., and Price,D.L. (1982). Alzheimer disease: plaques, tangles, and the basal forebrain. *Ann Neurol* 12, 494.

Wilson,S.M., Toth,P.T., Oh,S.B., Gillard,S.E., Volsen,S., Ren,D., Philipson,L.H., Lee,E.C., Fletcher,C.F., Tessarollo,L., Copeland,N.G., Jenkins,N.A., and Miller,R.J. (2000). The status of voltage-dependent calcium channels in alpha 1E knock-out mice. *J Neurosci.* 20, 8566-8571.

Winson,J. (1974). Patterns of hippocampal theta rhythm in the freely moving rat. *Electroencephalogr. Clin Neurophysiol.* 36, 291-301.

Womelsdorf,T., Schoffelen,J.M., Oostenveld,R., Singer,W., Desimone,R., Engel,A.K., and Fries,P. (2007). Modulation of neuronal interactions through neuronal synchronization. *Science* 316, 1609-1612.

Wurts,S.W. and Edgar,D.M. (2000). Circadian and homeostatic control of rapid eye movement (REM) sleep: promotion of REM tendency by the suprachiasmatic nucleus. *J Neurosci.* 20, 4300-4310.

Yamaguchi,H., Hirai,S., Morimatsu,M., Shoji,M., and Nakazato,Y. (1989). Diffuse type of senile plaques in the cerebellum of Alzheimer-type dementia demonstrated by beta protein immunostain. *Acta Neuropathol.* 77, 314-319.

Yang,S.N. and Berggren,P.O. (2005). CaV2.3 channel and PKC $\lambda$ : new players in insulin secretion. *J Clin Invest* 115, 16-20.

Yasuda,R., Sabatini,B.L., and Svoboda,K. (2003). Plasticity of calcium channels in dendritic spines. *Nat. Neurosci.* 6, 948-955.

Zaman,T., Lee,K., Park,C., Paydar,A., Choi,J.H., Cheong,E., Lee,C.J., and Shin,H.S. (2011). Cav2.3 channels are critical for oscillatory burst discharges in the reticular thalamus and absence epilepsy. *Neuron* 70, 95-108.

Zhang,Y., Mori,M., Burgess,D.L., and Noebels,J.L. (2002). Mutations in high-voltage-activated calcium channel genes stimulate low-voltage-activated currents in mouse thalamic relay neurons. *J Neurosci.* 22, 6362-6371.

Zhao,J., Fu,Y., Yasvoina,M., Shao,P., Hitt,B., O'Connor,T., Logan,S., Maus,E., Citron,M., Berry,R., Binder,L., and Vassar,R. (2007). Beta-site amyloid precursor protein cleaving enzyme 1 levels become elevated in neurons around amyloid plaques: implications for Alzheimer's disease pathogenesis. *J Neurosci.* 27, 3639-3649.

## **6. Acknowledgements**

First and foremost I would like to thank my PhD advisors, PD. Dr. Marco Weiergräber and Dr. Anna Papazoglou for their great support during my past three years and giving me the opportunity to develop further each day and believing in me in times of struggle. Without you it would not have been possible to write this PhD thesis. I would also like to thank my university supervisor, Professor Büschges, for taking care of me. I am greatly thankful to my former colleges at the laboratory. Spending time with you was always a lot of fun. Special thanks are going to my collaborates, Ralf Müller and Dr. Dan Ehninger. Last but not least I want to thank all my friends for their words of cheer and my wonderful family, my parents and my sister. No matter what, I can always count on you.



## 7. Author's contribution to publications

To the present work I have substantially contributed as follows:

In all three studies I performed implantations and telemetric recordings of the animals independently. I conducted additional experiments (sleep deprivation and urethane injections) and evaluated sleep analysis and seizure scorings. Time frequency analysis of the data was done in cooperation with Ralf Müller at the Psychiatry and Psychotherapy Institute of the University of Cologne. Assessment and performance of behavioural and molecular data of 5XFAD mice was done in cooperation with the German Center for Neurodegenerative Diseases (DZNE) in Bonn and the Institute of Molecular Psychiatry of the University of Bonn.

### **The Ca<sub>v</sub>2.3 R-Type Voltage-Gated Ca<sup>2+</sup> Channel in Mouse Sleep Architecture.**

**Siwek M.E\***, Müller R\*, Henseler C, Broich K, Papazoglou A, Weiergräber M (2013); Sleep, **accepted**; \*shared authorship

Concept: 20%

Experiments: 70%

Analysis: 20%

Figures: 80%

Text: 15%

### **Limited effects of an eIF2 $\alpha$ <sup>S51A</sup> allele on neurological impairments in the 5XFAD mouse model of Alzheimer's disease.**

Paesler K, Hettich M.M, **Siwek M.E**, Ryan D.P, Schröder S, Papazoglou A, Broich K, Müller R, Becker A, Garthe A, Kempermann G, Weiergräber M, Ehninger D (2013); PlosOne, **submitted**

Concept: 10%

Experiments: 20%

Analysis: 15%

Figures: 20%

Text: 15%

**Altered muscarinic signalling in 5XFAD mice – Bridging the gap between seizure activity, theta oscillations and Alzheimer’s disease**

**Siwek M.E\***, Müller R\*, Becker A, Lundt A, Wormuth C, Henseler C, Broich K, Ehinger D, Weiergräber M, Papazoglou A (2014).; Journal of Alzheimer’s Disease, **submitted**; \*shared authorship

Concept: 25%

Experiments: 90%

Analysis: 80%

Figures: 90%

Text: 70%

## 8. Erklärung

Ich versichere, dass ich die von mir vorgelegte Dissertation selbständig angefertigt, die benutzten Quellen und Hilfsmittel vollständig angegeben und die Stellen der Arbeit einschließlich Tabellen, Karten und Abbildungen, die anderen Werken im Wortlaut oder dem Sinn nach entnommen sind, in jedem Einzelfall als Entlehnung kenntlich gemacht habe; dass diese Dissertation noch keiner anderen Fakultät oder Universität zur Prüfung vorgelegen hat; dass sie – abgesehen von unten angegebenen Teilpublikationen – noch nicht veröffentlicht worden ist sowie, dass ich eine solche Veröffentlichung vor Abschluss des Promotionsverfahrens nicht vornehmen werde.

Die Bestimmungen der Promotionsordnung sind mir bekannt. Die von mir vorgelegte Dissertation ist von PD Dr. Dr. Marco Weiergräber und Prof. Dr. Ansgar Büschges betreut worden.

Köln, den 27.06.2014

---

Magdalena Elisabeth Siwek

## 9. Teilpublikationen

**The Ca<sub>v</sub>2.3 R-Type Voltage-Gated Ca<sup>2+</sup> Channel in Mouse Sleep Architecture.**

**Siwek M.E\***, Müller R\*, Henseler C, Broich K, Papazoglou A, Weiergräber M (2013); Sleep, **accepted**; \*shared authorship

**Limited effects of an eIF2 $\alpha$ <sup>S51A</sup> allele on neurological impairments in the 5XFAD mouse model of Alzheimer's disease.**

Paesler K, Hettich M.M, **Siwek M.E**, Ryan D.P, Schröder S, Papazoglou A, Broich K, Müller R, Becker A, Garthe A, Kempermann G, Weiergräber M, Ehninger D (2013); PlosOne (submitted)

**Altered muscarinic signalling in 5XFAD mice – Bridging the gap between seizure activity, theta oscillations and Alzheimer's disease**

**Siwek M.E\***, Müller R\*, Becker A, Lundt A, Wormuth C, Henseler C, Broich K, Ehninger D, Weiergräber M, Papazoglou A (2014).; Journal of Alzheimer's Disease (submitted); \*shared authorship

# 10. Curriculum Vitae

## Personal Data

---

Name SIWEK, Magdalena Elisabeth  
Date of Birth 15.05.1984  
Address Plittersdorferstr. 168,  
53173 Bonn, Germany  
Telephone: + 49 (0)1638658427  
E-mail: [magdasiwek@gmx.de](mailto:magdasiwek@gmx.de)  
Citizenship German

## Education

---

03/2011- 03/2014 **PhD student** at the Federal Institute for Drugs and Medical Devices – Bundesinstitut für Arzneimittel und Medizinprodukte (BfArM)

PhD Thesis: *„Electrophysiological and Molecular Insights into Thalamocortical Rhythmicity and Hippocampal Theta Oscillations”*

10/2008 - 10/2010 **Degree: MSc Neuroscience (Grade: 1.9)** University of Cologne

Master thesis: *„The Influence of Spatial Distortion during Body Perception- an event-related potential study”* at the Ruhr-University Bochum, Chair of Professor Irene Daum, Institute of Cognitive Neuroscience

10/2006 - 9/2008 **Degree: BSc Neuroscience** University of Cologne

Bachelor thesis: *„Psychovegetative Dysregulation bei einem Patienten mit orbitofrontaler und temporaler Hirnläsion“* at the University of Cologne, Chair of Professor Niels Galley, Institute of Anatomy

10/2003 - 10/2006 **Pre-degree of Dentistry** University of Cologne

08/1994 - 06/2003 General qualification for university entrance (allgemeine Hochschulreife) Dietrich Bonhoeffer High School, Wiehl

08/1990 - 04/1994 Elementary school Wiehl

## **Practical Courses**

---

08/2009 - 02/2010    **Clinic of Psychiatry Cologne**

Project:                    Group therapy in Patients with Asperger-syndrome

01/2009 - 03/2009    **Max Planck Institute of Neurological Research Cologne**

Project:                    Motion Perception during Visual Stimulation – An ERP Investigation

04/2007 - 10/2007    **Institute of Anatomy University of Cologne**

Project:                    Characterization and Comparison of MP4-, MOG:35-55 and PLP:178-191 induced EAE in C57BL/6 mice

## **Professional Experience**

---

10/2009 - 03/2010    **Student Assistant** Institute of Anatomy  
University of Cologne

10/2008 - 03/2009    **Consultant of the Study of Neuroscience**  
University of Cologne

09/2007 - 09/2008    **Student Assistant** Institute of Anatomy  
University of Cologne

## **Professional Conferences and Workshops attended**

---

- **Substance Application and Blood Sampling Techniques in Mice and Rats; Charles River Seminar**, 21.06.2011, Essen
- **FELASA B**: 5-09.12.11.11, Berlin
- **International Neuroscience Symposium- Neuronal and glial signalling: From physiology to epilepsy**: 01.03.12-03.03.12, Bonn
- **MCS Microelectrode Array Workshop, Neuronal Applications on Microelectrode Arrays**: 29.03.12, Reutlingen
- **Basics of Medical Statistics**: 9-13.07.12, Cologne
- **Roche Academy (Real-time PCR)**: 13.06.13, Cologne

## Software Skills

---

- Office advanced knowledge
- SPSS basic
- MatLAB basic
- Origin intermediate knowledge
- GraphPad Prism intermediate knowledge
- Neuroscore advanced knowledge
- Dataquest A.R.T advanced knowledge

## Languages

---

- German (mother tongue)
- English (fluent)
- Polish (fluent)

## References

---

Prof. Dr. med. Hannsjörg Schröder, Institut II für Anatomie, Zentrum Anatomie Joseph-Stelzmannstr.9, 50931 Köln, Germany.  
Tel: +49-221-478-5209, 5000, Fax: +49-221-478-5318,  
E-Mail: schröder.anatomie@uni-koeln.de

Prof. Dr. Ansgar Büschges, Neurobiologie/Tierphysiologie, Zoologisches Institut, Universität zu Köln, Zùlpicherstr.47 b, 50674 Köln, Germany.  
Tel: +49-221-470-2607, Fax: +49-221-470-4889,  
E-Mail: ansgar.bueschges@uni-koeln.de

PD Dr. Dr. Marco Weiergräber, Bundesinstitut für Arzneimittel und Medizinprodukte (BfArM), Kurt-Georg-Kiesinger-Allee 3, 53175 Bonn, Germany.  
Tel: +49-228-99-307-3196, Fax: +49-228-99-307-3896,  
E-Mail: Marco.Weiergräber@bfarm.de

Dr. Dan Ehninger, German Center for Neurodegenerative Diseases (DZNE), Ludwig-Erhard-Allee 2, 53175 Bonn, Germany.  
Tel: +49 228 43302-530; fax: +49 228 43302-689,  
E-mail: Dan.Ehninger@dzne.de

## Publications

---

- **Voltage-gated Ca<sup>2+</sup> channel mediated Ca<sup>2+</sup> influx in epileptogenesis.**  
Siwek M, Henseler C, Broich K, Papazoglou A, Weiergräber M. (2012); Adv Exp Med Biol. 740:1219-47
- **The Ca<sub>v</sub>2.3 R-Type Voltage-Gated Ca<sup>2+</sup> Channel in Mouse Sleep Architecture.**  
Siwek M.E\*, Müller R\*, Henseler C, Broich K, Papazoglou A, Weiergräber M (2013); Sleep, **accepted**; \*shared authorship

- **Limited effects of an eIF2 $\alpha$ <sup>S51A</sup> allele on neurological impairments in the 5XFAD mouse model of Alzheimer's disease.**  
Paesler K, Hettich M.M, Siwek M.E, Ryan D.P, Schröder S, Papazoglou A, Broich K, Müller R, Becker A, Garthe A, Kempermann G, Weiergräber M, Ehninger D (2013); PlosOne; **submitted**
- **Altered muscarinic signalling in 5XFAD mice – Bridging the gap between seizure activity, theta oscillations and Alzheimer's disease**  
**Siwek M.E\***, Müller R\*, Becker A, Lundt A, Wormuth C, Henseler C, Broich K, Ehninger D, Weiergräber M, Papazoglou A (2014).; Journal of Alzheimer's Disease; **submitted**; \*shared authorship

## **Presentations**

---

### *Oral Presentations*

- **EURON PhD Days 2011:** *The influence of spatial distortion during body perception: an event-related potential study*, 22-23.09.2011, Bad Honnef
- **Young Physiologists' Symposium:** *The Ca<sub>v</sub> 2.3 R-Type Voltage-Gated Ca<sup>2+</sup> Channel in Rodent Sleep Architecture*, 10-11.10.13, Frankfurt

### *Poster Presentations:*

- **20. Annual meeting of the German Sleep Society (DGSM) e.V:** *The Ca<sub>v</sub> 2.3 R-type voltage-gated Ca<sup>2+</sup> channel in rodent sleep architecture*; 6-8.12.12, Berlin
- **10th. Göttingen Meeting of the German Neuroscience Society:** *The Ca<sub>v</sub> 2.3 R-type voltage-gated Ca<sup>2+</sup> channel in rodent sleep architecture*; 13.03-16.03.2013, Göttingen